NASA CR-72422
R-7492

DEVELOPMENT OF A BREADBOARD MODEL OF AN ALL-PNEUMATIC NEUTRON FLUX DETECTOR

by

S. E. Milleman

prepared for

NATIONAL AERONAUTICS AND SPACE ADMINISTRATION

Contract NAS 3-7989

ROCKETDYNE
A Division of North American Rockwell, Inc.
6633 Canoga Avenue, Canoga Park, California

NAS CR-72422
R-7492

FINAL REPORT

DEVELOPMENT OF A BREADBOARD MODEL OF AN ALL-PNEUMATIC NEUTRON FLUX DETECTOR

by

S. E. Milleman

prepared for

NATIONAL AERONAUTICS AND SPACE ADMINISTRATION

23 May 1968

CONTRACT NAS 3-7989

Technical Management
NASA-Lewis Research Center
Cleveland, Ohio
Advanced Systems Division
Miles O. Dustin, Project Manager
Nuclear Systems Division
John C. Liwosz

ROCKETDYNE
A Division of North American Rockwell Corporation
6633 Canoga Avenue
Canoga Park, California

NOTICE

This report was prepared as an account of Government sponsored work. Neither the United States, nor the National Aeronautics and Space Administration (NASA), nor any person acting on behalf of NASA:

a. Makes any warranty or representation, expressed or implied, with respect to the accuracy, completeness, or usefulness of the information contained in this report, or that the use of any information, apparatus, method, or process disclosed in this report may not infringe privately owned rights; or

b. Assumes any liabilities with respect to the use of, or for damages resulting from the use of any information, apparatus, method or process disclosed in this report.

As used above, "person acting on behalf of NASA" includes any employee or contractor of NASA, or employee of such contractor, to the extent that such employee or contractor of NASA, or employee of such contractor prepares, disseminates, or provides access to, any information pursuant to his employment or contract with NASA, or his employment with such contractor.

Requests for copies of this report should be referred to:

National Aeronautics and Space Administration
Office of Scientific and Technical Information
Attention: AFSS-A
Washington, D. C. 20546

FOREWORD

This report was prepared by Rocketdyne, a Division of North American Rockwell, Inc. under National Aeronautics and Space Administration Contract NAS 3-7989.

ABSTRACT

A breadboard Model was constructed of an All-Pneumatic Neutron Flux Detector. Subassemblies of the detector consisted of a sensing element which was electrically heated to simulate neutron heating effects, a precooler, a temperature equalizer, and a fluid interaction logarithmic function generator. The detector was designed to produce a pneumatic output signal proportional to the logarithm of incident neutron flux. Performance tests were made on all system subassemblies except the sensing element. Sensing element heater development tests were completed.

CONTENTS

ILLUSTRATIONS

INTRODUCTION AND SUMMARY

This report describes the work performed by Rocketdyne under NASA-Lewis contract NAS 3-7989, "Development of a Breadboard Model of an All-Pneumatic Neutron Flux Detector". It was a follow-on effort to "Feasibility Study of All-Pneumatic Neutron Flux Density Measurement Device," NASA CR 54736 (Ref. 1). As such, its intent was to demonstrate hardware feasibility of the all-pneumatic neutron flux measurement method recommended in the initial study effort.

A conceptual schematic of the flux detector system is shown in Fig. 1. It consists of a regulated gas supply, a precooler, an active leg connected in parallel with a compensating leg, a temperature equalizer, and a fluid interaction log function generator. The active and compensating legs are each comprised of an inlet sonic orifice, a sensing element and an outlet sonic orifice connected in series. In operation, the pressure regulator and precooler maintain the sensor inlet gas pressure and temperature constant. The mass flowrate through the inlet orifice of the active element is constant since the orifice is choked and the inlet pressure temperature are constant. Heat, q_a proportional to the incident neutron and gamma flux is generated by the fuel loaded sensing element in the active leg. It is transferred to the fluid flowing over the heated element, causing the pressure between the two sonic orifices to increase. Thus the active element pressure, P_a, is functionally related to the neutron and gamma flux at the sensor. The compensating leg of the detector provides a similar relationship for the incident gamma flux heating effect.

The fluid interaction log function generator converts the differential pressure developed between the active and compensating elements to a differential pressure proportional to the logarithm of the incident neutron flux level. The temperature equalizer heats up the log function generator control gas to the same temperature as the supply gas.

The scope of this effort was to conduct an experimental program to aero-thermodynamically evaluate a breadboard model of this flux detector system using electrical heating elements in place of the thermally sensitive fission activated sensing elements.

A Log Function Generator was fabricated and statically evaluated for an input range of nearly two and a half decades. The flux detector system was not fully evaluated because the electrical heaters selected failed to perform. An alternate heater configuration was fabricated and successfully tested at the design environmental conditions. It is believed the problems which prevented completion of the planned effort have now been solved and continuation of the original program to completion is feasible and desirable.

SYSTEM SPECIFICATIONS AND REQUIREMENTS

The breadboard model pneumatic neutron flux detector system was designed to be compatible with the following specifications.

1. The thermally sensitive fission activated elements described in the preceding section shall be replaced by electrical heating elements which shall yield heat generation rates comparable to those determined in Ref. 1.

2. The response time of the system shall be less than 0.02 seconds for the designed operating range. The response time is defined as the time required for the system output to reach 63 percent of its final steady-state value following a step change on the input.

3. The system shall be capable of measuring a minimum of three decades of neutron flux. The neutron flux spectrum and range is to be that defined by Ref. 1.

4. The overall accuracy of the system shall be ± 10 percent of the indicated flux while operating under the environmental conditions stated below. This shall include the inaccuracy caused by incomplete gamma discrimination.

5. The system shall be compensated for gamma radiation.

6. The system output shall be an analog pneumatic signal proportional to the logarithm of the neutron flux.

7. The system shall be capable of continuous operation for 40 minutes and capable of at least four shutdown and restart operations. The total time of operation of full power shall be at least 1-1/2 hours.

8. The working fluid shall be helium with an ultimate goal of a capability of using hydrogen.

ENVIRONMENTAL CONDITIONS

1. Temperature where the detector will be located with be from 200 to 800 R.
2. Gamma flux up to 5×10^9 ergs/gm(c) hr.

It was found necessary, due to trade-off considerations between resolution and speed of response, to deviate from the 0.02 seconds speed of response specification. The reasons for this are discussed more fully in the next section. The resultant calculated speed of response, after designing for good resolution, was about 0.10 seconds.

SENSOR SPECIFICATIONS

At a meeting between NASA-Lewis and Rocketdyne representatives, the design philosophy for the breadboard model all-pneumatic flux detector was established. It was agreed that the working gas supply pressure would be maintained at 250 psia with the signal pressure, P_a, at the 100 percent power level restricted to a maximum value of 125 psia (Fig. 1). This reduction of the operating pressure levels reduces the severity of the problems involved in the differential amplifier of the Log Function Generator (i.e., detection os small differential pressure at a very high absolute pressure). Reduction of pressure level also decreases the operating range of pressures, unless the corresponding temperature range over which the flux detector is operated is increased.

$$P_a(\max) - P_a(\min) = P_a(\max)\left[1 - \sqrt{\frac{T_a(\min)}{T_a(\max)}}\right] \qquad (1)$$

Therefore, it was agreed to increase the temperature, at 100 percent power level, to near room temperature. For the design heating rate, it may be seen that the flow is reduced for increased temperature range from the equation of heat balance:

$$q_a = \dot{m}_a C_{pa} (T_a - T_r) \qquad (2)$$

Although the speed of response is slower at higher temperatures, it was reasoned that calculated analytical values may be correlated with test results such that predictions may be extrapolated with good accuracy for flight type hardware. In the analytical feasibility study, it was shown that range, pressure levels, and speed of response of this device are considerably improved at low operating temperatures.

It was also agreed that the inlet and exit areas would be designed as sharp edged orifices rather than venturi nozzles, which had been discussed

previously as a means of reducing the required supply gas pressure. This also eliminated the long diffuser section required to attain high pressure recovery. It should be noted that with plain orifices at the 100 percent power level, i.e., 125 psia, the inlet orifice flow is not choked since the critical pressure ratio for helium is 0.492. The flow-rate error at a pressure ratio of 0.500 (corresponding to 100 percent power level) is 0.45 percent.

The basic design concept is briefly reviewed to aid in discussion. Referring to Fig. 1, the flow through the inlet orifice of the active element is:

$$\dot{m}_a = \frac{P_r A_{ra} f\,(P_a/P_r)}{\sqrt{T_r}} \tag{3}$$

By maintaining constant supply pressure and temperature and maintaining choked flow in the inlet orifice, the flow remains constant throughout the operating regime. Neglecting losses, the heat transferred from the active element to the passing gas is given by Eq. 2. Since the flow and fluid specific heat are constant in this application, the temperature rise is proportional to the heat generated in the heating elements. The flow through the discharge orifice is:

$$\dot{m}_a = \frac{P_a A_a f\,(P_d/P_a)}{\sqrt{T_a}} \tag{4}$$

By maintaining constant flow and a choked discharge orifice, the signal pressure, P_a, is then a function of the generated heat:

$$P_a = K_1 \sqrt{T_r + K_2 q_a} \tag{5}$$

The operating pressures and temperatures of the device were determined using Eq. 4. The pressure range from 0 to 100 percent flux is:

$$P_a(\max) - P_a(\min) = \frac{\dot{m}_a \sqrt{T_a(\max)}}{A_a f\,(P_d/P_a)} - \frac{\dot{m}_a \sqrt{T_a(\min)}}{A_a f\,(P_d/P_a)} \tag{6}$$

which may be manipulated to give Eq. 1. Thus the pressure range which is directly related to resolution may be increased by:

1. Decreasing $T_a(\min)$
2. Increasing $T_a(\max)$
3. Increasing $P_a(\max)$

The 63 percent time constant, τ, for the flux detector is of the form:

$$\tau = \frac{C_{ma} M_a}{\dot{m}_a C_{pa}} = \frac{C_{ma} (T_a - T_r)}{q_a} \tag{7}$$

Noting that $T_r = T_a(\min)$ and that the specific heat of the heating elements decreases with temperature, it is observed that the speed of response is increased by decreasing the supply temperature and temperature rise for a given heat input. In summary, the conditions desired for good response and range are:

1. Low supply gas temperature
2. High operating pressures
3. A tradeoff between response and resolution

The minimum supply temperature was limited by the temperature of the liquid nitrogen coolant which was assumed to be 140 R. The supply gas pressure at the inlet orifice was limited to 250 psia. For helium, the critical pressure ratio of 0.492 means that the inlet orifice unchoked at a signal pressure of 122 psia (assuming no pressure drop). The maximum signal pressure at 100 percent power was selected at 125 psia. The reduction in flow due to unchoked flow at this pressure was less than 0.5 percent and could be calibrated out. For the breadboard model, it was decided to design for as high a gas temperature as was feasible to obtain a large operating pressure range, while sacrificing speed of response.

Pressure range is plotted vs temperature rise for a maximum signal pressure of 125 psia in Fig. 2. In Fig. 3, the change in Reynold's number and pressure drop through the sensing element due to increased temperature range is plotted. See Appendix A for sample calculations. From these results, a design temperature range of 200 R was selected at a flowrate of 3.13×10^{-3} lb/sec. The Log Function Generator Specification was calculated using these design values and is shown in Appendix B.

SENSOR COMPONENT ANALYSIS

SENSING ELEMENT ANALYSIS

For the system parameters defined, the required orifice effective areas were calculated. The inlet area was calculated as 7.03×10^{-4} sq in., and the exit orifice area as 2.22×10^{-3} sq in. For design purposes, it was necessary to define various factors affecting the orifice discharge coefficients in order to physically size the orifice areas. These factors were Reynold's number, velocity of approach, orifice type (i.e., knife edge, thick plate, nozzle), orifice size, and pressure ratio across the orifice. The Reynold's numbers for the inlet and exit orifices were calculated at 286,000 and 90,400 respectively. Discharge coefficients are relatively constant with changes in Reynold's numbers of these magnitudes (Ref. 2 and 3). The velocity of approach factor on flow was about 1.0001 for the inlet and 1.021 for the exhaust. Discharge coefficients for sonic orifices vary considerably with orifice type; maximum values range between 1.0 and 0.80. Values also vary for different sizes, especially small diameters, tending to yield higher values for small diameters (Ref. 3). Although sonic flow is maintained, the discharge coefficient is subject to change with changes in pressure ratio. This effect is more evident in sharp edged orifices than in nozzles.

Calibrations were made on basic sensor inlet and discharge orifices. The reduced data from this orifice test program are presented in Fig. 4. The values of C_D fell within a rather narrow band when plotted against pressure ratio; and it was concluded that, in the range of interest, C_D was a very weak function of orifice Reynold's number. Hence, no attempt was made to obtain a secondary correlation with orifice Reynold's number.

A digital program was written to calculate discharge coefficients for the sensing element inlet and discharge orifices as functions of pressure ratio across the orifice and orifice Reynold's number. Based on this data the basic sensor orifices were sized as follows: inlet 0.0361 in. and exit 0.0589 in.

A brief digital program, GROG, was written to determine output ΔP_o vs power input for variable orifice discharge coefficients and variable pressure drop across the heater elements. It was predicted that due to the variation of discharge coefficients with pressure ratios, active element flowrate would vary from 3.40×10^{-3} lb/sec at 0 power to 3.18×10^{-3} lb/sec at 100 percent power (200 R temperature rise). This resulted in a control output pressure of 87.05 psid at 0 power and 122 psid at 100 percent power as shown in Table 1 of Appendix B.

The heater slab configuration used for the above calculations is shown in Fig. 5. The calculated average wall temperature was 355 R. The temperature distribution on the silicon slabs was also calculated to ensure that their electrical properties would not be destroyed. Uniform heat generation in the slabs was assumed and the results are plotted in Fig. 6. The maximum wall temperature calculated was 445 R, which was satisfactory.

The thermal contraction of the aluminum pressure shell was found to be 0.00375 in. per in. of length while that of the silicon heater slab was 0.0002 in. per in. of length. Allowances for differential thermal expansion were necessary in design of the pressure shell to avoid crushing the slabs. Another necessary precaution was the avoidance of thermal stresses in the physical design of the heater slab.

Work was done to ensure that the pressure shell wall thickness was sufficient to prevent rupture or excessive deflection during pressurization. Calculations showed that stresswise, the factor of safety with an 0.020 wall thickness was 3.24. The maximum deflection outward of the tube was 0.0003 in. and the maximum inward deflection was 0.00018 in. However, certain considerations led to the adoption of 0.030 in. for the nominal wall thickness. These considerations included tolerance buildups, the problem of maintaining "concentricity" of the outer and inner shell contours over the 3-in. length, and reduction of effective load carrying wall thickness by anodization. Assuming other factors constant, the additional

wall material would degrade the response of the detector, based on the linearized analysis presented in the final report of the feasibility study (Ref. 1). However, this degradation is amenable to analysis and can be corrected for a flight type design.

Sensing Element Analog Study

The analog model was designed to study the effect of thermal lags on the response of the active element output pressure to both large and small amplitude steps in power input to the heater elements.

Effects due to flow dynamics would have appeared at frequencies at least an order of magnitude higher than those of interest (0.01 to 100 rad/sec); consequently, steady flow was assumed. However, thermal capacitance of the gas was taken into account. The approximating lumped parameter equations and a schematic of the resulting representation are shown in Appendix C. Two lumps were used in the (single equivalent) heater element, gas, and wall; lump temperature (indicated by $\bar{T}$....) was taken as the arithmetic mean of the section end-point temperatures. Two additional lumps were included at either end of the wall to represent material (flanges, etc.) outside the area in which the heater elements were located. Heat transfer across the vacuum chamber and from the end flanges to the outer shell of the vacuum chamber was neglected. All other possible paths between regions indicated in the schematic of the Appendix were considered.

A computer diagram of the model is also shown in Appendix C. The potentiometer settings shown are the nominal (as calculated) heat transfer coefficients and masses. A tabulation of nominal parameters is given in Table 1 of Appendix C.

For nominal conditions Fig. 7 and 8 exhibit the behavior of various system parameters when power level to the heaters was stepped from zero to 100 percent. Three facts stand out here.

1. Output ΔP_a reached 90 percent of its final value in about 0.20 seconds.

2. Time required for the change in wall temperature to reach 90 percent of its final value was about 45 seconds.

3. The long wall temperature transient did not noticeably affect the output ΔP_a; in fact, the output ΔP_a appeared to have completely settled out after 0.5 seconds.

The same characteristics are exhibited on the small-amplitude step response traces. Frequency response plots derived from the small amplitude step response at 0, 50, and 100 percent power levels are shown in Fig. 9, 10, and 11. Note that the 3 db down point occurs at approximately 110 radians (90 ms response) in each case.

It should be noted that the above model assumed zero contact conductance between the walls and the heater elements. What the results above imply are that, if this condition does indeed occur, then the mass of the walls is not a significant factor in the overall response of the detector.

Figure 12 shows the pressure trace obtained when all gas film coefficients were increased by a factor of 4. For a step in power level from 0 to 100 percent, the output ΔP_a reached 90 percent of its final value in about 0.10 seconds, one-half the time required for the nominal case.

Figure 13 shows the pressure trace obtained when all gas film coefficients were decreased by a factor of 2. In this case, due to a couple of overloaded analog amplifiers (corresponding to heater element temperatures in excess of 600 R), an 0 to 100 percent power level step was not used. However, for a 71.5 percent step in power level, 90 percent of the final value ΔP_a was achieved in 0.33 seconds. (For the same size step under nominal conditions, 1.18 seconds was required.)

In the last two runs mentioned, the wall temperature transients were again very slow compared to the gas temperature and pressure transients, with negligible feedback effects from the walls on the gas outlet temperature and pressure.

It should also be noted that, due to the small values of conductance within the heater elements and negligible wall effects, the effects obtained by changing heater element masses are similar to those obtained by changing heat transfer coefficients. For example, increasing heater mass by a factor of 2 would have essentially the same effect on response as decreasing film heat transfer coefficients by a factor of 2, and so forth.

In Fig. 14, the heat transfer coefficient between the heater and gas was left at its nominal value, and the coefficient between the walls and flanges and gas was increased by a factor of 4. No discernible difference exists between these results and those of Fig. 7.

Finally, an attempt was made to determine what effect contact conductance between the heater elements and walls had on detector response. To accomplish this, an overall heat transfer coefficient between the walls and the heater element was arbitrarily assumed to be 1/5 of that between the gas and the heater element. Figures 15 and 16 indicate response of various system parameters when a 0 - 100 percent step in power level was applied. Note that the initial transient in Fig. 15, similar to that shown in Fig. 7, is followed by an extremely long settling transient. In fact, 70 percent of the final value change is reached in 0.15 seconds; however, the 90 percent point is reached only after 1.64 seconds, and complete settling requires something on the order of 16 seconds. Time required for the wall temperature to reach 90 percent of its final value change was cut from 45 to 6 seconds. The small amplitude output response was also degraded; a frequency response plot (obtained from the small aplitude step response) is shown in Fig. 17.

It is not known whether the figure assumed for contact conductance is reasonable; this number is obviously a function of such nebulous variables as tightness of fit of the heater elements in the shell, etc. A qualitative index of the significance of contact conductance may be obtained from tests of the breadboard flux detector transient by examining the output. The presence of a long (on the order of seconds) settling transient would probably indicate that contact conductance is large enough to be a problem.

The major conclusions to be drawn from this study may be summarized as follows. These are, of course, applicable to future flight type hardware.

1. Active element mass should be minimized and heat transfer coefficient between gas and active element should be maximized.
2. If care is taken to insulate the active element from the surrounding walls, the interaction between walls and gas is negligible; and the mass of the walls is not critical.
3. If significant contact conductance exists between the walls and the active element, a reduction of wall mass by at least an order of magnitude would probably be necessary to cut the long settling time to an acceptable value. Since this appears to be a physically unrealized accomplishment, it is recommended that future attention be given to item 2.
4. If extremely long settling times are noted in testing the flux detector, the principal influence would probably be contact conductance between the heater elements and walls, indicating that this would indeed be a design problem on the flight hardware.

PRECOOLER ANALYSIS

The precooler was designed to cool the helium supply gas to the pneumatic flux detector down to the vicinity of 140 R. The cooling medium chosen was boiling liquid nitrogen at ambient pressure; the helium flowed through

coiled tubing immersed in the liquid nitrogen, while level was controlled within appropriate limits by an on-off type level controller. The heat exchanger coils were designed with the following criteria in mind:

1. Lack of susceptibility to clogging due to ice formation.
2. Ease of fabrication.
3. Availability and cheapness of material.
4. Large factor of safety on the amount of heat transfer area supplied.

Some testing was done on heat transfer rates for helium flowing through 0.040 OD tubes immersed in liquid nitrogen. Severe problems were encountered with tube blockage due to ice formation, and consequently the results of the testing were inconclusive. Because of this experience it was decided to use larger tube sizes for the precooler, making no serious attempt to minimize package size.

In order to maintain turbulent flow in the tubes, and in order to adhere to criterion (1), the precooler was designed in two sections. The first section consisted of four parallel parths of 1/4 inch OD tubing in which helium was cooled to -116 F, at which temperature 90 percent of the water vapor was calculated to have condensed as ice, assuming a dew point of -70 F.

For a helium flowrate of 0.00626 lb/sec., approximately 0.000277 pound of water would be condensed in one hour's testing. Assuming this appeared as frost with a density 1/5 that of ice, this corresponded to 0.0415 $in.^3$ of material, 90 percent of which theoretically would condense out in 14 inches of the 1/4 in. OD tubing. This gave a predicted thickness on the walls of about 0.005 in. thus eliminating clogging as a problem with this precooler.

The remainder of the cooling to 145 R took place in the second section, which consisted of 15 parallel paths of 1/8 in. OD tubing. Pressure drop was predicted to be about 30 psi.

Calculation of heat transfer coefficients on the boiling side was done using a correlation (Ref. 14) for stable pool film boiling of liquid nitrogen at ambient pressure around a horizontal cylinder. In the precooler, boiling took place around helically coiled tubing with a large bend radius, small helix angle, and vertical helix axis; however, it was expected that applying the cited correlation to this case would be conservative for the following reasons:

1. Increased turbulence around the upper coils due to the influence of bubbles leaving the lower coils.
2. Improved heat transfer coefficient on the helium side due to tube curvature.

A safety factor of 5 was used on the calculation of all heat transfer areas. The calculations are shown in Appendix D.

TEMPERATURE EQUALIZER ANALYSIS

The temperature equalizer was designed to equalize the temperatures of the two control flows to the Log Function Generator. This was done by passing the control flows through tubes on the outside of which flows the supply gas for the flux detector and Log Function Generator.

Since one of the control flows varied in temperature, pressure, and flowrate, it was necessary to design the temperature equalizer so that the rates of change of control flow outlet temperature with respect to its variables were negligible at the worst conceivable heat transfer conditions. This was accomplished by providing enough heat transfer area to heat

0.000313 lb/sec (maximum total LFG control flow) at 140 R (lowest temperature) to within 5 R of the helium supply temperature. There were three conflicting requirements for the temperature equalizer:

1. Large overall heat transfer coefficient dictated by the considerations mentioned above.
2. Low pressure drops on the control gas side to assure that differences in the pressure drops in the two control gas paths were also small.
3. Good dynamic response to perturbations in control pressures.

After several false starts, the configuration shown in Appendix E was decided on as a reasonable compromise among these three requirements. In order to minimize pressure drop in the control gas (cold) side, it was necessary to accept laminar flow which in turn gives rise to poor heat transfer coefficients on the cold side. So, in order to provide as much wall-to-fluid ΔT as possible on the cold side, it was decided to use a cross flow pattern on the hot side to accept the fairly large hot side pressure drop associated with this configuration. This gives a large gas film coefficient on the hot side and a wall temperature close to the supply gas temperature.

Due to the very small value of the ratio of (cold side outlet wall-to-fluid ΔT) to (cold side inlet wall-to-fluid ΔT) thermal response of the temperature equalizer was a matter of somewhat academic interest. This was confirmed on a brief analog computer study of the linearized dynamic heat transfer equations. The only transients visible on the outlet temperature trace were spurious ones introduced by the approximate lumped parameter representation used.

Of more significance was the pressure response on the control gas side; this was investigated in another, more detailed analog study. Again, due to the basic dislike of analog computers for distributed parameter systems, an approximate lumped parameter representation was formulated. This is shown diagramatically on Page 5, Appendix E, along with the basic equations used. The model included the control gas lines from the flux detector to the temprature equalizer and flow inertia, resistance, and capacitance were considered.

Figure 18 illustrates a typical trace of the outlet pressure of the active control leg in response to a step change in flux detector output pressure. Time required to reach 90 percent of the steady state pressure change was less than 5 ms, which was well within acceptable limits.

LOG FUNCTION GENERATOR ANALYSIS AND FABRICATION

This section describes both analysis and fabrication of the Log Function Generator since the two were so closely intertwined due to the large amount of dependence upon empirical information in the design of fluidic circuits. As previously noted, the Log Function Generator requirements were specified by Appendix B. The original scheme for the LFG is shown in Fig. 19. The system was open loop and simply gave a power gain to the input signal, then broke the signal into several parts and multiplied each part by a different gain. The individual gain block outputs saturated at some input level less than the maximum input signal, and then their outputs were recombined to give an approximation of a logarithm.

The Log Function Generator was mathematically described to find how much gain was needed, how many segments were needed, and what the segment gains and saturation levels should be. Appendix F derives the mathematical model used for the LFG. The following equation is the mathematical approximation arrived upon by computer solution

$$\Delta P_o = 0.867 \sin \frac{\pi}{2} \frac{\Delta P_i}{0.03} + 1.16 \sin \frac{\pi}{2} \frac{\Delta P_i}{0.09} + 1.28 \sin \frac{\pi}{2} \frac{\Delta P_i}{0.28} +$$
$$1.26 \sin \frac{\pi}{2} \frac{\Delta P_i}{0.90} + 1.36 \sin \frac{\pi}{2} \frac{\Delta P_i}{3.0} + 1.22 \sin \frac{\pi}{2} \frac{\Delta P_i}{9.99} +$$
$$1.30 \sin \frac{\pi}{2} \frac{\Delta P_i}{30.0} + 2.3 \sin \frac{\pi}{2} \frac{\Delta P_i}{130.0}$$

where

$$\Delta P_i = P_a - P_b$$

The value of each segment is constant for ΔP_i less than the value A, where A is the number inside the sine and under ΔP_i. Through the use of this model, the conclusion was reached that the system should have 8 segments and that each segment should have the pressure gain and saturation shown in Table 1 to enable approximation of a logarithm within 5 percent.

At the start of the program it was known that several basic improvements could be made on the basic Corning standard center dump amplifier. By reducing the aspect ratio to 2, pointing the controls slightly at the power jet and reducing the control edge width to 1.5 power nozzle widths, the pressure and flow gain could be increased.

A sample fabrication lot of modified amplifiers showed the amplifier to have a pressure gain of 7.3 and flow gain of 11.0 (Fig. 20). The standard center dump has a pressure gain of 5.3 and flow gain of 3.7 (Fig. 21).

TABLE 1

LOG FUNCTION GENERATOR SATURABLE GAIN SEGMENT REQUIREMENTS

Segment	Pressure Gain at $P_i = 0$ (psi/psi)	Segment Output Saturation Level, psid
1	45.4	0.867
2	20.2	1.16
3	7.18	1.28
4	2.20	1.26
5	0.712	1.36
6	0.612	1.22
7	0.0680	1.30
8	0.0278	2.30

The only bad feature noted with this amplifier was that there was a great deal of cross coupling between controls when the amplifier was overdriven.

Performance tests (Fig. 22) on the basic amplifier indicated that a lot of noise was present above 100 cps. Since the system needed to respond only to 15 cps it appeared possible to filter this noise. A Ladder Filter type configuration was designed for the low pass filters. Figure 23 shows the performance curve of the selected filter for 1 psig input signals indicating fair roll off in the critical area above 100 cps.

The power amplifier was originally proposed as an open loop amplifier. However, system tuning problems dictated that the power amplifier be closed loop so that better system stability could be obtained. The original closed loop power amplifier had two stages. One stage was a 0.005 x 0.010 amplifier which had its output feed into a 0.010 x 0.020 amplifier. This system proved to have insufficient output to power eight segments. The gain obtained ranged from 2.3 to 1.6 depending upon what resistors were used between the power amplifier and the saturable segments.

A third 0.020 x 0.040 amplifier was added to the power amplifier. The resulting increase in output available stabilized the power amplifier gain. The complete power amplifier assembly consists of five Corning No. 2 resistors and one Corning amplifier 47500-262. The assembly has 20 cps frequency response with a 0.5 cu. in. output volume and a gain of 1.0. When operated in a 50 psia atmosphere of helium and supplied with a 135 to 195 psia helium supply, the output of the amplifier varied from 55 to 90 psia depending upon the input signal. An extra input provided to the saturable amplifier is used as a zero adjust.

The saturable amplifier was the main component in the LFG. A schematic representation of one segment of the Function Generator Circuit is shown in Fig. 24. Typical input-output characteristic curves of a segment depicting various gains are shown in Fig. 25. Single ended inputs were used in this circuit, primarily to reduce the overall circuit noise. In Fig. 24, when the control input of amplifier A of a segment was sufficiently large, its output signal was zero and amplifier B became saturated. The output signal at this point was not affected by noise from the input power gain circuit for that particular segment. However, this feature did not relieve the noise problem at the lower input signal levels. The effect of varying supply gas pressure and the resistors for a particular segment was investigated experimentally with the following results:

1. The supply gas pressure controlled the magnitude of the output differential pressure signal at saturation.
2. Resistance R_4 controlled the overshoot of the output signal.
3. Resistances R_1, R_2, and R_3 affected the shape of the nonsaturated portion of the input-output curve and the circuit balance.
4. Resistance R_5 controlled the circuit gain.

Figure 26 shows typical data from the saturable amplifier breadboard. Once the circuit was breadboarded, two things became apparent. One was that the input to the saturable amplifiers (the power amplifier output) did not start from zero so that all the segments started from saturation. This problem necessitated adding a bias to the saturable amplifier.

Adding the bias and the necessary dropping resistors caused the second problem. When the input to the saturable was high, the saturable amplifier first stage was overdriven and the cross-talk caused a pressure buildup on the bias side of the first amplifier. The dynamics of the pressure buildup and discharge were such that a hysteresis loop resulted. Therefore, isolators were added to the input and bias of the saturable amplifier and between the fixed resistor and the second stage bias. These isolators were two-dimensional vented jets with a 0.005 x 0.020 supply nozzle, a 0.010 x 0.020 receiver and a 14 degree included angle diffuser. The saturable amplifier consisted of quite a few components and was quite bulky, so the circuit was integrated.

Performance tests on the integrated saturable amplifier showed the saturation to be completely flat. The output vs input curve very closely approximated the sine function assumed. Also, the frequency response of the circuit was over 20 cps with less than 0.1 cu in. volume on the output.

A Diode type summer was planned originally. However, it was found that when more than four inputs were used, the poor front to back ratio of the diodes caused tuning problems. Therefore, another type summer was needed. The only summer which was accurate enough and had small enough crosstalk to allow the circuit to be tuned was the feedback stabilized type of summer. The summer configuration arrived at is shown in Fig. 27. During final assembly and tuning the summer had to be modified to allow a ninth input to be added. The ninth input was used as a zero balance of the output.

The initial assembly demonstrated that it was not feasible to breadboard the complete system as fittings and tubing required too much space. Therefore, the system was combined into several integrated circuits. These integrated circuits were the power amplifier, the saturable amplifiers and the summer. Subsequent assembly showed the system components to be too interdependent to tune. If the gain of a segment was changed, the gain of the power amplifier was changed and so the gain of all other segments changed. To attempt to stabilize the system, the power amplifier and the summer were made closed loop. The saturable amplifiers were left open loop.

A Log Function Generator system was assembled with all fixed value resistors and proved to be quite difficult to tune. The major problem was that the entire system needed to be removed from the tank to change any of the fixed value resistors. The system was modified by the addition of needle valves which could be adjusted from the outside of the tank. This system was quickly tuned. The Brooks elf type needle valves were used since these valves had the fine adjustment and repeatability needed in tuning.

SYSTEM COMPONENT FABRICATION

SENSING ELEMENT

The Sensing Element Assembly Drawing is shown in Fig. 28. Each assembly contains three electrical heater slabs mounted in spacers and held in place by a heater support tube. This support tube is in turn enclosed in a vacuum tube which is evacuated during tests through an appropriate tube connection. This feature reduces the heat loss from the heater support tube and thus any consequent signal degradation. The sensor inlet and exit orifices are mounted in the support tube. Each heater slab is fabricated such that each surface has a controlled, specified resistance. Each of these surfaces is electrically insulated from the other by the heater substrate material. Thus six resistive surfaces are available in the sensing element. These are mechanically connected in series with electrical conducting wires to each other and to hermetically sealed electrical pass-throughs. In addition, tubing connections are provided to enable pressure sensing and signal extraction and thermocouples are provided for temperature sensing. Figure 29 shows some of the sensing element components just described while Fig. 30 shows the assembled sensing elements.

SENSOR ASSEMBLY

Figure 31 shows the Flux Detector Sensor Assembly. Two Sensing Element Assemblies, an active element and a compensating element, are each enclosed in vacuum tube support housings and both are mounted on a support plate within a single tube mounting shell. This support plate assembly is mounted in a coolant exhaust shell and both are then attached to a coolant manifold cover plate. The wiring used to provide electrical power to the heater slabs and part of the pressure and temperature instrumentation probes are brought out through the sides of the cover plate. Access to the sensor output signal lines and the rest of the instrumentation lines

is provided through the back of the coolant exhaust shell. This entire assembly is shown in Fig. 32. It is mounted upright as shown on top of the precooler.

Gaseous helium at 250 psia and at 140 R is provided directly to this assembly after passing through the precooler. It enters the common volume shown in Fig. 31 between the precooler cover plate and the coolant manifold cover plate. Thereafter it passes through each sensing element assembly exhausting into the aft ends of the two vacuum tube support housings. This gas is then recirculated back past the outside of the Sensing Element Assemblies, out into the tube mounting shell and finally through the coolant exhaust shell to an atmospheric exhaust. By recirculating the Sensing Element exhaust gas as described, the differential temperature between the inside and outside of the elements is reduced and thus any heat loss which might erroneously effect the signal obtained.

The exhaust gases from the precooler are vented up through the precooler cover plate, the coolant manifold cover plate, and sensing element support plate into the coolant exhaust shell. From there it combines with the exhaust helium from the sensing element before being dumped overboard.

TEMPERATURE EQUALIZER ASSEMBLY

The Temperature Equalizer Assembly drawing is shown in Fig. 33. The signal lines from the two sensing elements bring the helium into the heat exchanger tubes where it is heated to near room temperature by counterflow circulation outside these tubes of the sensor assembly supply helium prior to its entrance to the precooler. The warm sensing element helium flow is then ported to the Log Function Generator. Figure 34 shows the Temperature Equalizer components prior to assembly and the assembled Temperature Equalizer can be seen in Fig. 38.

PRECOOLER ASSEMBLY

The precooler just prior to assembly is shown in Fig. 35. This assembly was a true breadboard in the sense that no assembly drawings were used. The tubing specified in the analysis of Appendix D was wrapped on a mandrel such that it fit in the insulated metal container shown. The tube exit ends were connected to fittings in a distribution manifold on the precooler cover. The sensor assembly mounted to this manifold as previously discussed. The tube entrance ends connected to tube fittings, also on the precooler cover. The exit gas tubing from the temperature equalizer was connected to these fittings, also as previously discussed. In operation, the tank was filled with liquid nitrogen to cover the tubing through which the gaseous helium flowed. When the boil off from the liquid nitrogen (through the sensor assembly) caused the liquid level in the tank to fall below a pre-determined level, more nitrogen was added. The supply gas temperature was maintained fairly easily at 140 R with this configuration and required little attention as far as maintaining the liquid level.

LOG FUNCTION GENERATOR

An internal view of the Log Function Generator is shown in Fig. 36. The entire assembly was fabricated to fit inside a heavy pressure vessel capable of containing the specified 50 psia vent pressure. The fluidic components were mounted on a metal plate which in turn was attached to the cover plate of the pressure vessel. All inputs and outputs to the various components also passed through this plate. As shown in the photograph, the integrated three-stage input power amplifier is mounted with external input and feedback resistors. The power amplifier supply is connected directly to the external 140 psia supply and an externally adjustable power amplifier output signal balance is provided. The eight saturable elements are stacked in the center of the plate and are all driven by the power amplifier. The common supply to all of them is externally adjustable as is the common bias to all of them. In addition, each segment is provided with

individual externally adjustable supply and bias control. Because of the high gain requirements at the low input pressure levels, three of the segments required an additional stage of amplification each. These stages can be seen just below the segment stack, above the summer. The differential outputs of the segments are brought into the summer through individual pairs of fixed resistors which can be seen just below the three amplifiers just discussed. The summers supply and output balance are externally adjustable. Figure 37 shows the top side of the pressure vessel cover plate and all of the external adjustments, instrumentation points and signal connect points. Figure 38 shows the Log Function Generator and Temperature Equalizer installed in the laboratory for evaluation tests.

LABORATORY EVALUATION

LOG FUNCTION GENERATOR

The Log Function Generator (LFG) was evaluated in the laboratory in a test setup per the schematic of Fig. 39. The eliminate crosstalk between the various controlled parameters, separate regulators were provided for the helium supply, vent, and both high and low side input pressures. The input was obtained by changing only the high side regulator. The input differential pressure and the deadheaded output differential pressure were observed by monometer readings, both water and mercury, and in the case of high inputs a gage was utilized.

The Log Function Generator (LFG) had been adjusted at Corning Glass Works, Corning, New York, prior to shipment to Rocketdyne. Upon its installation in the test facility, it was found not to be in adjustment. Following a procedure recommended by Corning engineering, the LFG was adjusted so that the logarithmic relation was attained within tolerance from 0.15 psid input to 30 psid input. It was noted during tests that the LFG was very sensitive to variations in either the vent pressure or the common bias pressure. This sensitivity showed up as a lack of repeatibility in the LFG. It was particularly evident at low input signals and seemed to show up every time the circuit was shut down a restarted.

Figure 40 shows the results of two consecutive runs. Figure 41 shows the results of two additional consecutive runs made after the LFG had been shut down about two hours. Only one curve is shown in the latter case since both were almost exactly identical. Figure 40 demonstrates that hysteresis existed at the low end, but that the curve was still fairly repeatable. Figure 41 again demonstrates repeatability, for both consecutive runs and for runs with an intervening shutdown period. However, the hysteresis had disappeared for some unexplained reason. The problem

of inconsistency in the input-output characteristics could not necessarily be associated with the LFG since the test setup could easily have been the cause. The answer to this dilemma was never satisfactorily determined.

Dynamic tests of the LFG showed that a very small volume was needed on the LFG outputs. With a 0.2 cu in. output volume the frequency response, at Corning, was about 10 cps. Response tests at Rocketdyne were conducted attempting to provide step inputs and recording the transient input and output differential pressure signals with the aid of an oscilloscope camera. Typical results are shown in Fig. 42 for the case of stepping from 24.1 psig input differential pressure to 26.9 psig and then back to 24.1 psig. The output differential pressure varied from 9.45 psig to 9.75 psig and back to 9.45 psig. Because of the excessive volume on the input circuit, the input signal was not a step. The output was able to follow this slow input, particularly in the case of decreasing input. Further transient evaluations would have to be performed after reducing the volumes of both the input and exit circuits. An additional possible problem is evident from the noisy output signal and further tests should investigate this area as well.

FLUX DETECTOR SYSTEM

Figure 43 shows schematically the test setup which was to be utilized to conduct laboratory evaluations of the Flux Detector System. The room temperature helium supply passed through the temperature equalizer to provide heating of the cold sensor output signal gas prior to its entrance to the Log Function Generator input circuit. After exiting from the temperature equalizer, part of this supply gas was ported to the Log Function Generator supply inlet and the rest was ported to the precooler and cooled to liquid nitrogen temperature (140 R). From there it went to the flux detector assembly after which most of it was vented overboard. That portion not dumped provided the flux detector output signal which

eventually found its way into the Log Function Generator. The electrical heaters in the flux detector used to simulate the nuclear fuel elements were provided with power from a supply capable of providing 7.5 amps at 120 volts. Separate voltage and current measurements would provide the input power information required. A vacuum pump was used to provide a vacuum around the sensing element assemblies and reduce undesirable heat loss.

Initial room temperature flow tests gave hints of a problem area of unforseen magnitude in that one of the sensing element null output signals was about 50 percent too high. No reason for this could be found without destructively dismanteling the sensor assembly, so the precooler was activated and attempts were made to apply electrical power at the cryogenic design temperature. At this time it became evident that the electrical heaters in both sensing element assemblies were open electrically. Upon disassembly the silicon heaters were found to be broken and with some of the gold solder pads pulled out.

Subsequent activity to determine the cause of this problem and its cure resulted in a heater development program being conducted at Rocketdyne expense. This program and its results are described in detail in Appendix G. It was determined that the silicon heaters suffered from thermally induced materials failures which occurred at the contact pads and they were subsequently discarded as unsatisfactory. Alternate heaters were fabricated and successfully tested at the environmental conditions which they would experience in the flux detector. These heaters utilized a thin metallic resistance foil which was epoxyed on a stainless steel substrate.

No further test effort was performed on either the system or its components.

RECOMMENDATIONS

It is recommended that the test evaluation and subsequent correlation of these results with the analytical model be completed. It is further recommended that fuel element fabrication be undertaken and that the existing breadboard hardware be altered as necessary to allow use of these fuel elements, in conjunction with the pneumatic neutron flux detector, in a nuclear reactor test.

REFERENCES

1. Mangion, C.; Fox, P.; Tomomatsu, H.; "Feasibility Study of All-Pneumatic Neutron Flux Density Measurement Devices," NASA CR54736 June 30 1965.

2. Perry, J. A., "Critical Flow Through Sharp Edged Orifices," Transactions of the ASME October 1949.

3. Grace, H. P. and Lapple, C. E.; "Discharge Coefficients of Small Diameter Orifices and Small Nozzles," Transactions of the ASME; July 1951.

4. Simmons, J. T.; "The Physical and Thermodynamic Properties of Helium," Wm. R. Whittaker Co. Ltd., July 1, 1957.

5. Chelton, D. B.; Mann, D. B.; "Cryogenic Data Book," NBS CEL, WADC Tech. Report 59-B; March 1959.

6. Hydrogen Handbook, Arthur D. Little Inc., AFFTC TR-60-19, April 1960

7. McAdams, W. H., "Heat Transmission," 3rd Edition; McGraw Hill Book Co., 1954.

8. Johnson, V. J., "A Compendium of the Properties of Materials at Low Temperature (Phase 1)" Part II, WADD Tech. Report 60-56; NBS CEL, October 1960.

9. Johnson, V. J., "A Compendium of the Properties of Materials at Low Temperatures (Phase 1)" Part I, WADD Tech. Report 60-56; NBS CEL, October 1960.

10. Cryogenic Materials Data Handbook; Supplement No. 6; Fourteenth Progress Report; PB 171809-6; Air Force Materials Lab; Wright-Patterson Air Force Base, December 1960.

11. Klainlogel, A.; "Rigid Frame Formulas," 2nd Edition; Ungar Publishing Co., 1964.

12. Peery, D. J.; "Aircraft Structures," McGraw Hill Book Co., 1949.

13. Roark, R. J., "Formulas for Stress and Strain," 3rd Edition; McGraw Hill Book Co., 1954.

14. Seader, J. S.; Miller, W. S.; Kalvinskas, L. A.; "Boiling Heat Transfer for Cryogenics," Final Report, Rocketdyne R-5598; Contract No. NAS8-5337; May 1964.

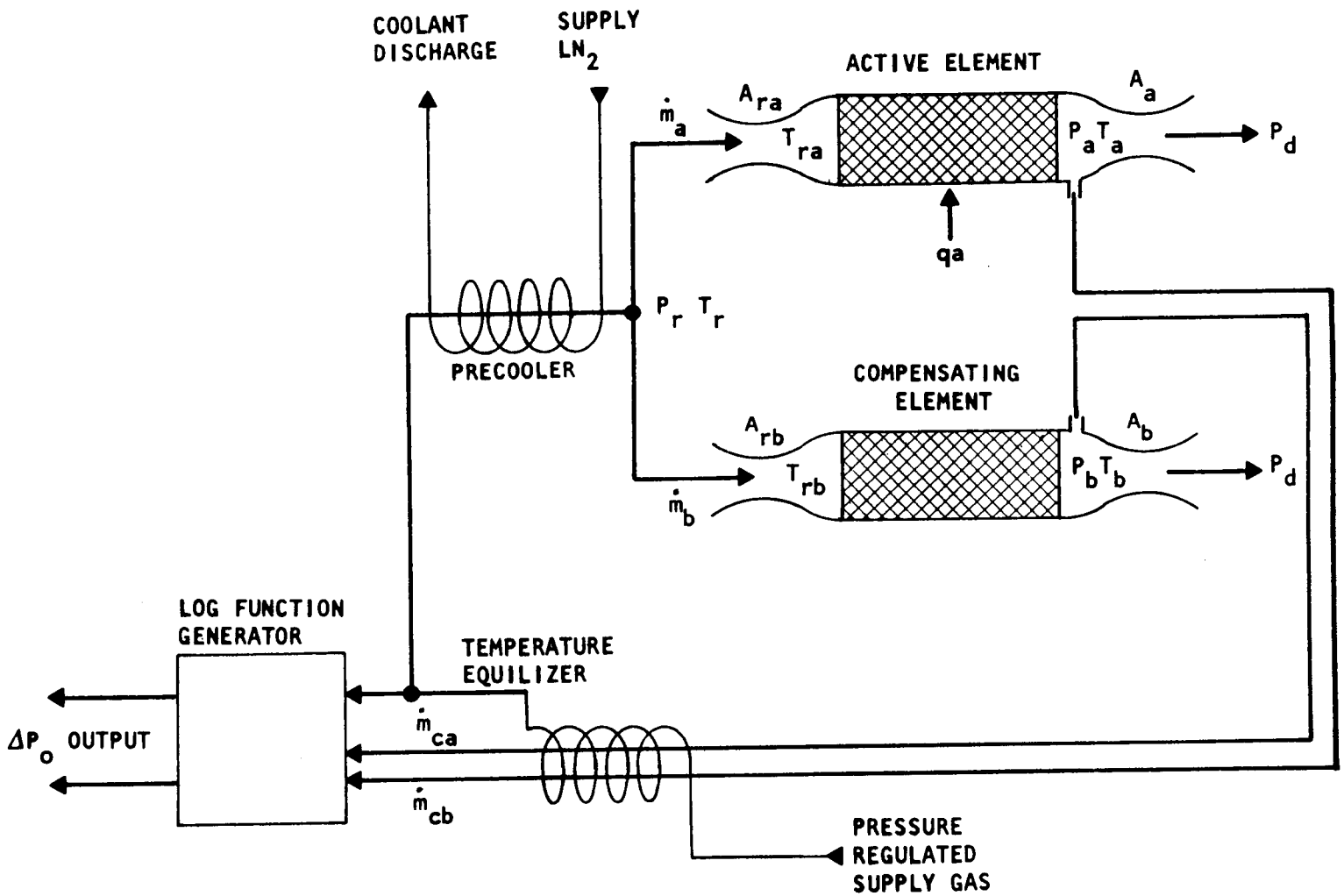

Figure 1. Flux Detector Schematic

FIGURE 2

FLUX DENSITY = ENTHALPY

CHANGE RATIO AS A FUNCTION OF TEMPERATURE RANGE

$T_H(max) = 125$ psia

$T_H(min) = 110$ °K

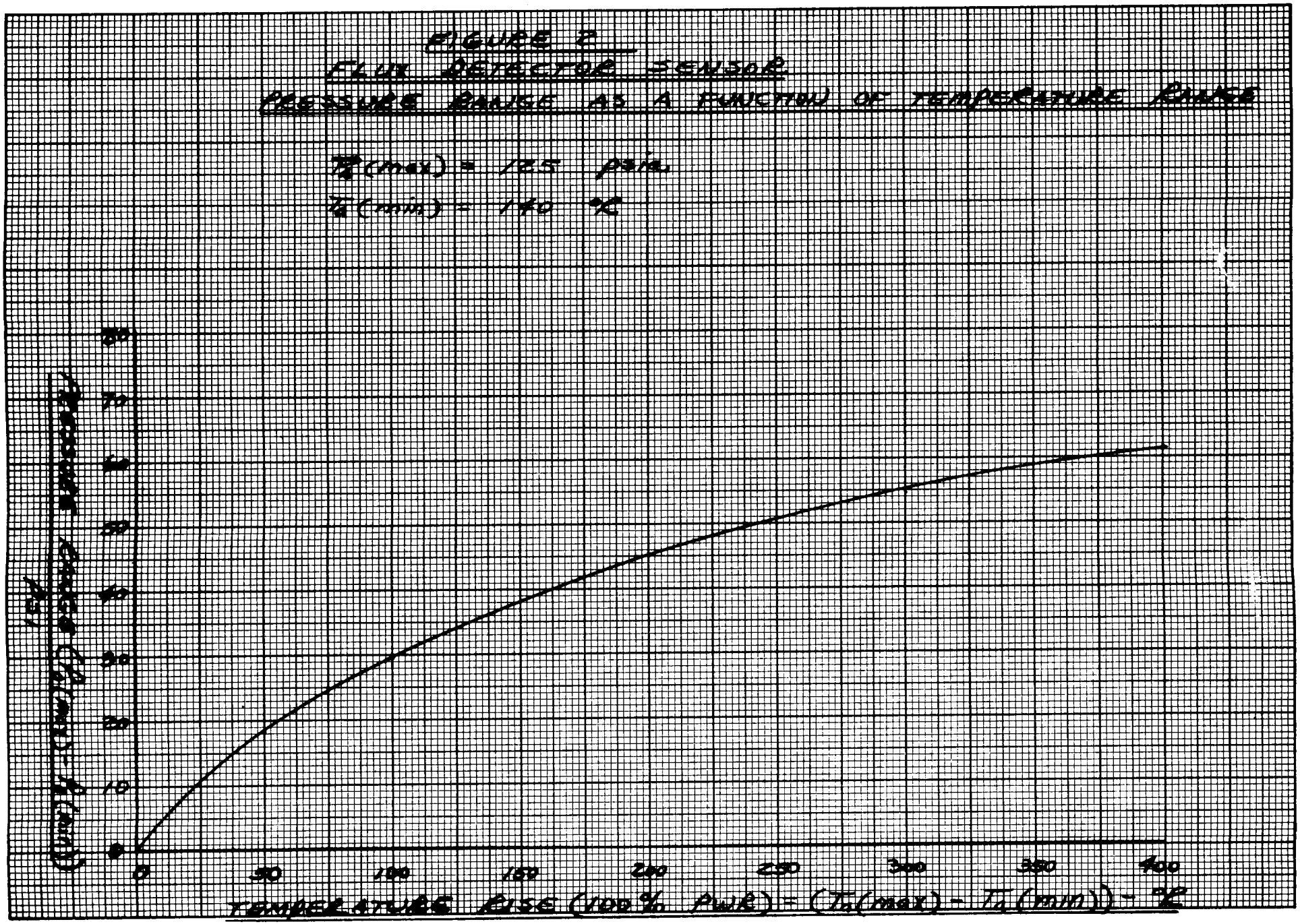

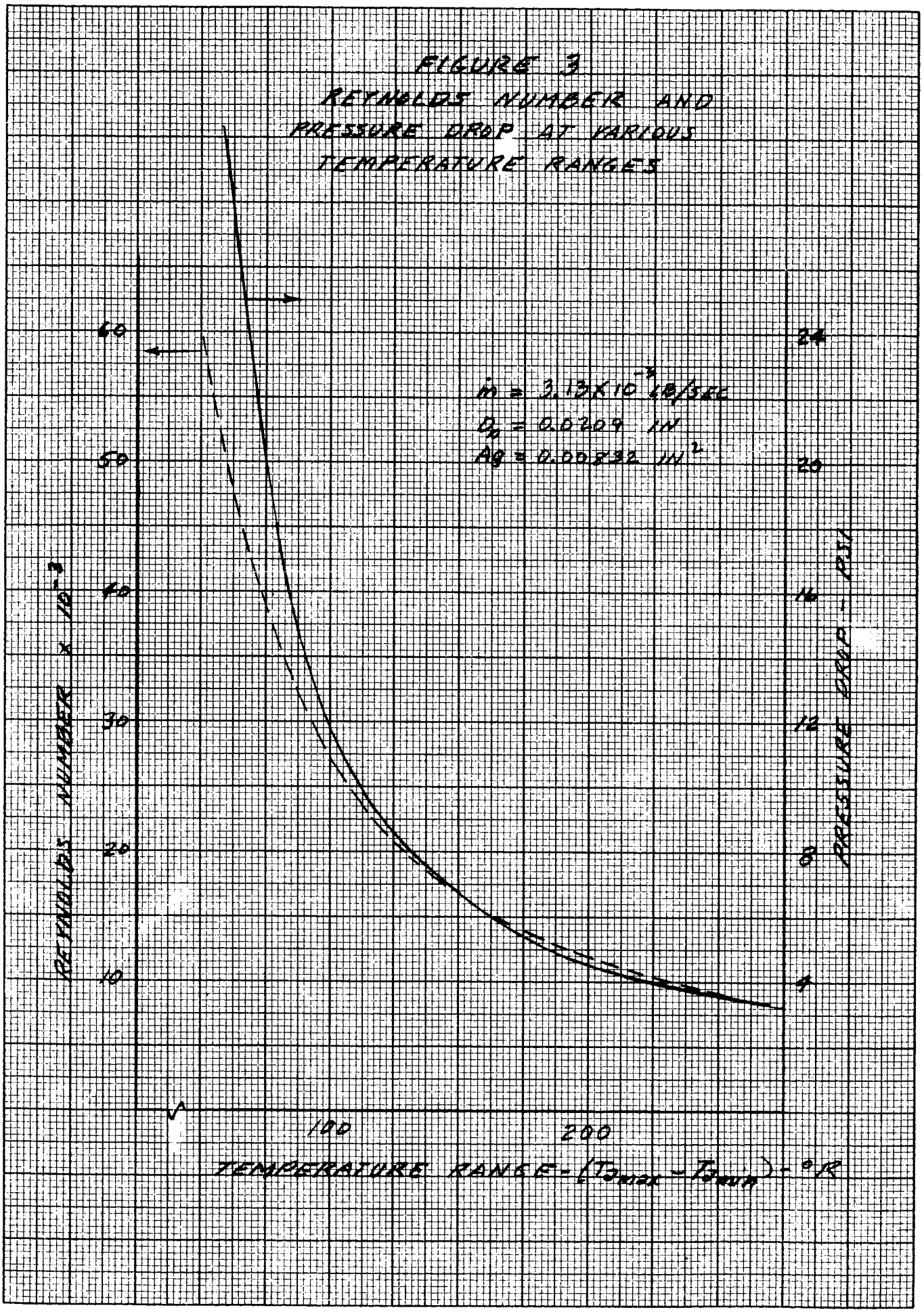

FOLDOUT FRAME

ORIFICE CALIBRATION TEST RESULTS

TEST FLUID: DRY HELIUM
UPSTREAM PRESSURE VARIATION: 64 - 290 PSIA
UPSTREAM TEMPERATURE VARIATION: 144 - 530°R
ORIFICE REYNOLDS' NO. VARIATION:
$.5 \times 10^6 - 3.2 \times 10^6$

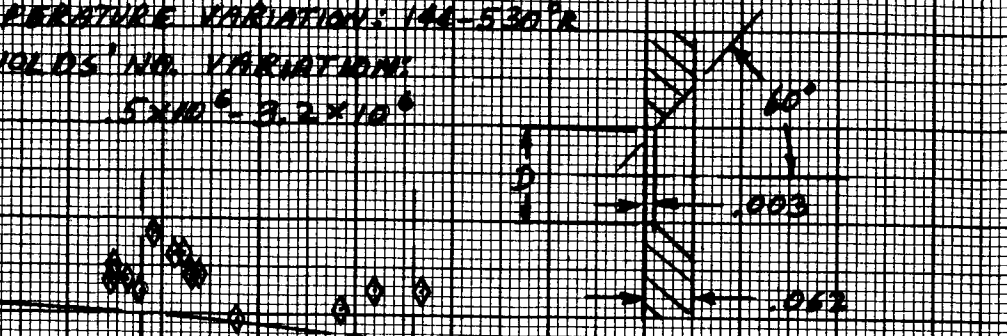

ORIFICE CONFIGURATION

DATA FROM
"CRITICAL FLOW THROUGH SHARP-EDGED ORIFICES"
J. A. PERRY, 1948

SYMBOL	ORIFICE I.D. (D)IN. IN.
◇	0.05870
○	0.03450

TEST CONFIGURATION

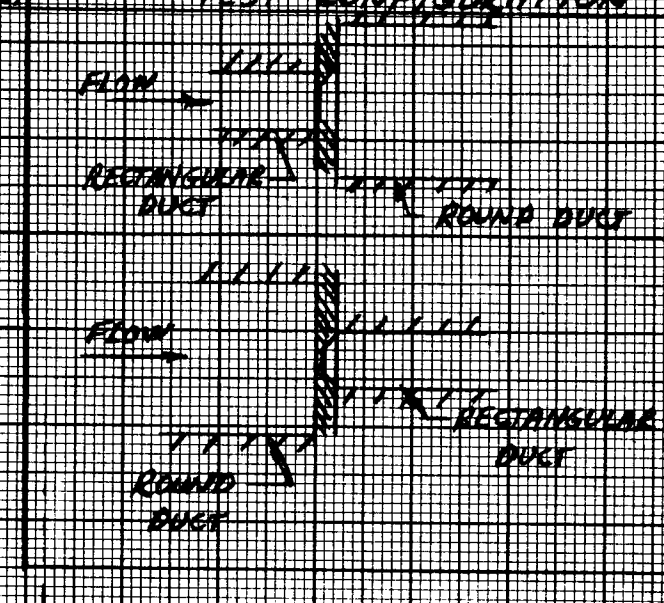

DISCHARGE COEFFICIENT, C_d

DISCHARGE ORIFICE OPERATING RANGE

INLET ORIFICE OPERATING RANGE

$\left(\frac{P_2}{P_1}\right)_{CRIT} = .887$

PRESSURE RATIO $\sim \frac{P_{2\,STATIC}}{P_{1\,TOTAL}}$

.9
.8
.7
0
.05
.1
.15
.20
.25
.30
.35
.40
.45
.50
.55
.60
.65
.70

RS 10/5/66

FOLDOUT FRAME 1

FOLDOUT FRAME 2

FIGURE 4

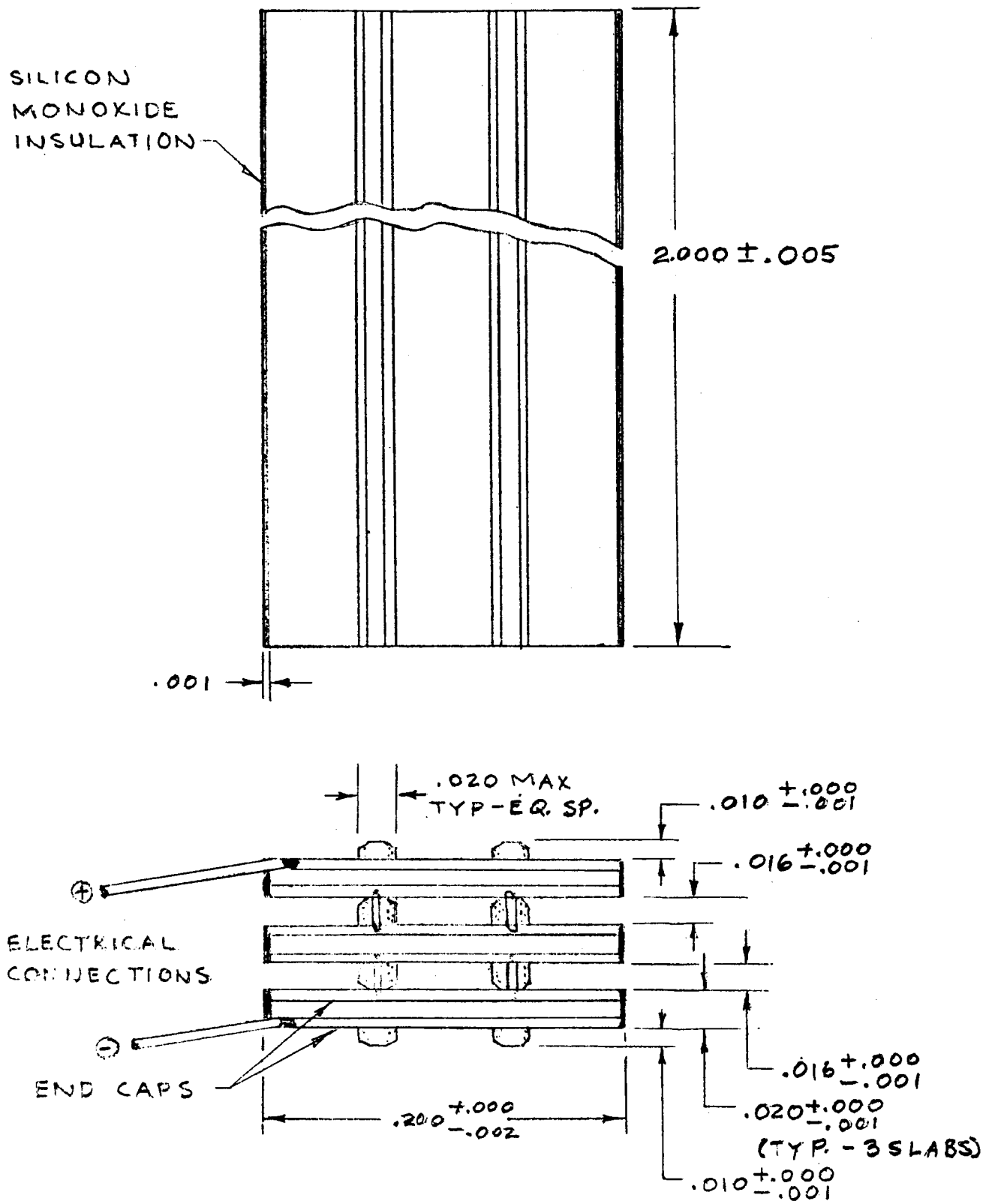

Figure 5. Heater Slab Typical Configuration

FIGURE 6

HEATER TEMPERATURE DISTRIBUTION

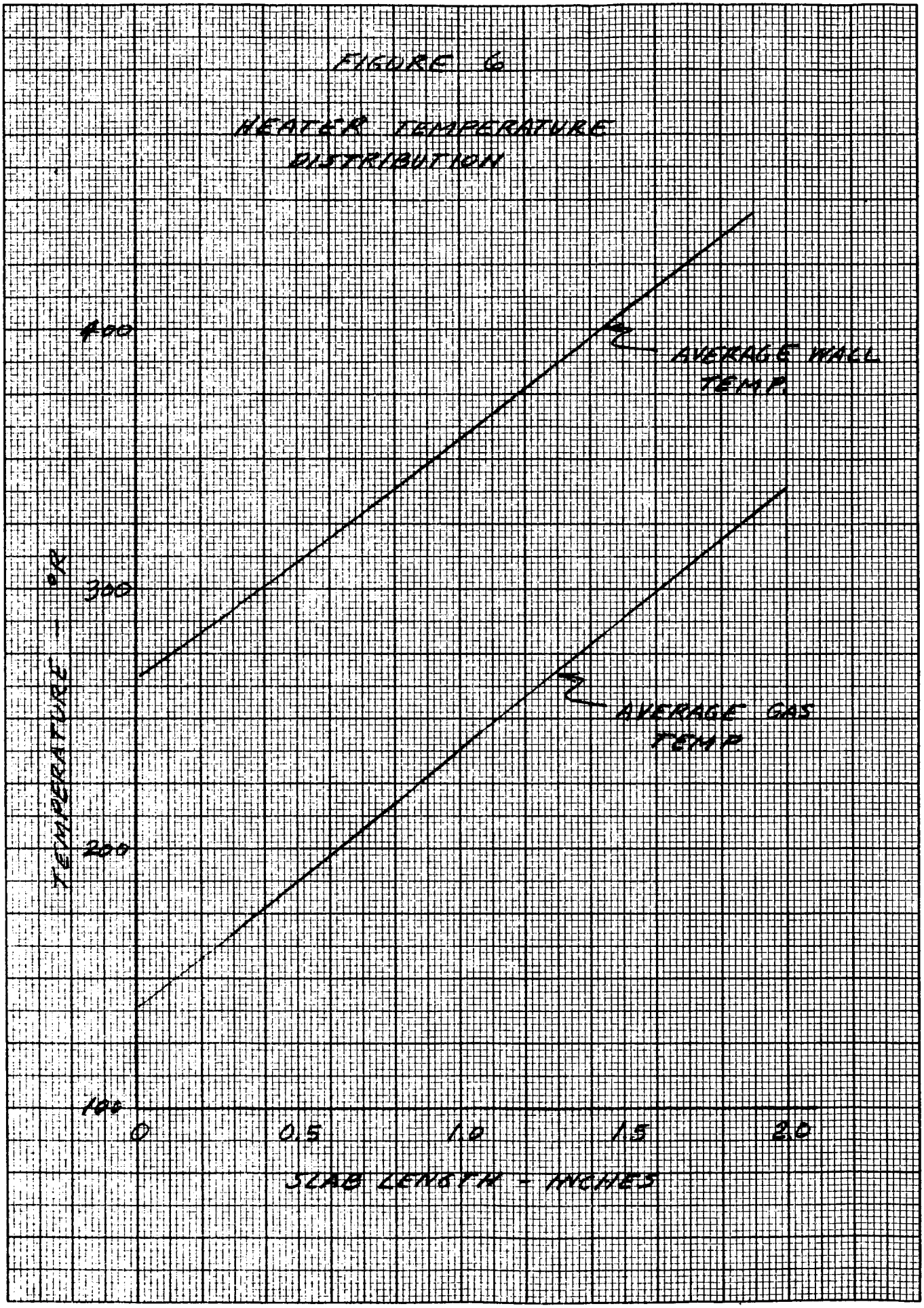

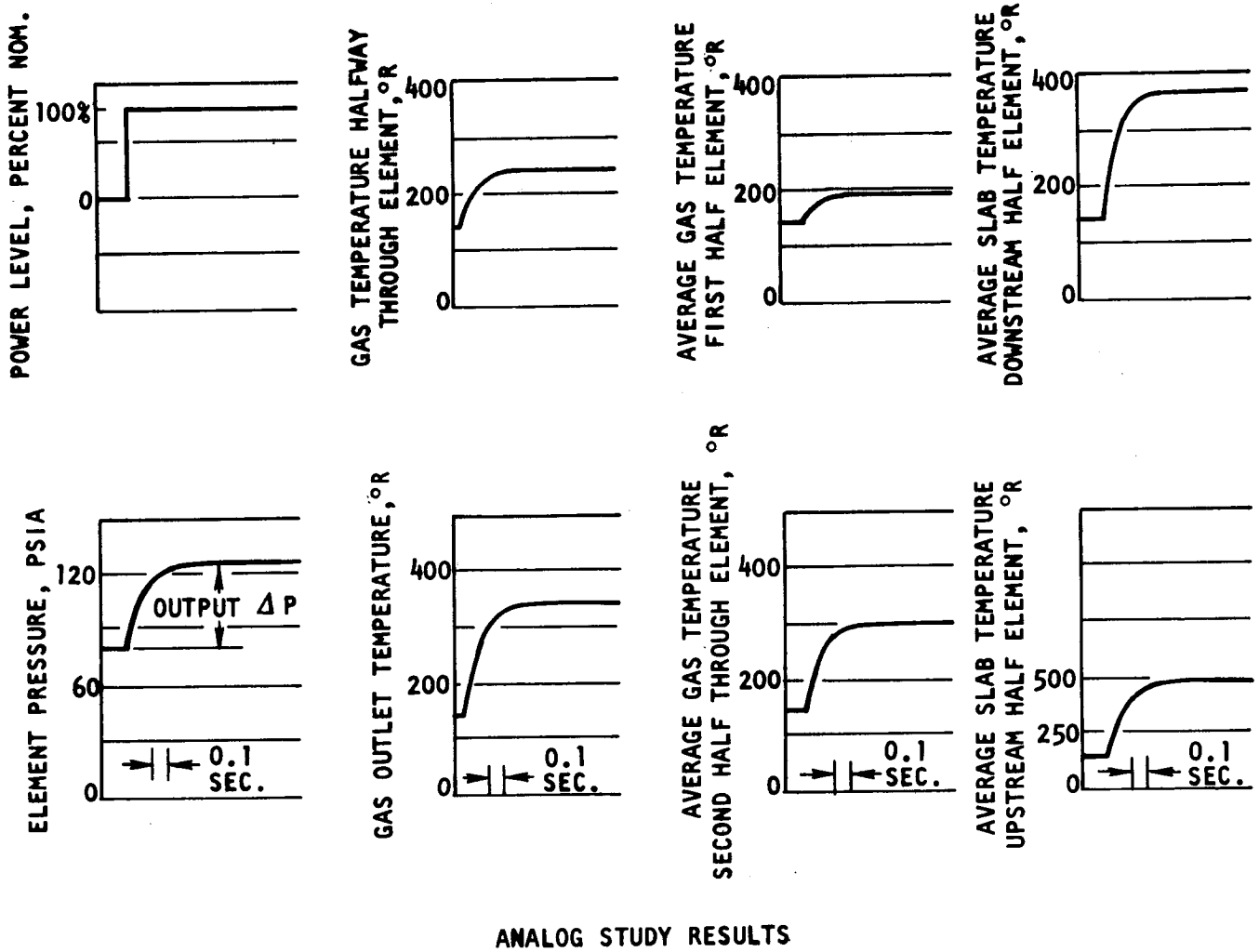

Figure 7. Analog Study Results Detector Response to 100 Percent Step in Power (Nominal Conditions)

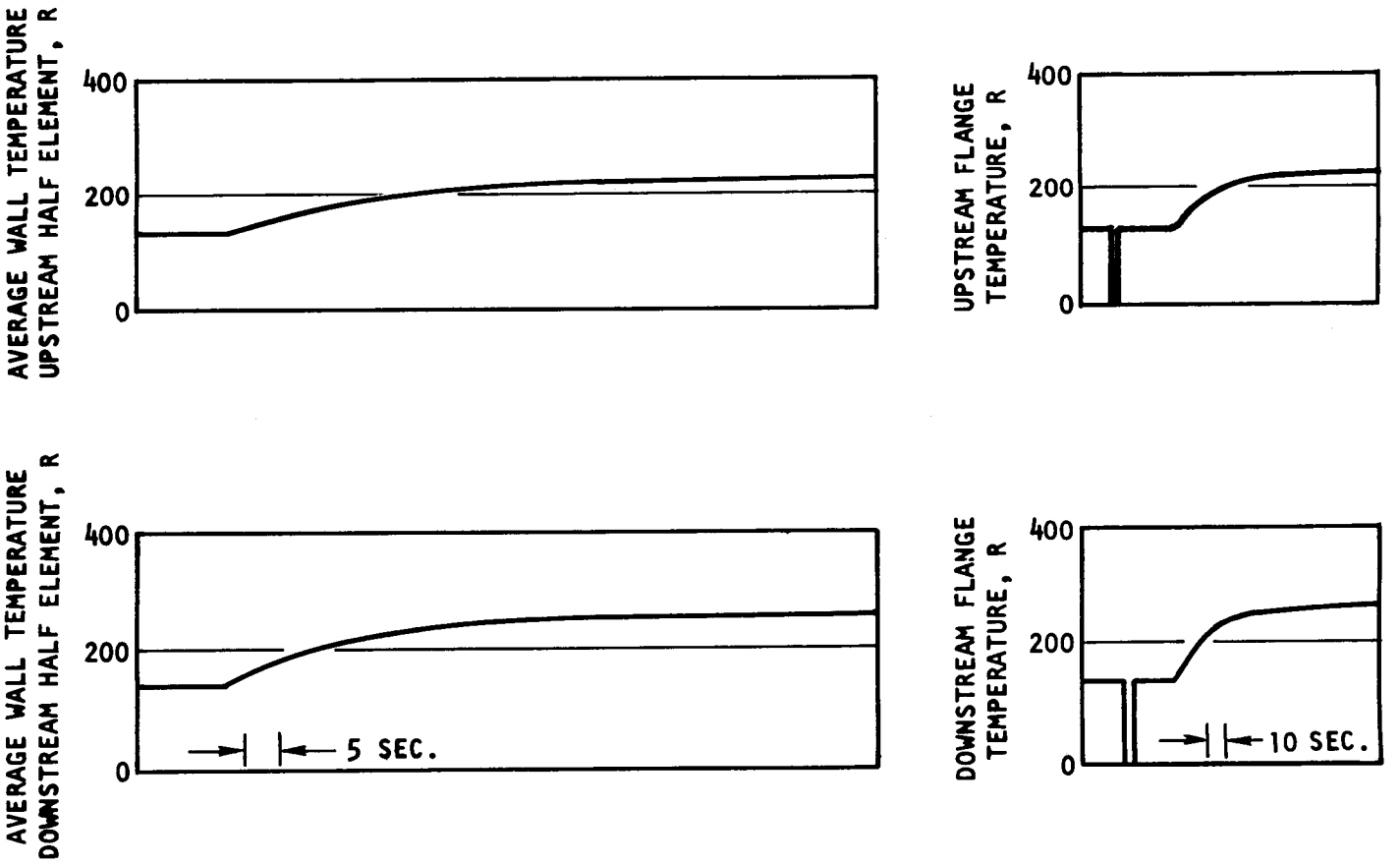

Figure 8. Analog Study Results Detector Response to 100 Percent Step in Power (Nominal Conditions)

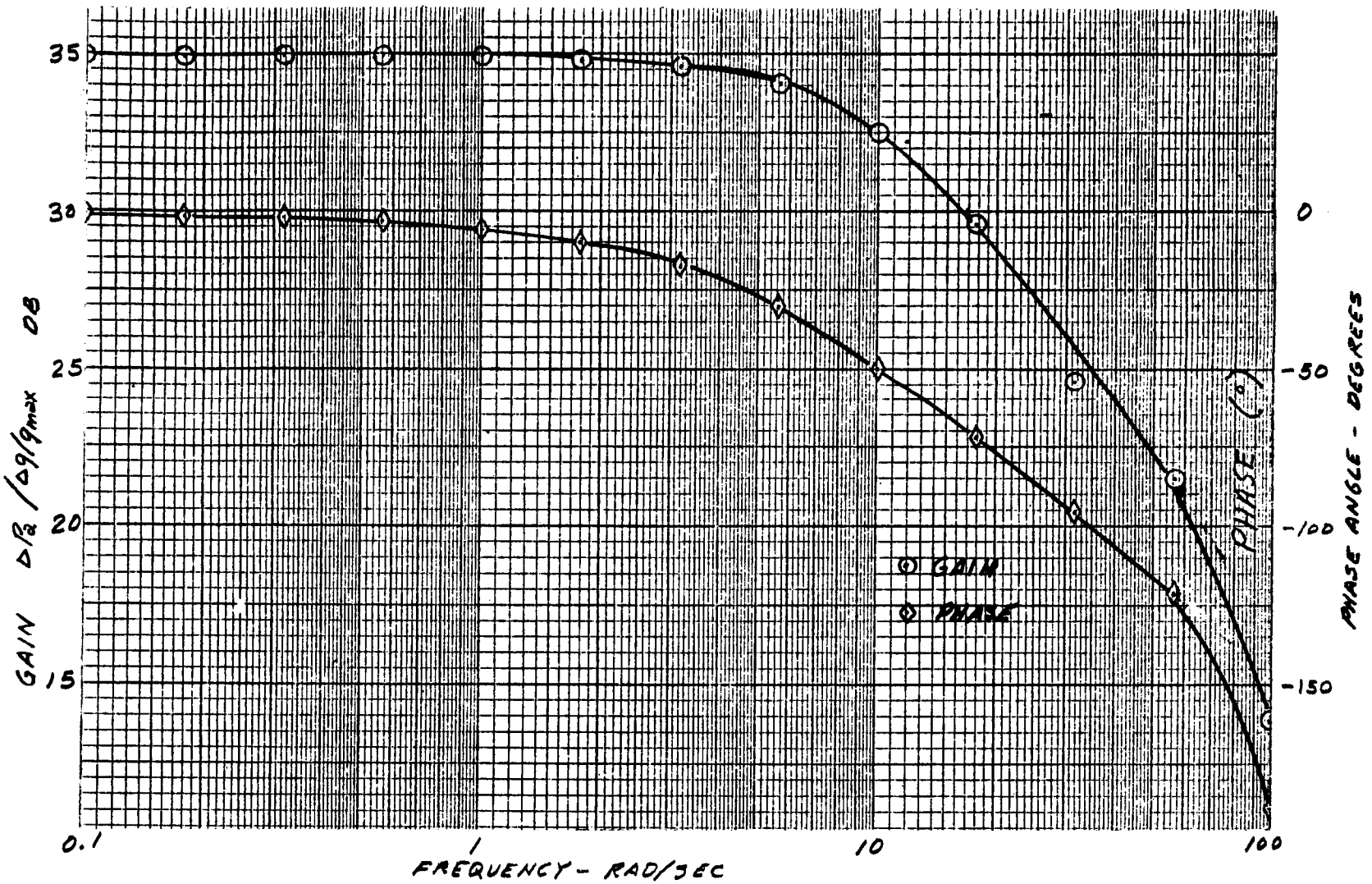

Figure 9. Analog Study Results Flux Detector Frequency Response (0 Power, Nominal Conditions)

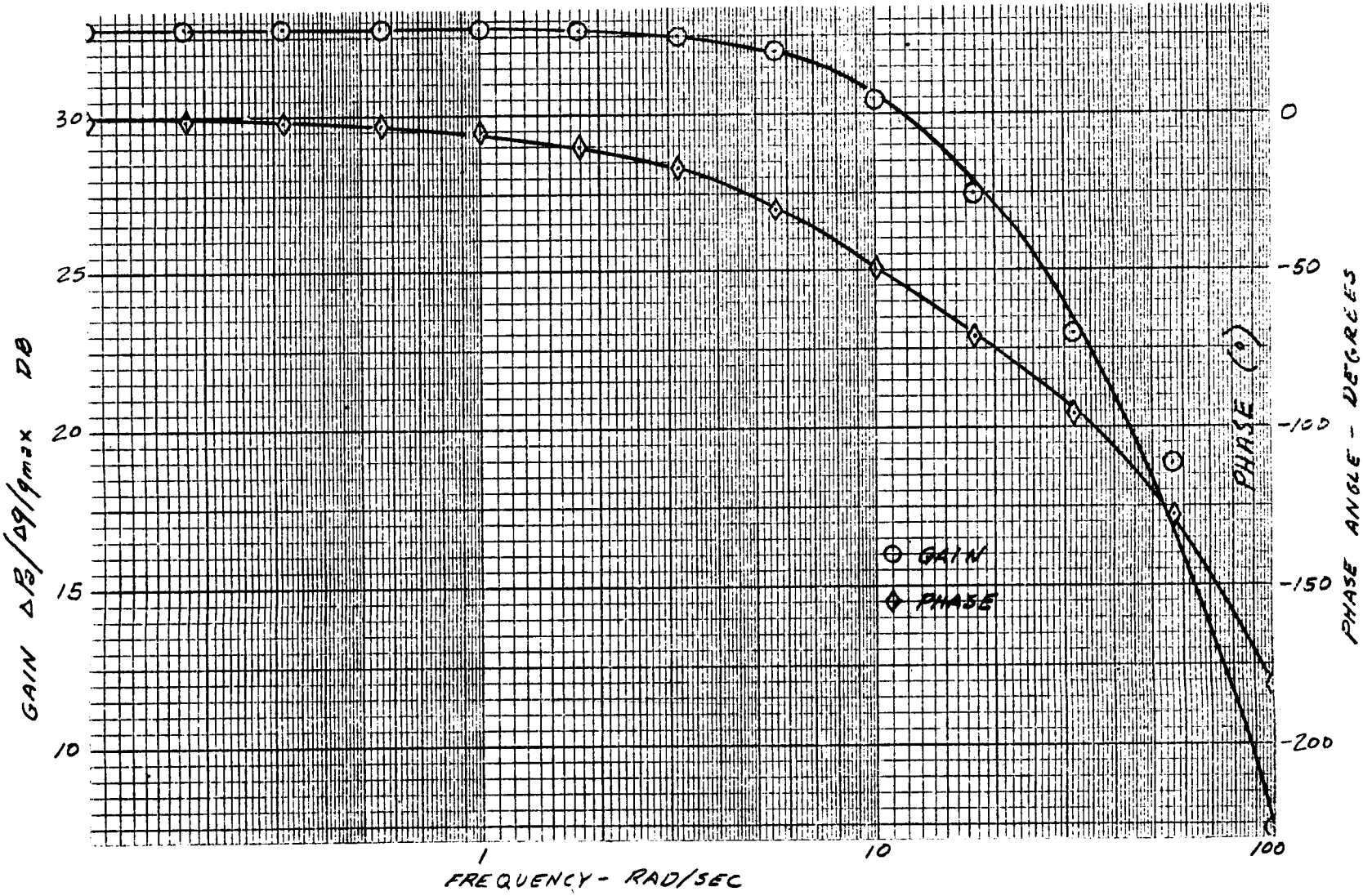

Figure 10. Analog Study Results Flux Detector Frequency Response (50 percent Power, Nominal Conditions)

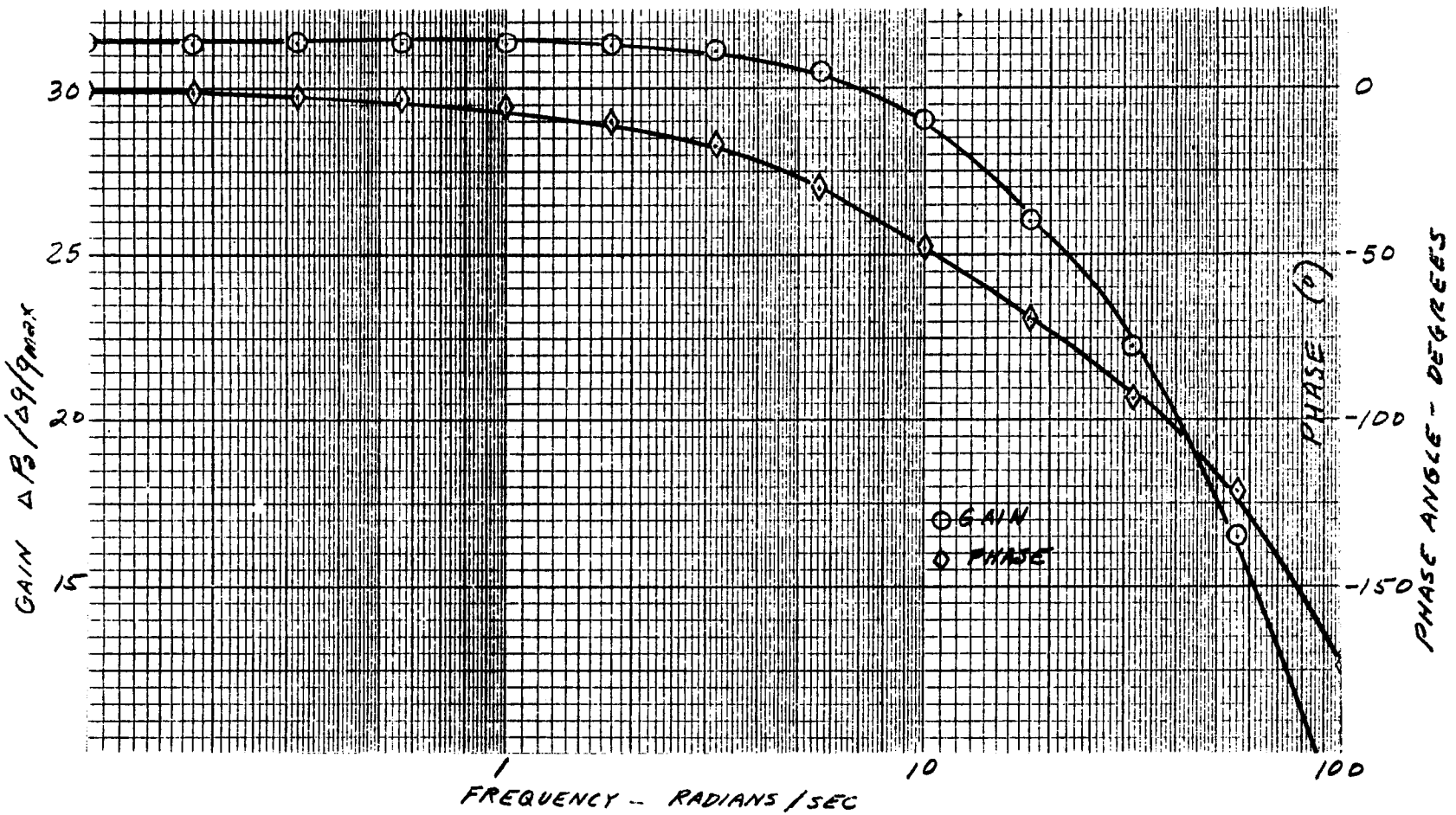

Figure 11. Analog Study Results Flux Detector Frequency Response (100 percent Power, Nominal Conditions)

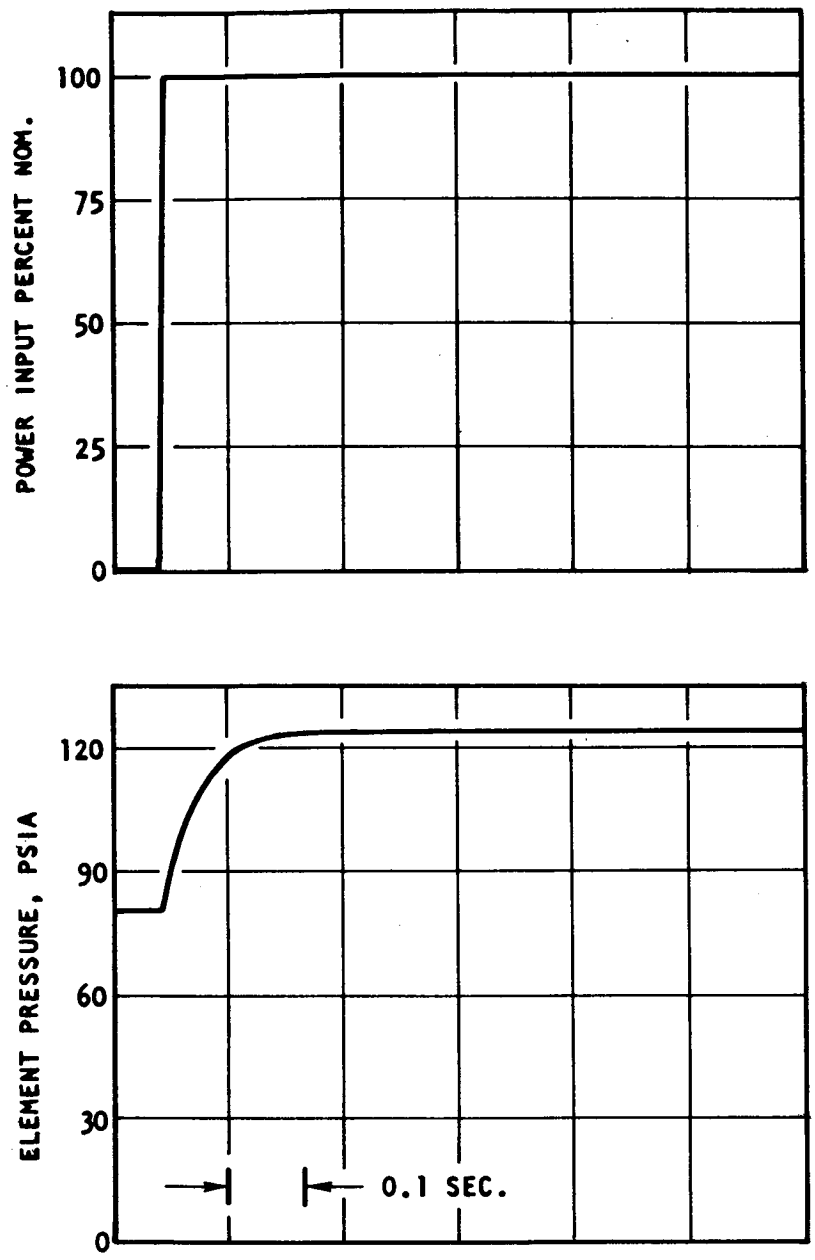

Figure 12. Detector Response to 100 percent Step in Power (Film Coefficients = 4 x Nominal)

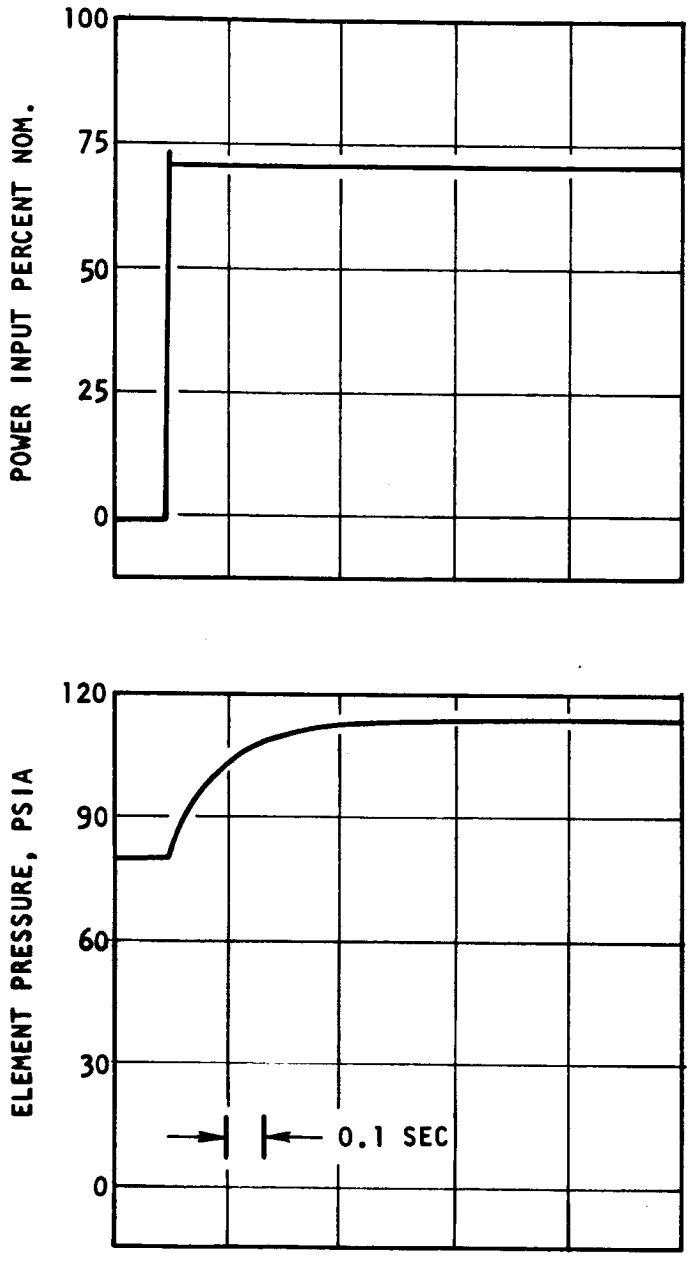

Figure 13. Detector Response to 100 Percent Step in Power (Film Coefficients = 1/2 x Normal)

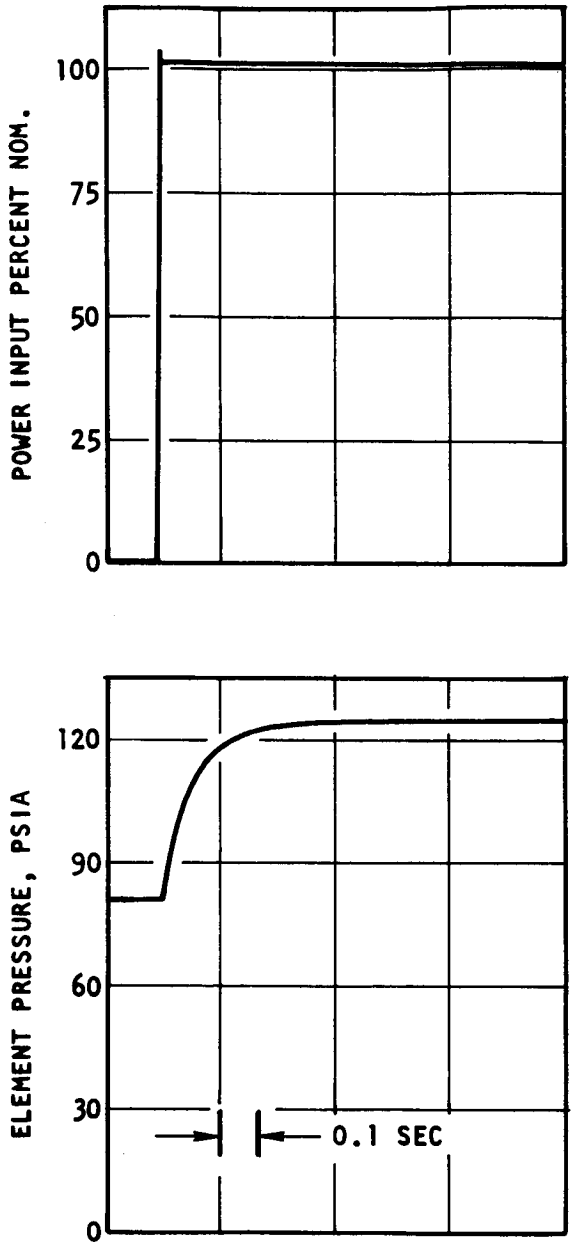

Figure 14. Detector Response to 100 Percent Step in Power (Gas to Wall and Gas to Flange Heat Transfer Coefficients = 4 x Nominal)

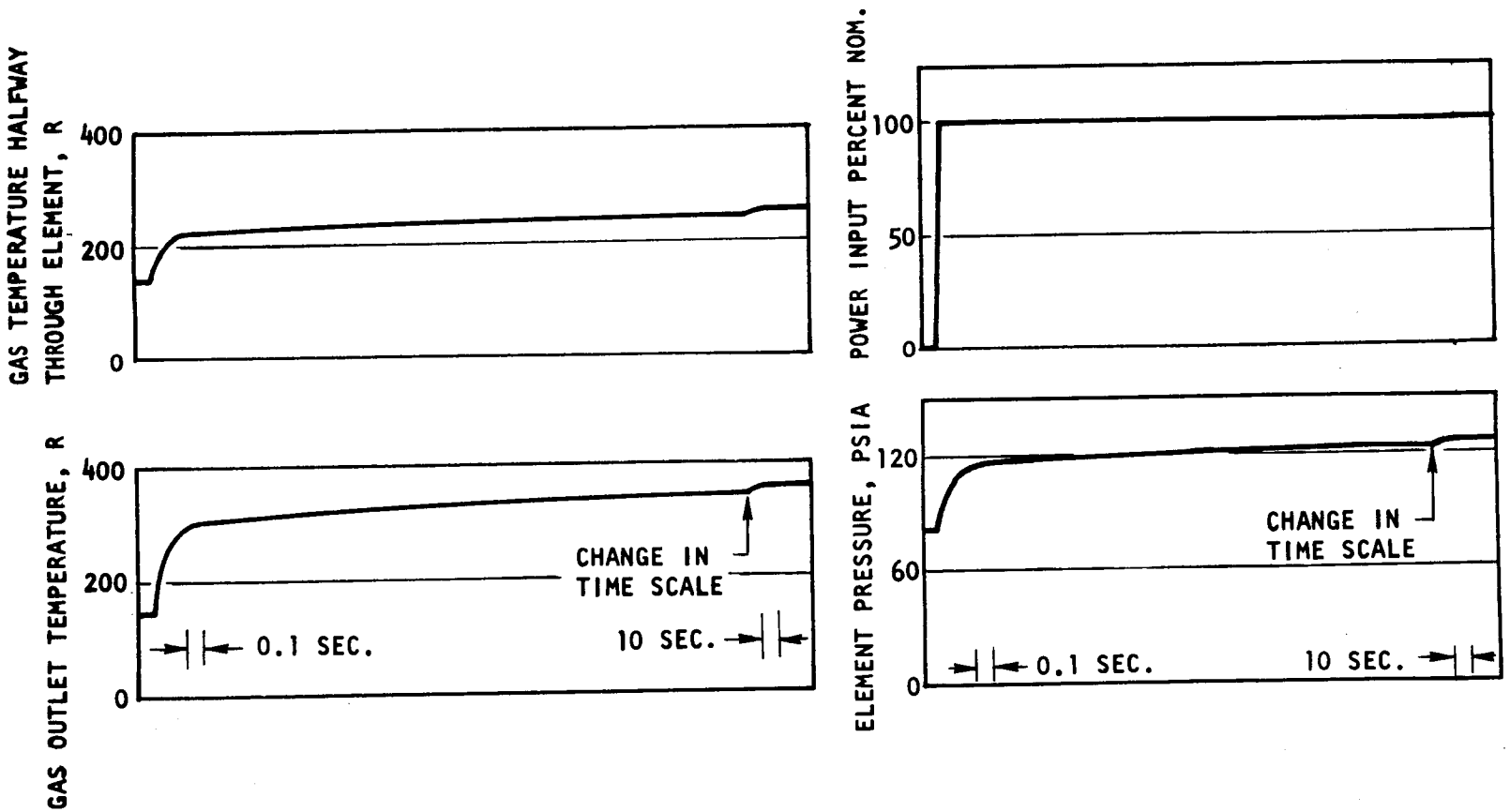

Figure 15. Analog Study Results Detector Response to 100 Percent Step in Power (Large Heater-To-Wall)

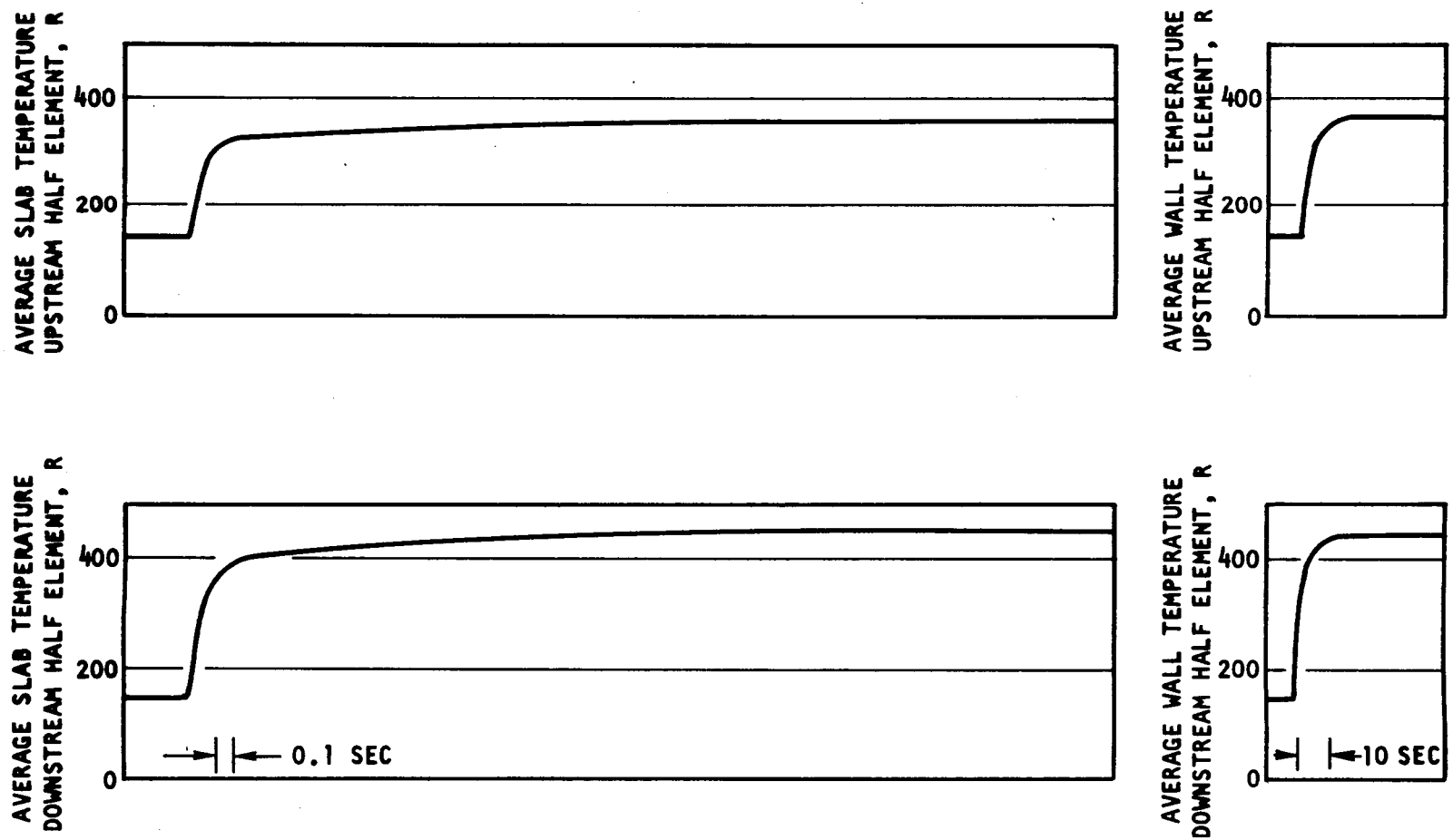

Figure 16. Lumped Heater Element Temperatures Detector Response to 100 Percent Step in Power (Larger Heater-to-Wall Contact Conductance)

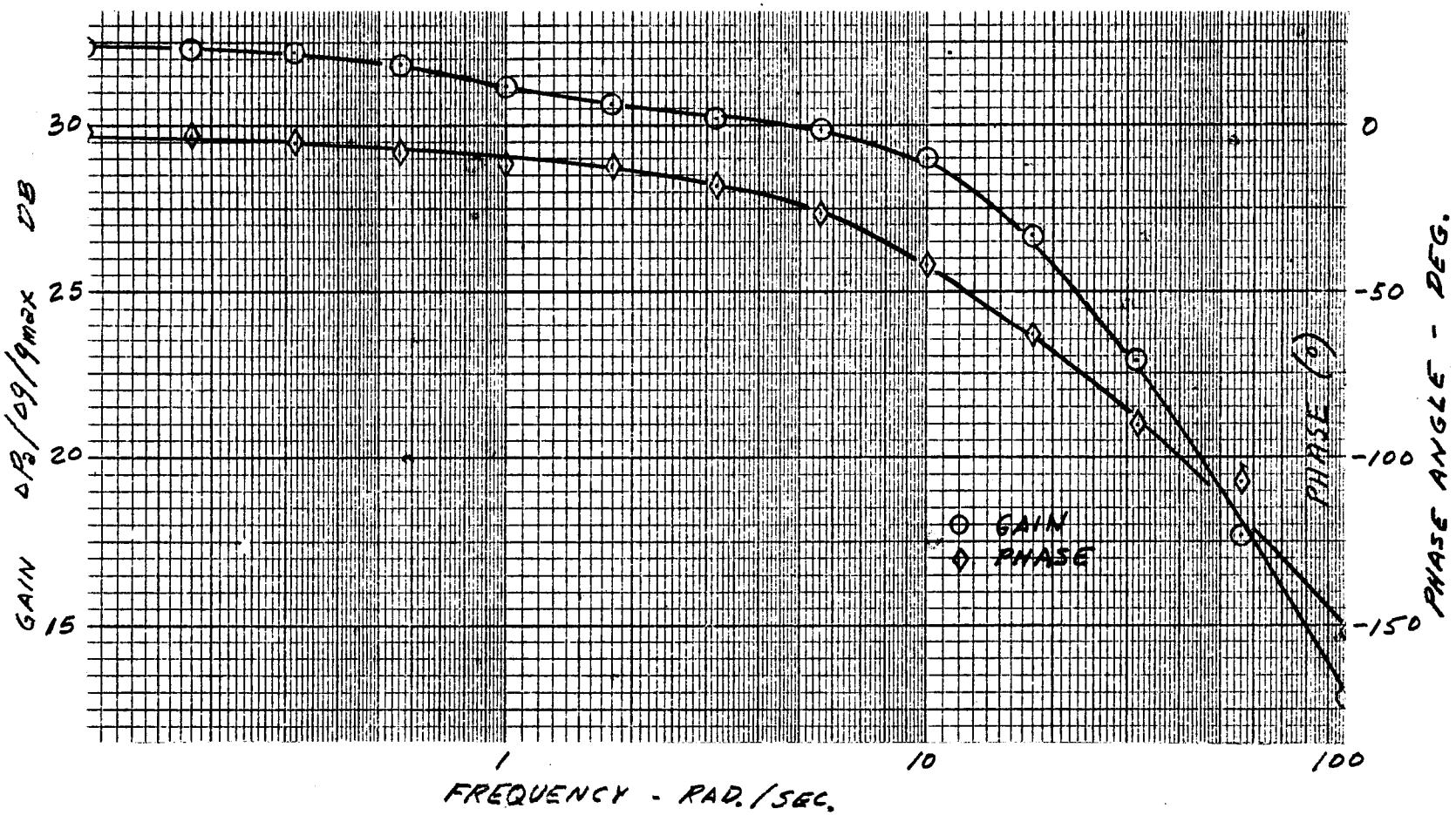

Figure 17. Analog Study Results Flux Detector Frequency Response (50 Percent Power Large Contact Conductance Between Heater and Wall)

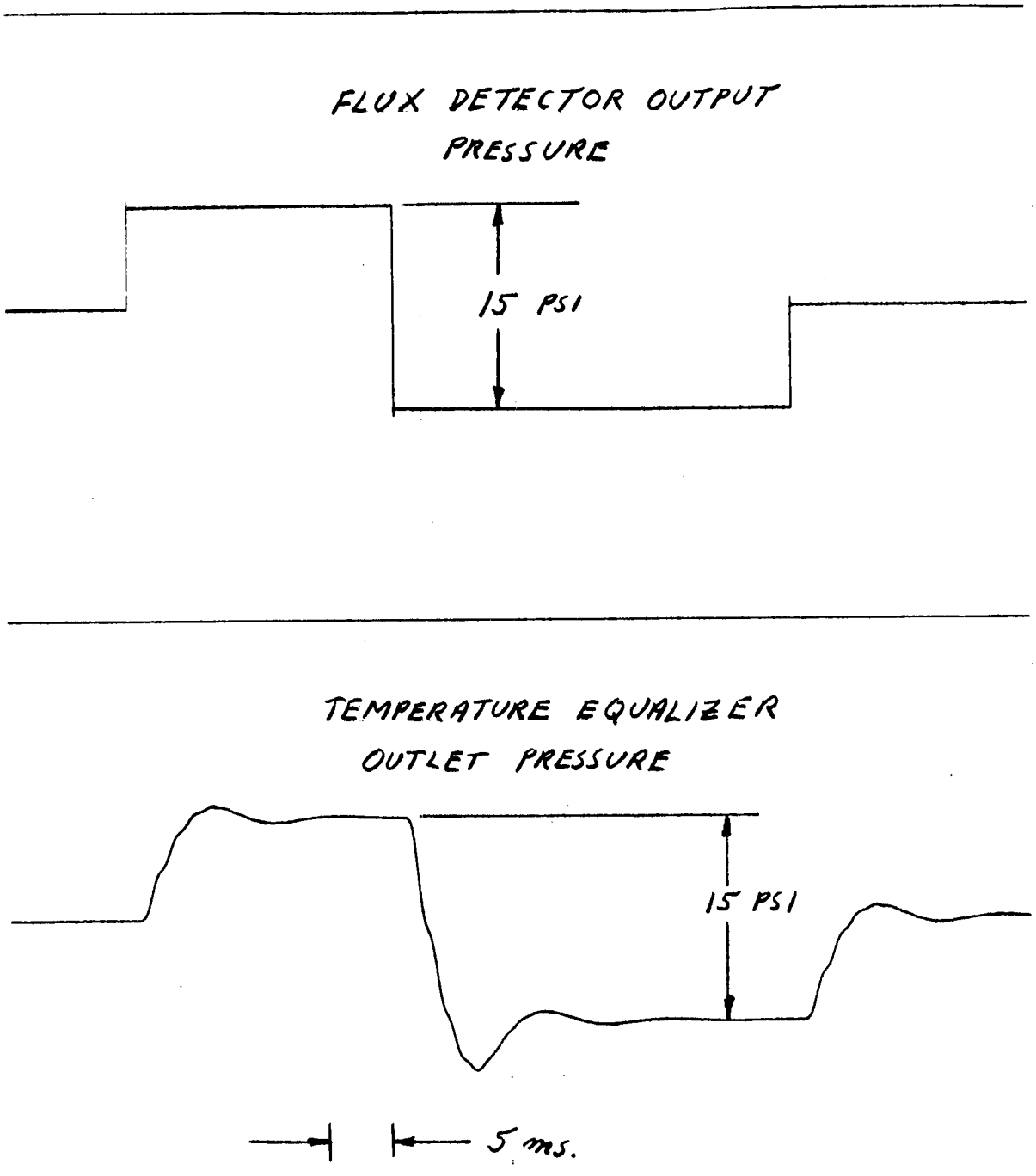

ANALOG RESULTS

Figure 18. Typical Temperature Equalizer Pressure Response

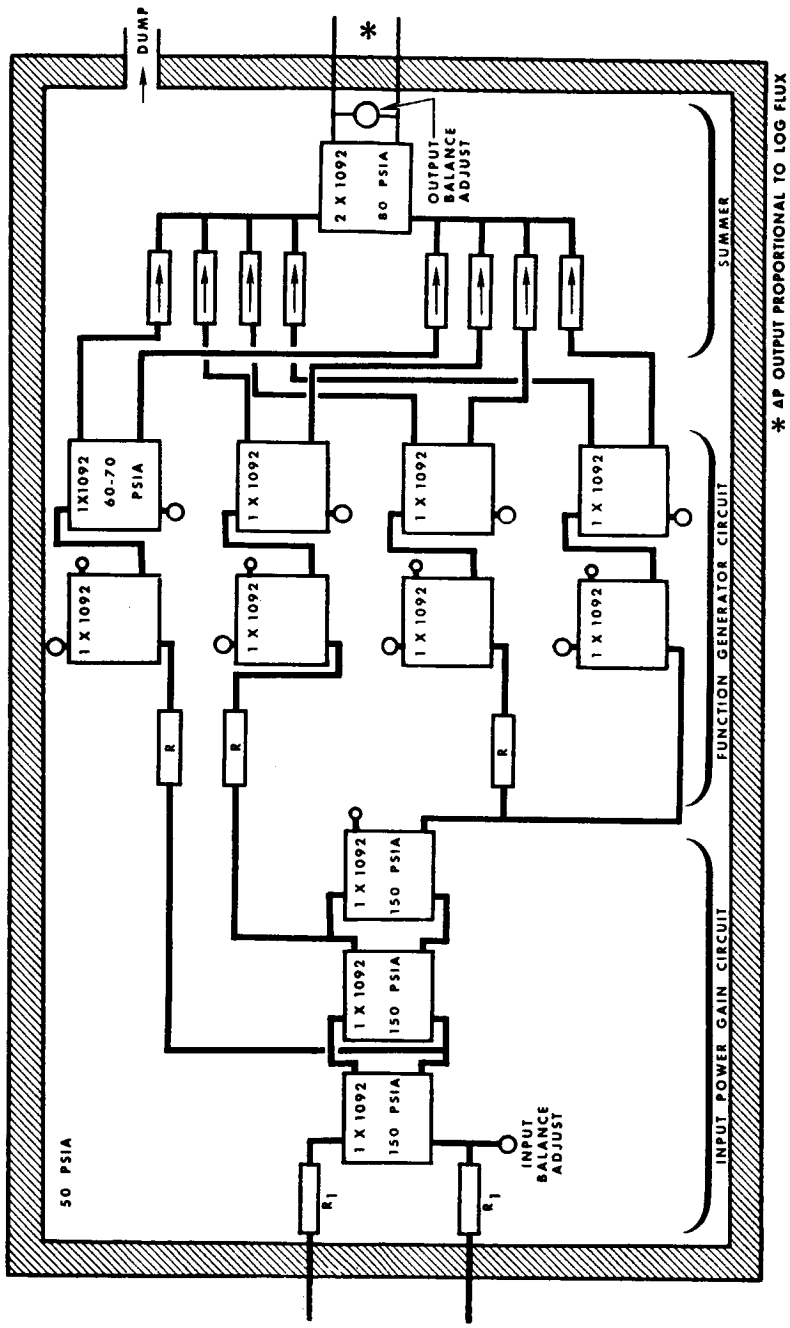

Figure 19. Schematic Log Function Generator Circuitry

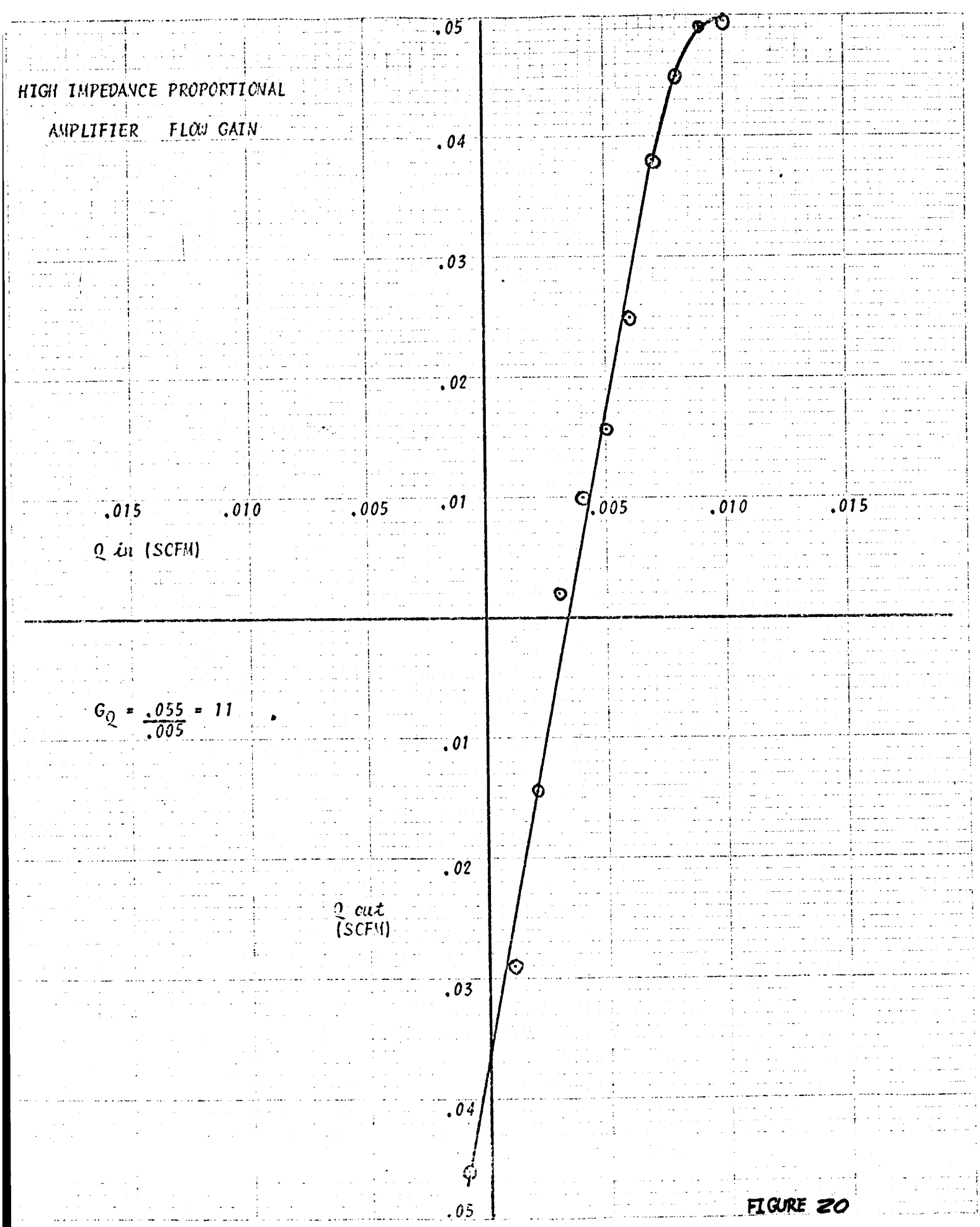
HIGH IMPEDANCE PROPORTIONAL
AMPLIFIER FLOW GAIN
.05
.04
.03
.02
.01
.015
.010
.005
.005
.010
.015
Q in (SCFM)
$G_Q = \frac{.055}{.005} = 11$
.01
.02
.03
.04
.05
Q out (SCFM)

FIGURE 20

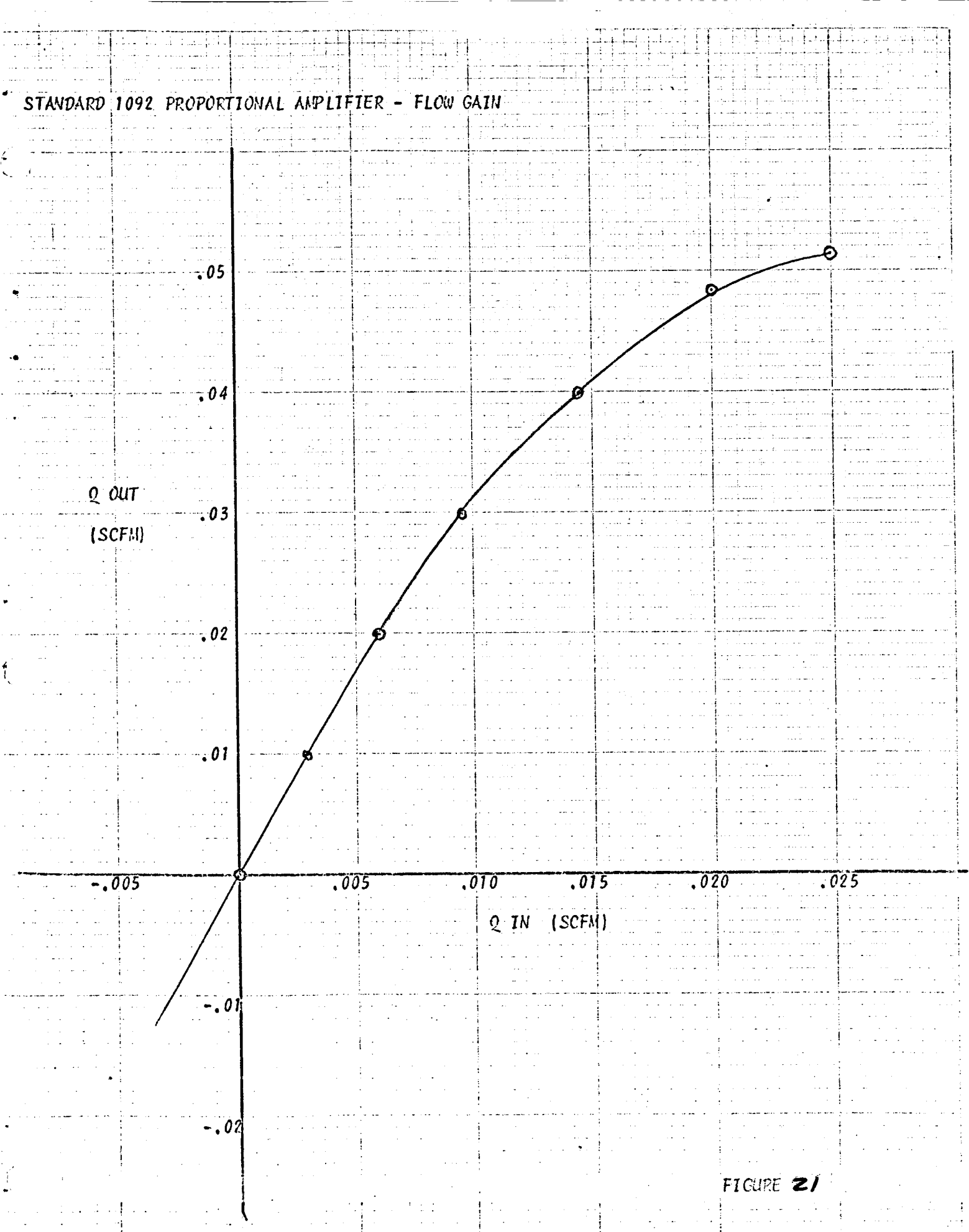
STANDARD 1092 PROPORTIONAL AMPLIFIER - FLOW GAIN
Q OUT
(SCFM)
.05
.04
.03
.02
.01
-.01
-.02
-.005
.005
.010
.015
.020
.025
Q IN (SCFM)

FIGURE 21

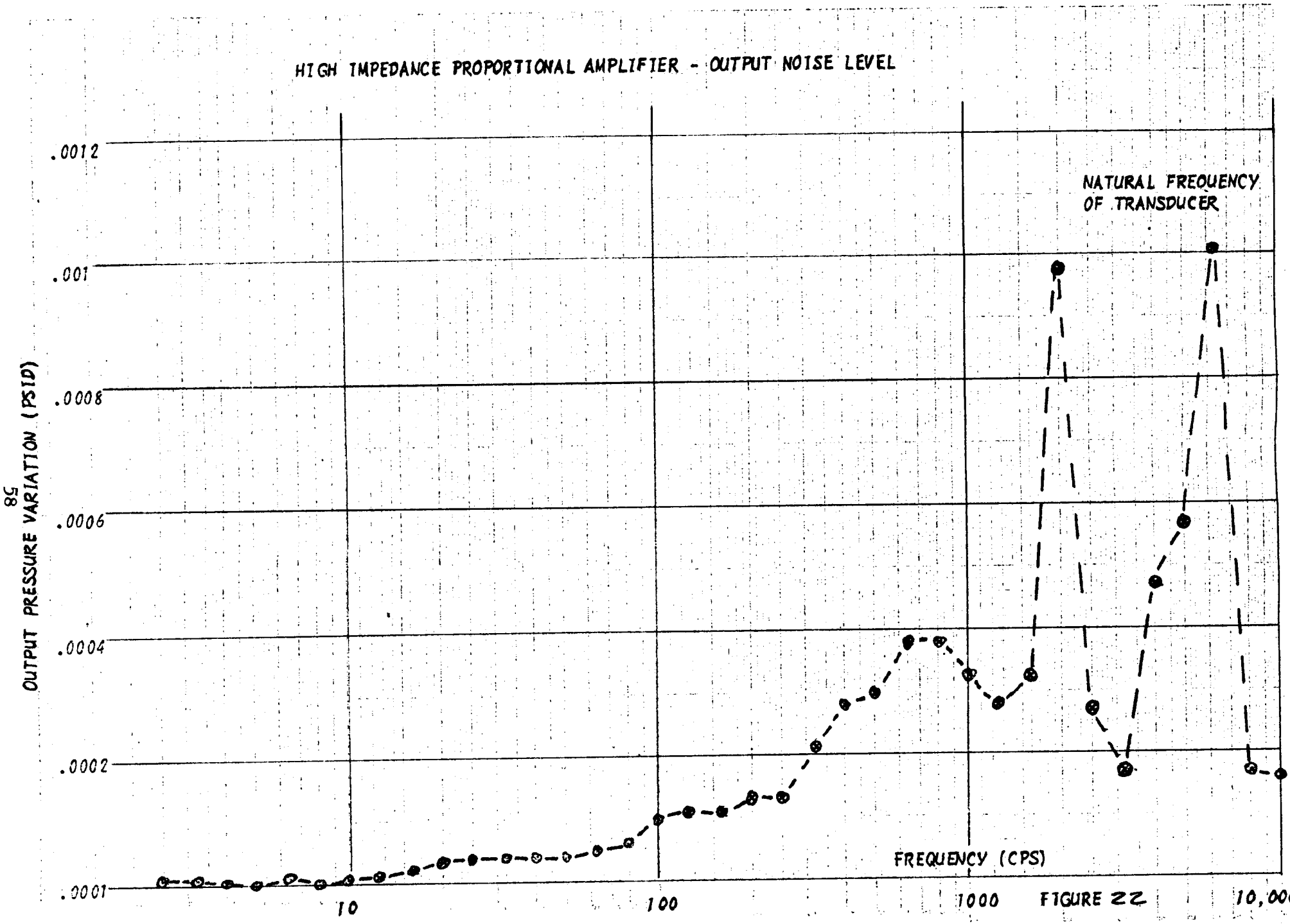
HIGH IMPEDANCE PROPORTIONAL AMPLIFIER - OUTPUT NOISE LEVEL
.0012
.001
.0008
.0006
.0004
.0002
.0001
OUTPUT PRESSURE VARIATION (PSID)
NATURAL FREQUENCY OF TRANSDUCER
FREQUENCY (CPS)
10
100
1000
10,000

FIGURE 22

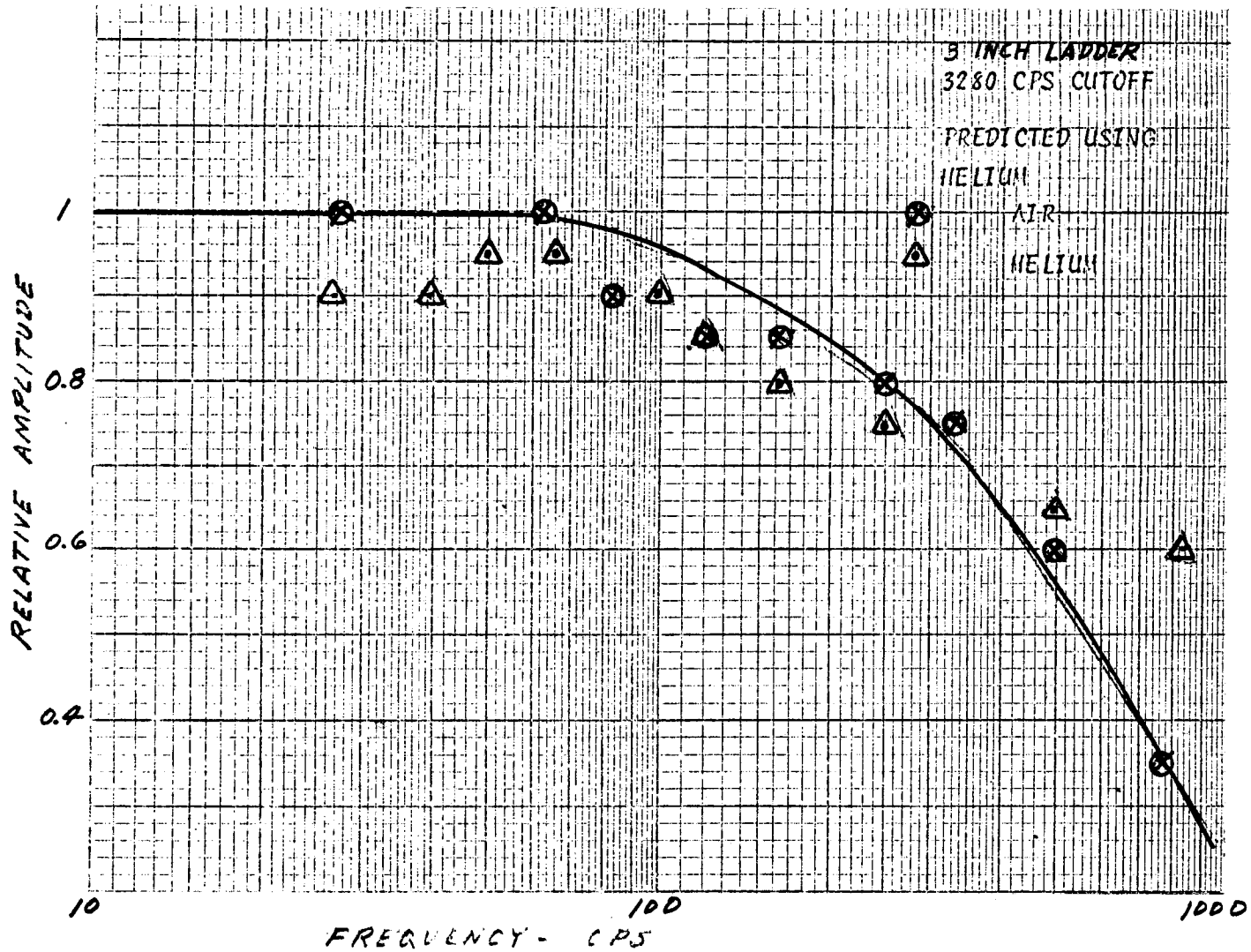

Figure 23. Ladder Filter Cutoff Response

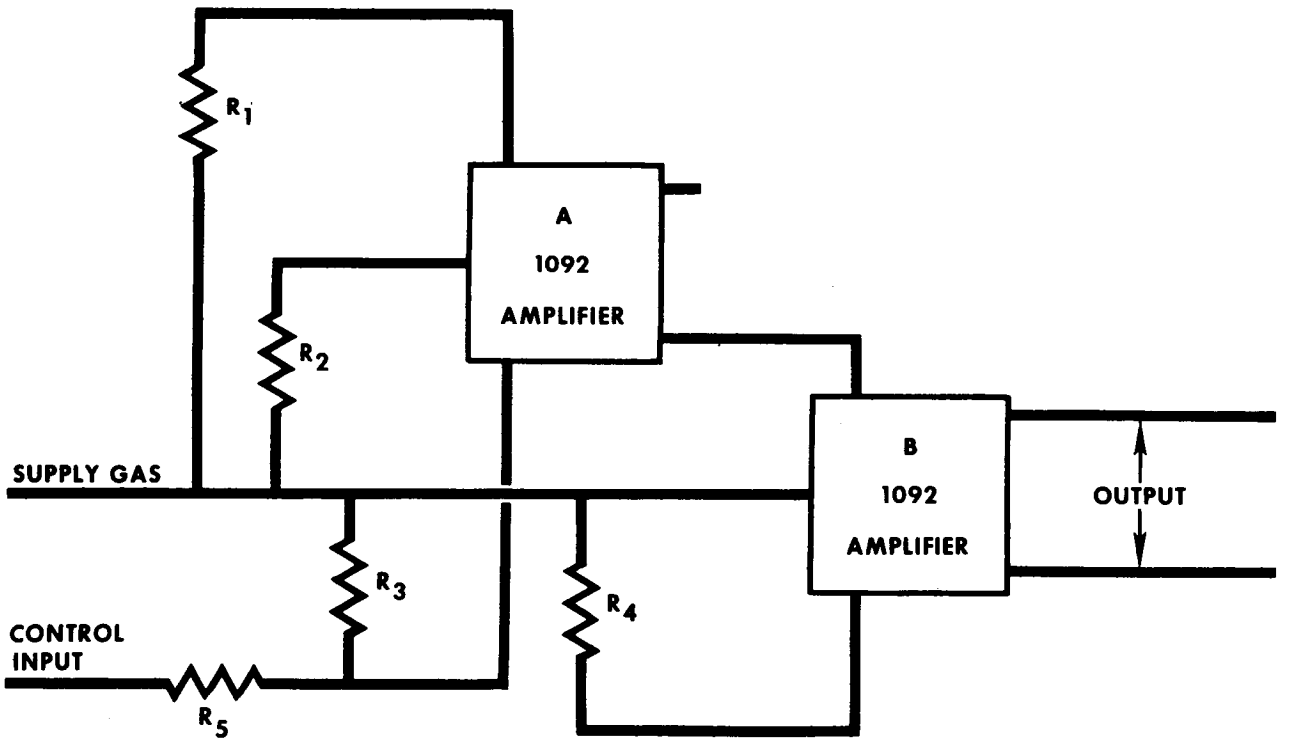

Figure 24. Function Generator Segment

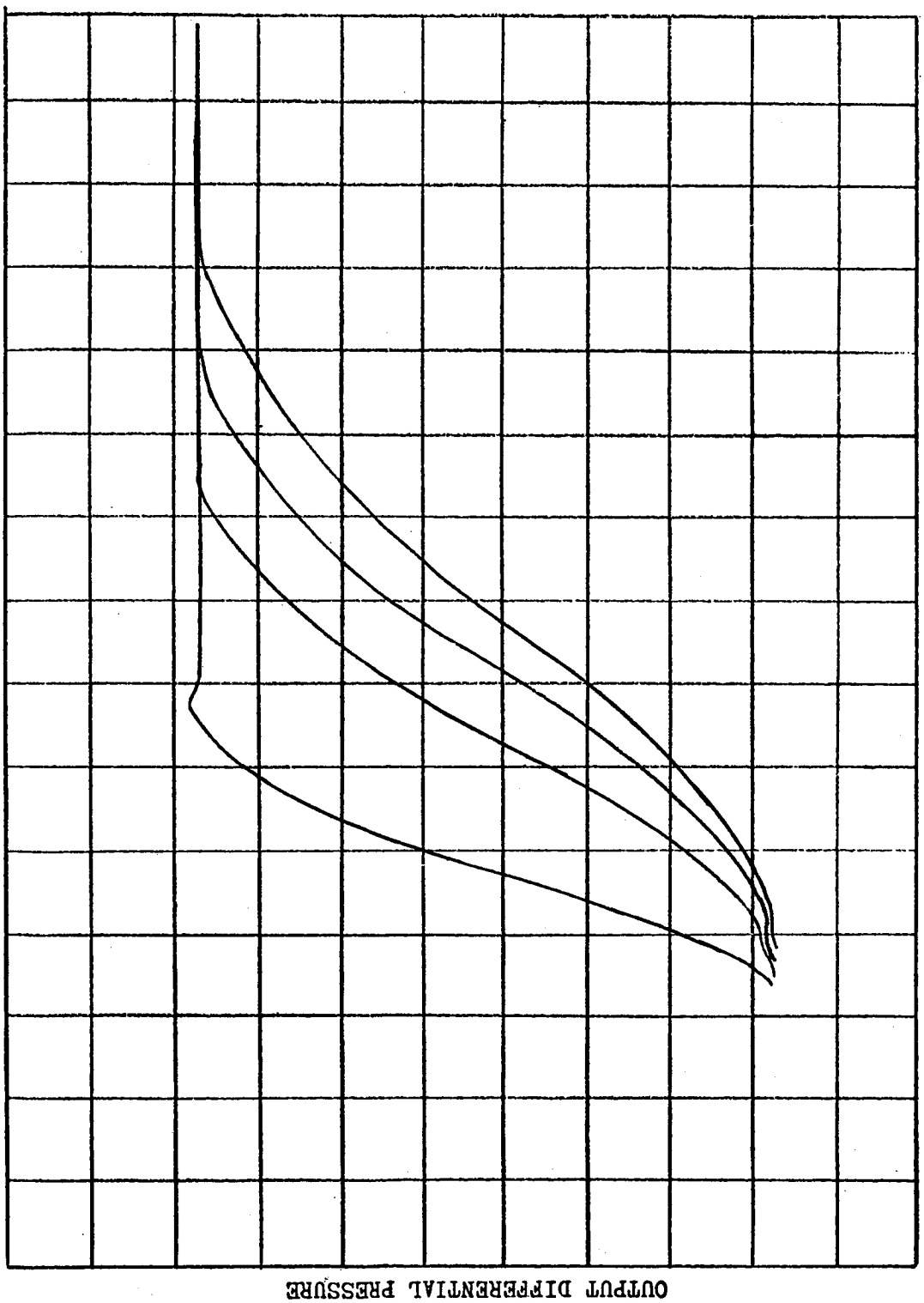

Figure 25 Typical Function Generator Segment Output Curves

SATURABLE AMPLIFIER BREADBOARD
TYPICAL DATA

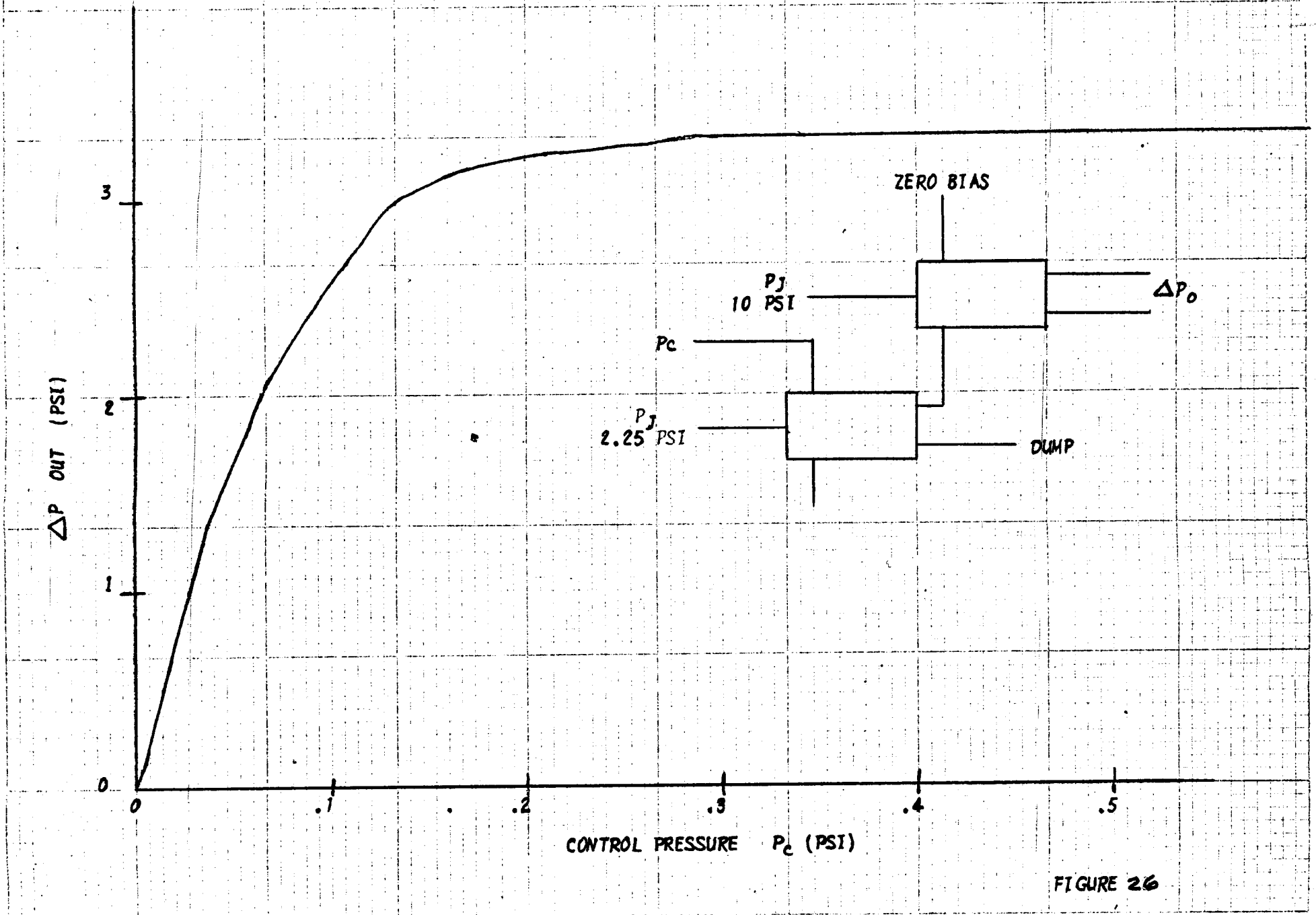

FIGURE 26

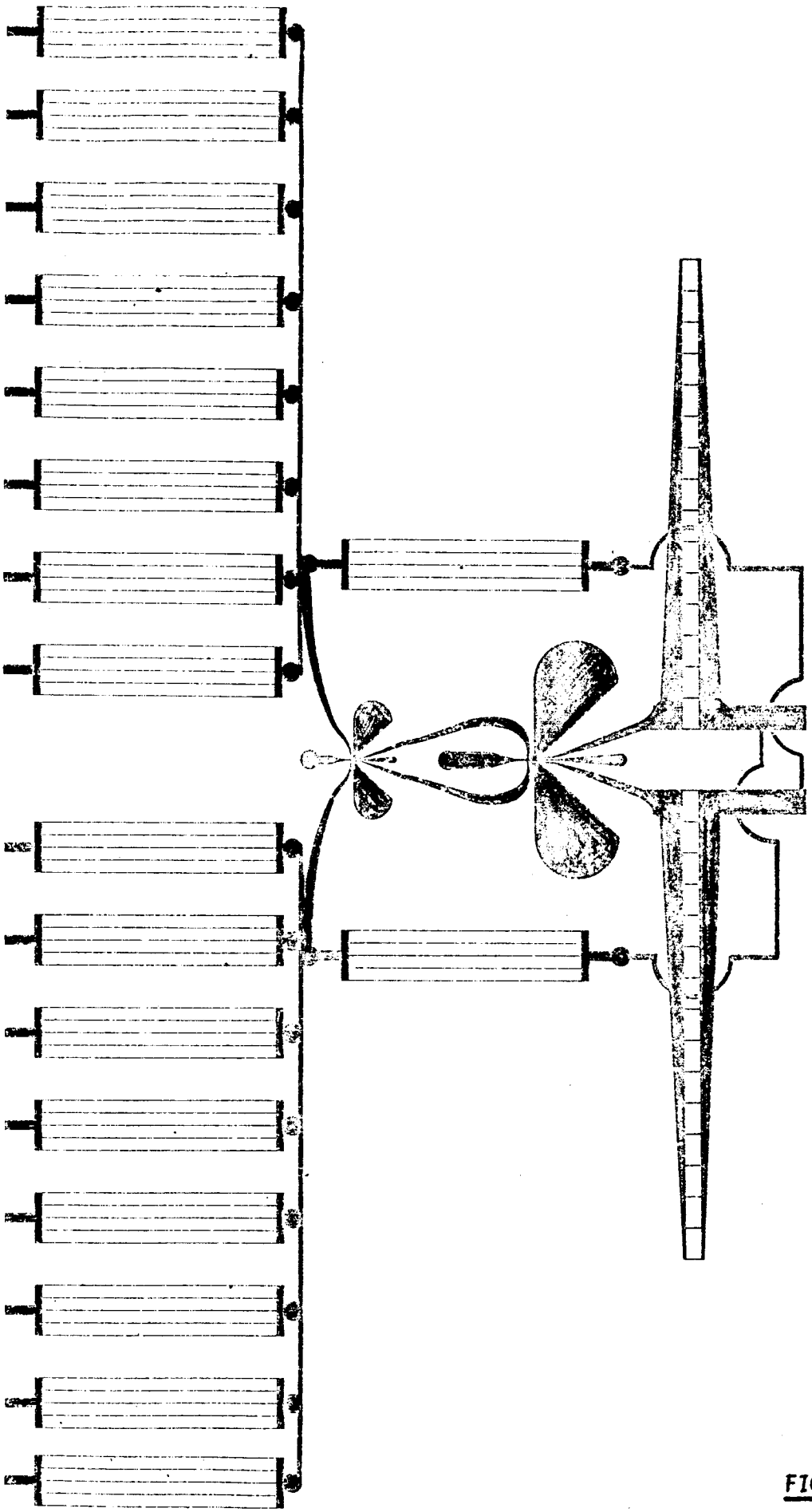

FIGURE 27

REVISIONS				
ZONE	LTR	DESCRIPTION	DIST CODE	DATE / APPROVED
		1. MAY BE REWORKED 3. RECORD CHANGE 2. CANNOT BE REWORKED 4. NOW SHOP PRACTICE 5. PARTS MADE OK		
	A	1) ADDED G/N (8). DELETED G/N (6) 2) ON F/D (8) WAS (4) (2) 3) (8) WAS "SEAL WITH GENERAL ELECTRIC RTV 102 SEALANT" 4) .010 GOLD LEAD WAS COPPER WIRE, #24 GA 5) DELETED G/N (5) 6) ADDED .090 DIA COPPER WIRE	4 4 4 4 4 4	5-5-67 3-16-67

99-108388 NOZZLE 1 REQD

99-108389 SPACER 2 REQD

99-108387 NOZZLE 1 REQD

99-108390-5 HEATER 2 REQD

99-108390-3 HEATER 1 REQD

VIEW **A-A** [4]

SECTION **C-C** [2]

VIEW **B-B** [1]

(-3) PRESSURE LINE 1 REQD

(1) 1097-2M-FKS THERMOCOUPLE 2 REQD 8 FEET LONG

(2) 2 PLACES

(3) CONNECTOR 4 REQD

(2) SOLDER ALL ELECTRICAL CONNECTIONS IN SERIES AS SHOWN

SECTION **D-D**

(A6) .090 DIA COPPER WIRE PER QQ-W-341 APPROX 4.00 (2 PLACES)

.010 DIA GOLD LEAD, APPROX 2.00 AS REQD (A4)

(-7) VACUUM LINE 1 REQD

99-108391 TUBE 1 REQD

99-108392 TUBE 1 REQD

(-3) PRESSURE LINE 1 REQD

(8) EPOXY WITH EPOXYLITE #6203 POTTING RESIN THE EPOXYLITE CORP. SOUTH EL MONTE, CALIFORNIA

7. FOR LIST OF MATERIAL SEE L/M 12GRING CORRESPONDING PART NO

~~(6) SELECTIVE COPPER PLATE PER RA0105-014~~

~~(5) WIRE SN WIRE CO., WARREN, OHIO~~

(4) IDENTIFY PER RA0104-008

(3) DEVICE SEALED INC, SUN VALLEY, CALIF.

(2) SOLDER PER MIL-S-6872 USING QQ-S-571 TYPE SN 20

(1) AGED RESEARCH INSTRUMENT CO INC, CHICAGO, ILL.

NOTE: UNLESS OTHERWISE SPECIFIED

-7	321 CRES TUBE	.0600D-.0570D x 8.00	ASTM 269 OR EQUIV
-5	321 CRES TUBE	.065 OD x .0620D x 6.00	ASTM 269 OR EQUIV
-3	321 CRES TUBE	.0390D, .0370D x 8.30	ASTM 269 OR EQUIV
V1	MATERIAL	SIZE	SPECIFICATION

HEAT TREAT / FINISH / MAT'L: NOTED

UNLESS OTHERWISE SPECIFIED DIMENSIONS ARE IN INCHES AND APPLY PRIOR TO FINISH. 125 MACH. SURF. ROUGHNESS V. TOLERANCES ON DECIMALS: XX = ± .01, XXX = ± .010; ANGLES ± 30'. HOLES NOTED "DRILL": .000 THRU .040 + .0015 - .001; .041 THRU .110 + .003 - .001; .111 THRU .230 + .0045 - .001; .231 THRU .500 + .006 - .001; .501 THRU .750 + .007 - .001; .751 THRU 1.000 + .009 - .001; 1.001 THRU 2.000 + .012 - .001. DO NOT SCALE PRINT.

DR BY	J.M. CONNOR	9-9-66
CHK BY		
DES		
MAT		
DEV		7-21-66
SUB		7-21-66
STR		

ROCKETDYNE
A DIVISION OF NORTH AMERICAN AVIATION, INC.
CANOGA PARK, CALIFORNIA · MCGREGOR, TEXAS

ELEMENT, SENSING, ASSY OF

CODE IDENT NO.	SIZE	
02602	E	99-108399
SCALE 10/1		SHEET

Q'ty P-NO 1

X-2

99-108399 A

THIS PRINT REDUCED
THIS IS NOT A RELEASED COPY

FIGURE 28

FOLDOUT FRAME 1

FOLDOUT FRAME 2

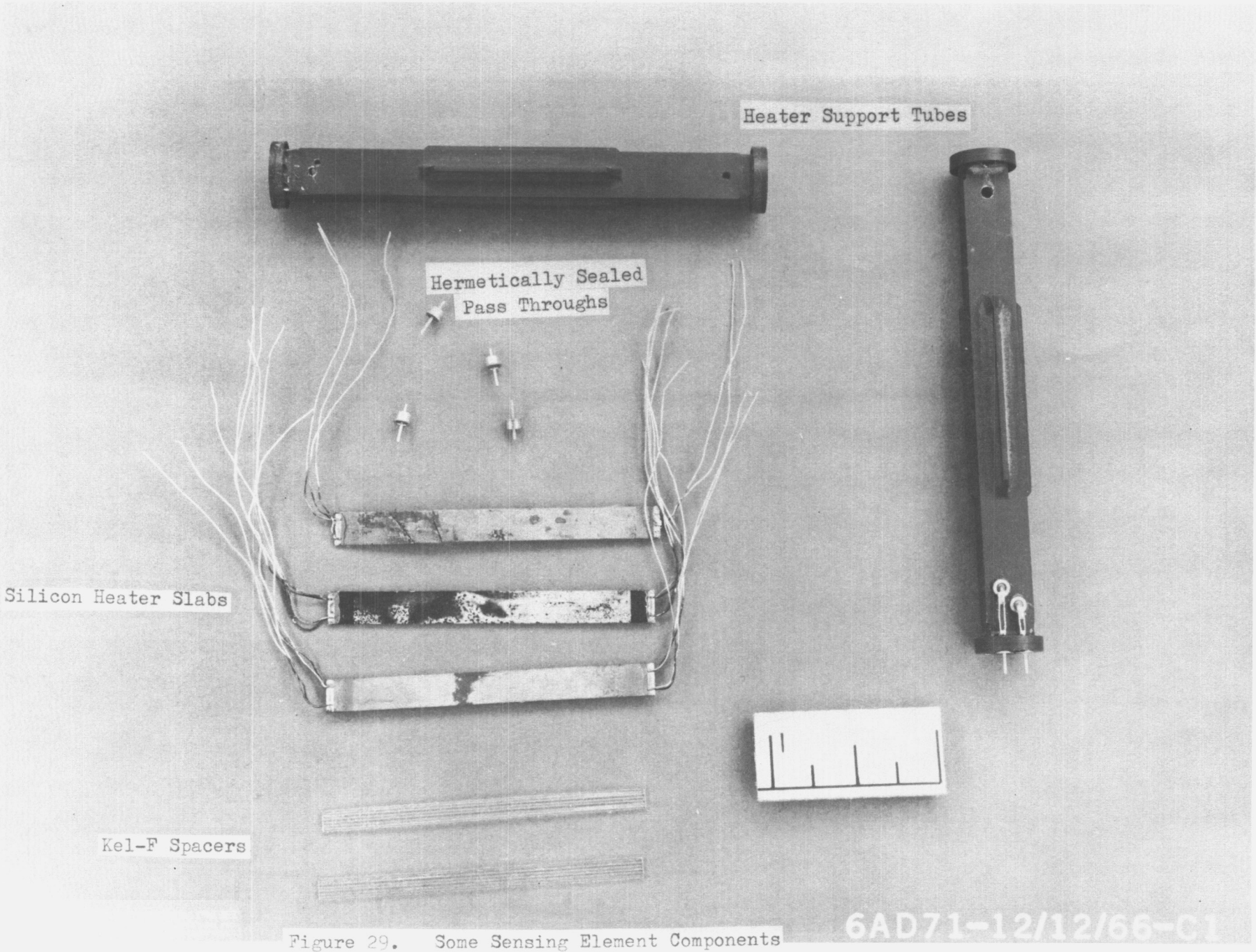

Figure 29. Some Sensing Element Components

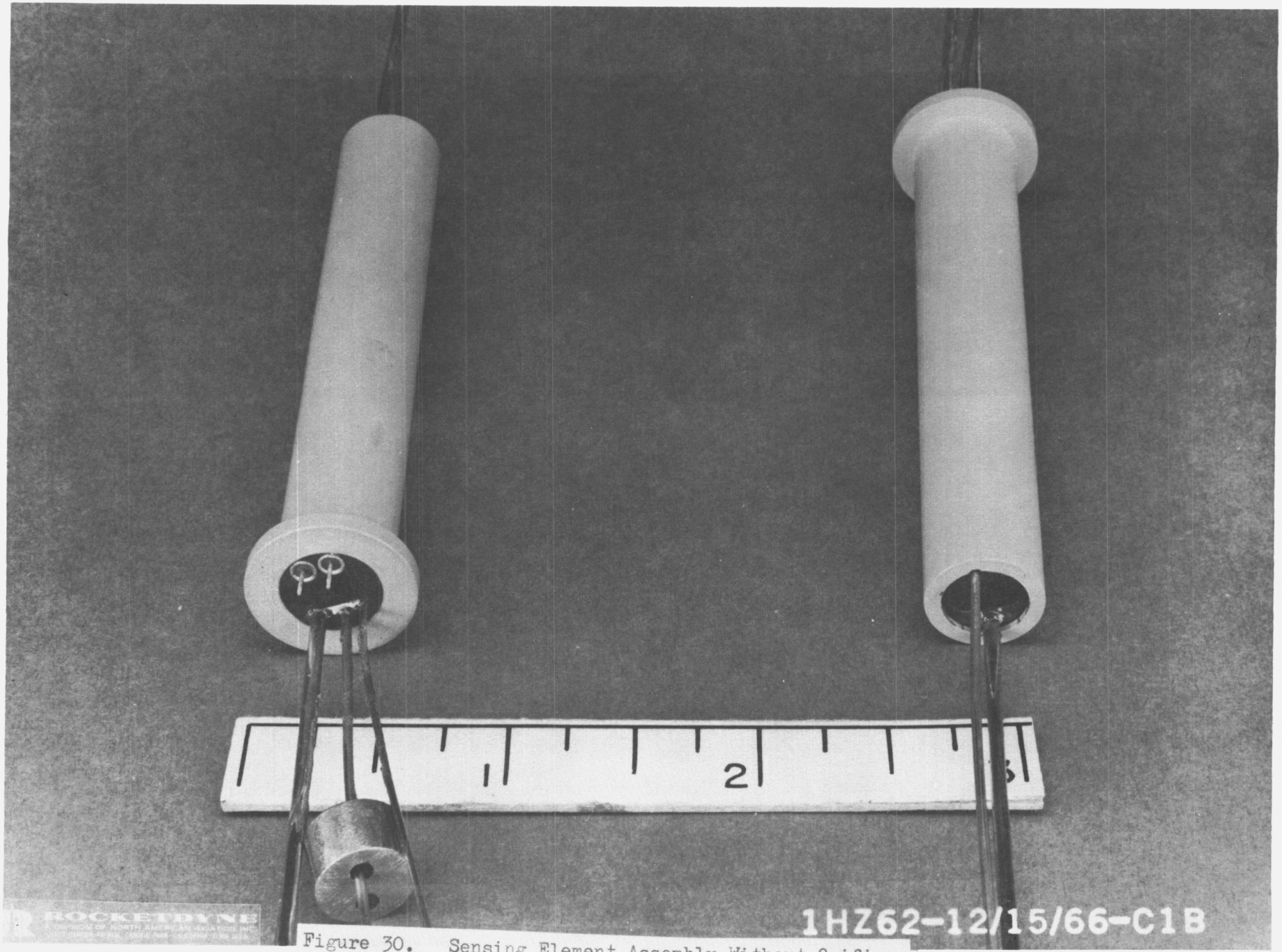

Figure 30. Sensing Element Assembly Without Orifices

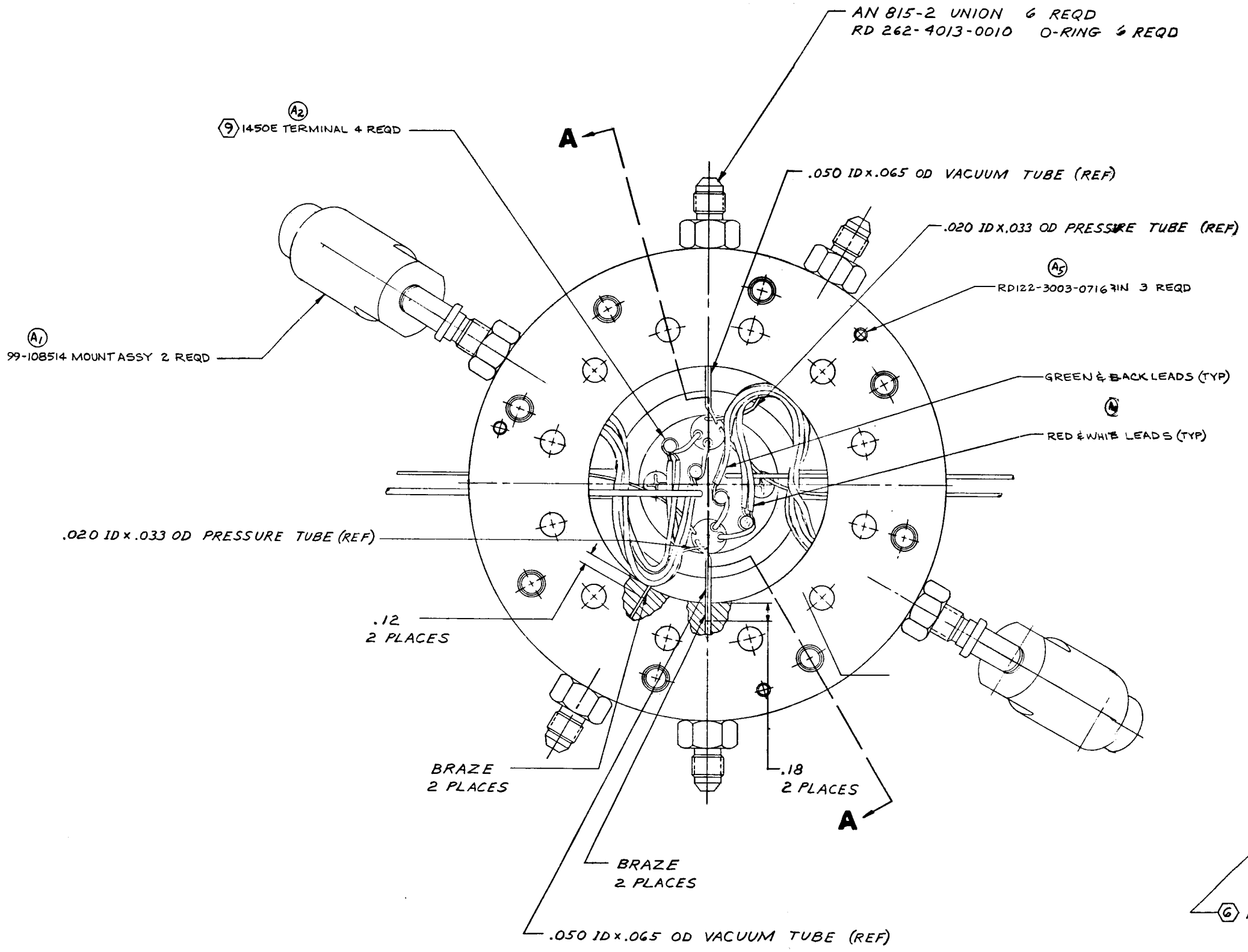

FOLDOUT FRAME 1

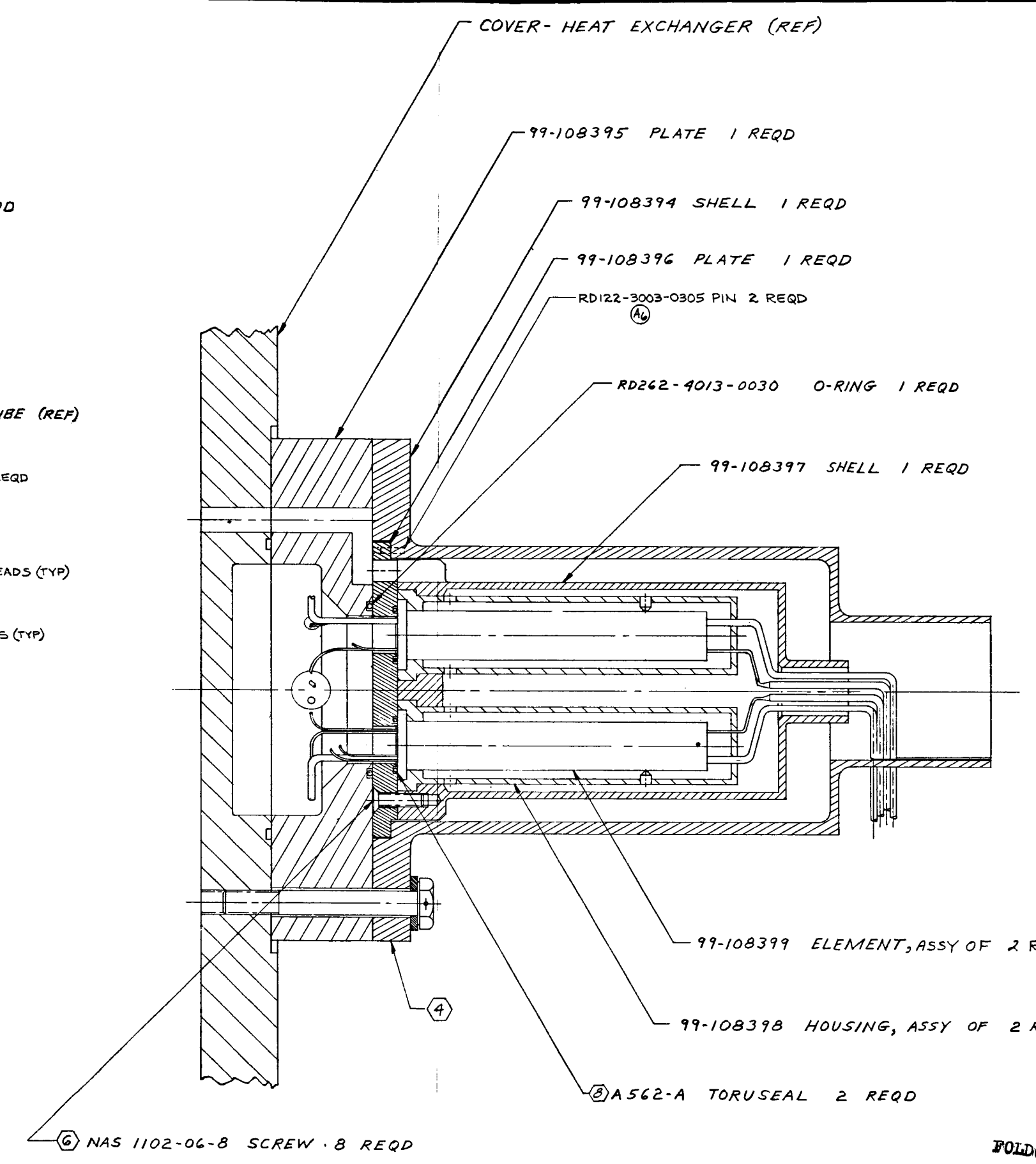

FOLDOUT FRAME 3

FOLDOUT FRAME 2

SECTION **A-A**

FIGURE 31
FLUX DETECTOR ASSY
ROCKETDYNE DWG. 99-108400

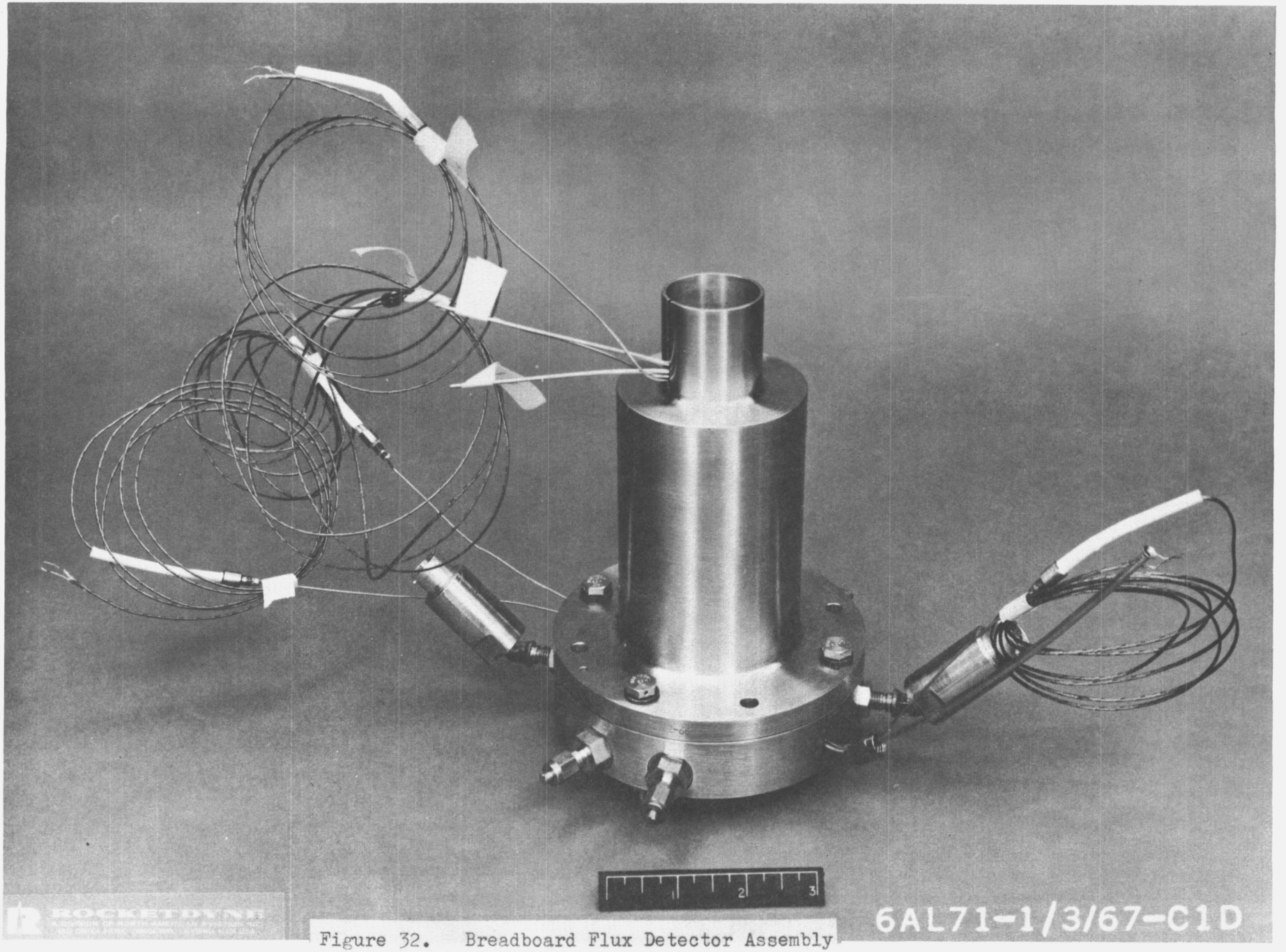

Figure 32. Breadboard Flux Detector Assembly

REVISIONS				
SYM	DESCRIPTION		DATE	APPROVED
	1. MAY BE REWORKED 3. RECORD CHANGE 2. CANNOT BE REWORKED 4. NOW SHOP PRACTICE 5. PARTS MADE OK			
X A	1) ADDED G/N 5	4	3-14-67	J. Smart 5-F-67 Horiyama

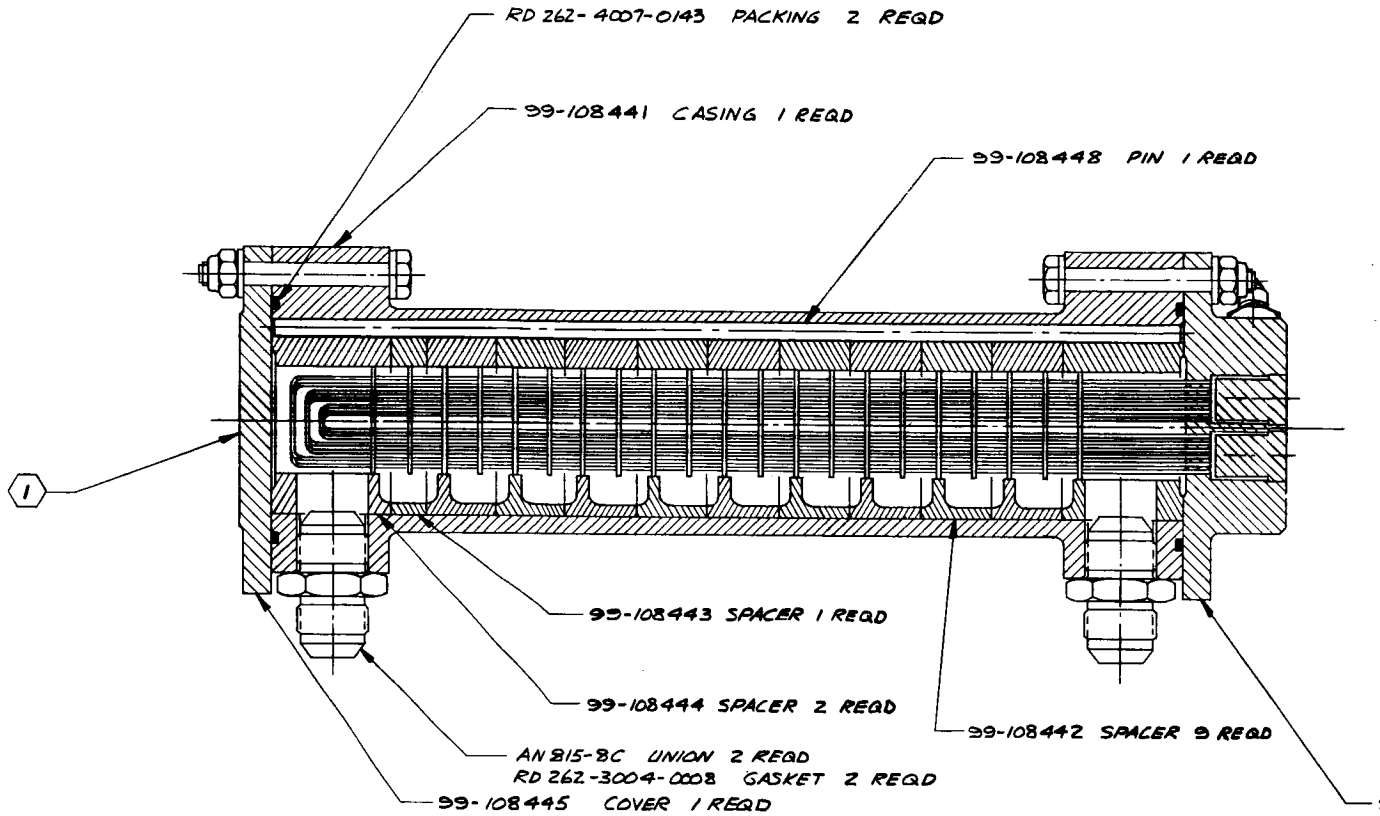

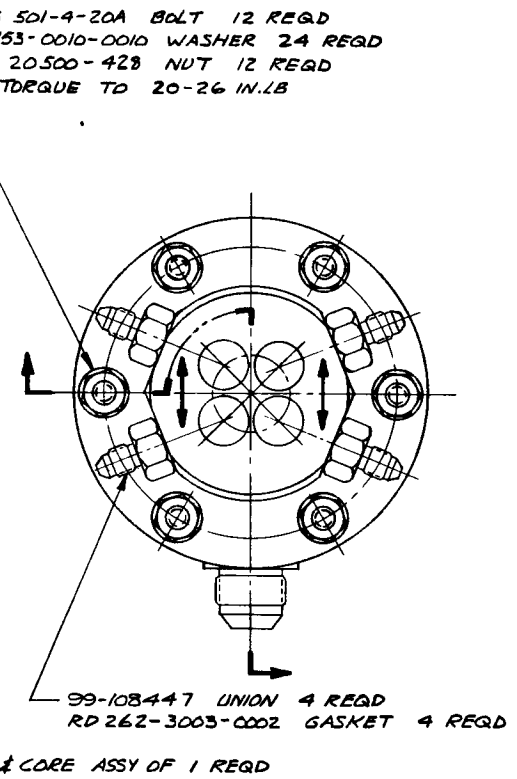

FOLDOUT FRAME 1

FIGURE 33

FOLDOUT FRAME 2

5. PROOF TEST WITH HELIUM TO 450 ± 5 PSIG, HOLD FOR 2 MINUTES MINIMUM. REPEAT FOR A TOTAL OF 5 CYCLES.
4. INSTALL FITTINGS PER RA0102-005
3. INSTALL THREADED FASTENERS PER RA0101-002
2. FOR LIST OF MATERIAL SEE LM BEARING CORRESPONDING PART NO.
(1.) IDENTIFY PER RA0104-008

NOTE: UNLESS OTHERWISE SPECIFIED

HEAT TREAT
FINISH
MAT'L

UNLESS OTHERWISE SPECIFIED: DIMENSIONS ARE IN INCHES AND APPLY PRIOR TO FINISH.
125/ MACH. SURF. ROUGHNESS
TOLERANCES ON DECIMALS .XX = ± .03, .XXX = ± .010 ANGLES ± 30'
HOLES NOTED "DRILL":
.000 THRU .040: +.0015 −.001
.041 THRU .130: +.003 −.001
.131 THRU .229: +.0045 −.001
.230 THRU .500: +.006 −.001
.501 THRU .750: +.007 −.001
.751 THRU 1.000: +.009 −.001
1.001 THRU 2.000: +.012 −.001
DO NOT SCALE PRINT

DR BY	R. BREMNER	9.23.66
CHK BY		9.28.66
DES	R. BREMNER	SUP 9.28.66
MAT		STR
DEV	9.28.66	9/29/66

ROCKETDYNE
A DIVISION OF NORTH AMERICAN AVIATION, INC.
CANOGA PARK, CALIFORNIA · McGREGOR, TEXAS

ASSY, HEAT EXCHANGER, PNEUMATIC FLUX DECTECTOR

CODE IDENT NO.	SIZE	
02602	D	99-108440
SCALE 1/1		SHEET

A 99-108440

7/65 DIETERICH-POST CLEARPRINT 3689H-2

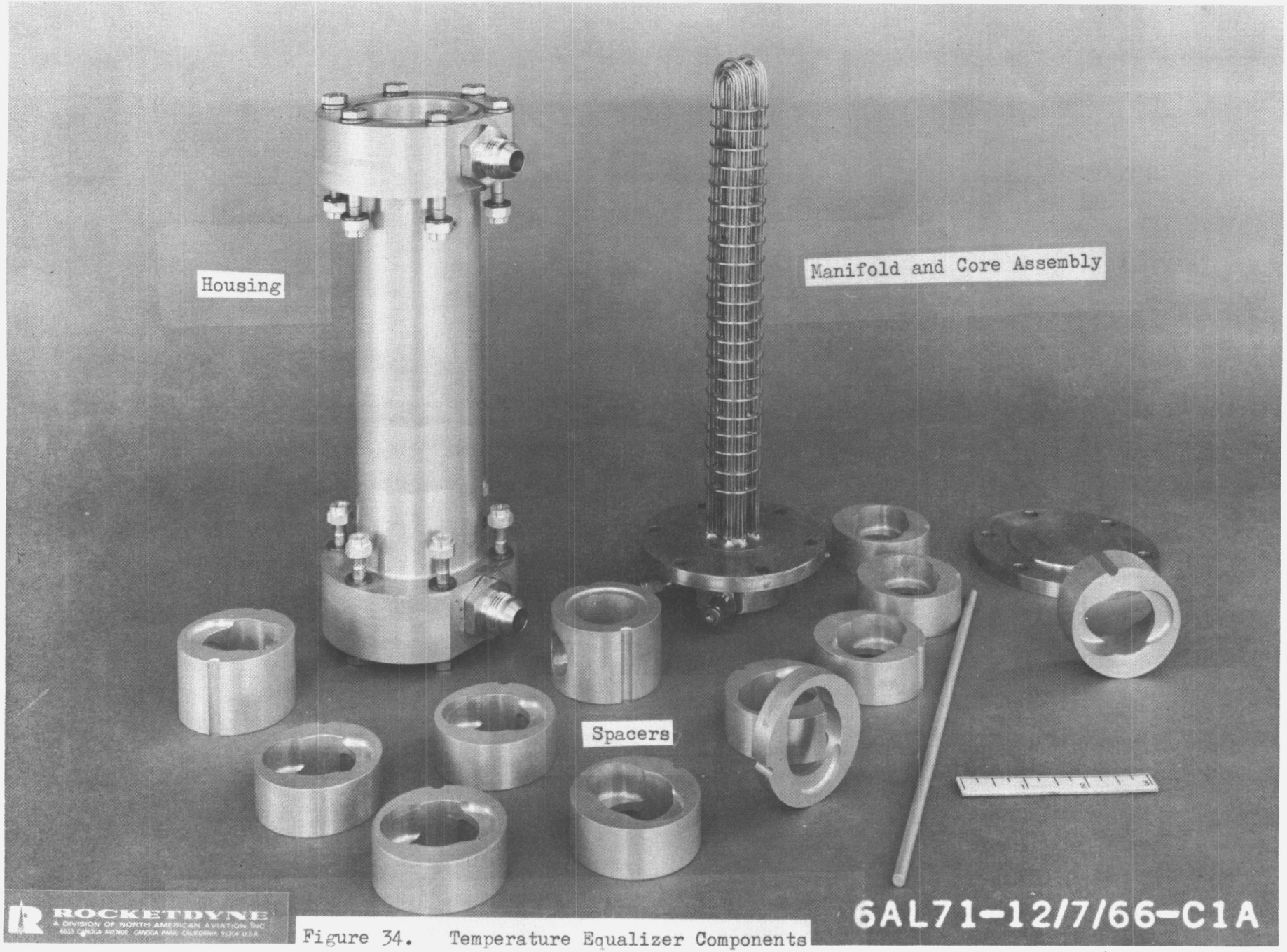

Figure 34. Temperature Equalizer Components

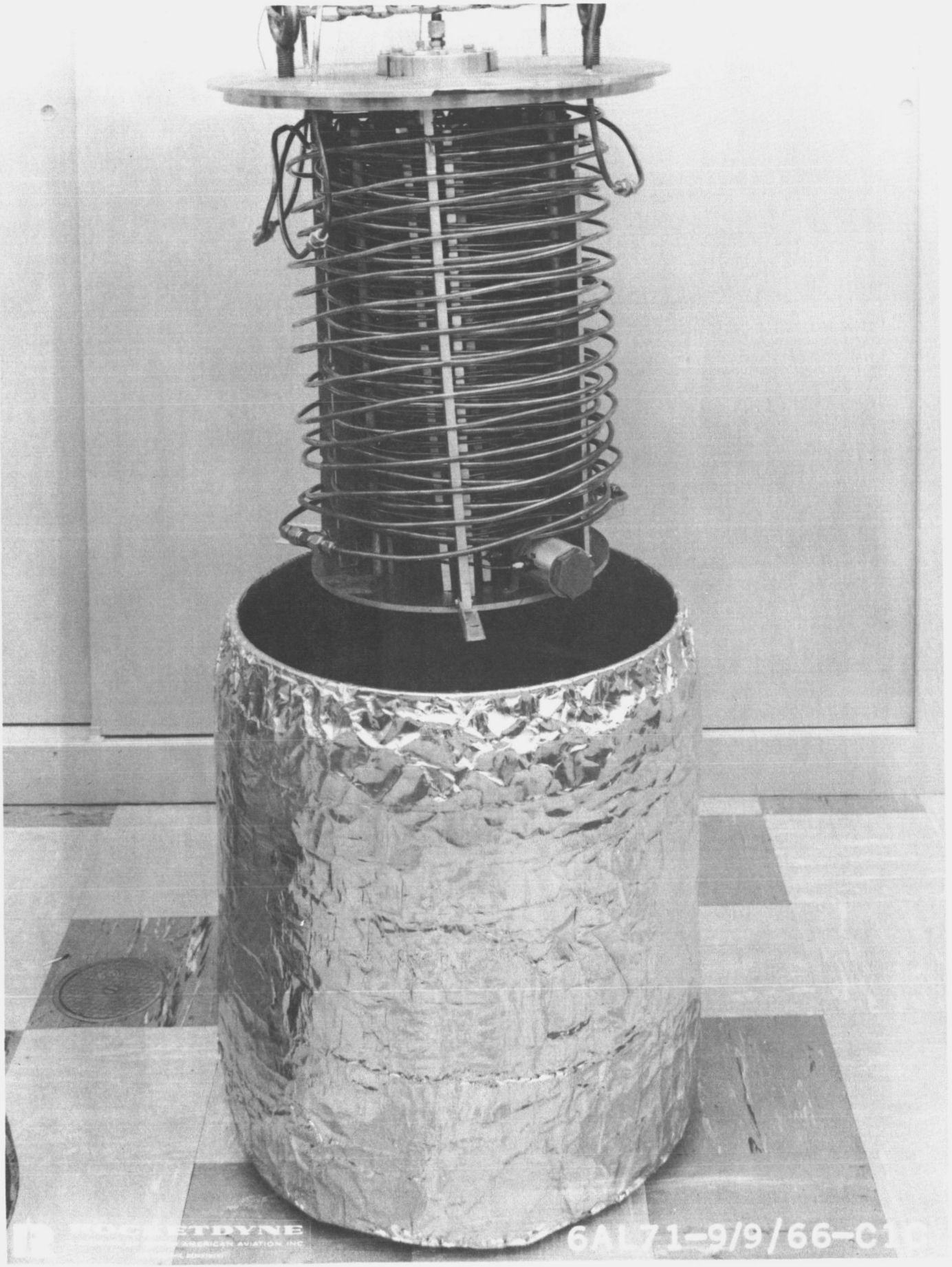

Figure 35. Precooler - Unassembled

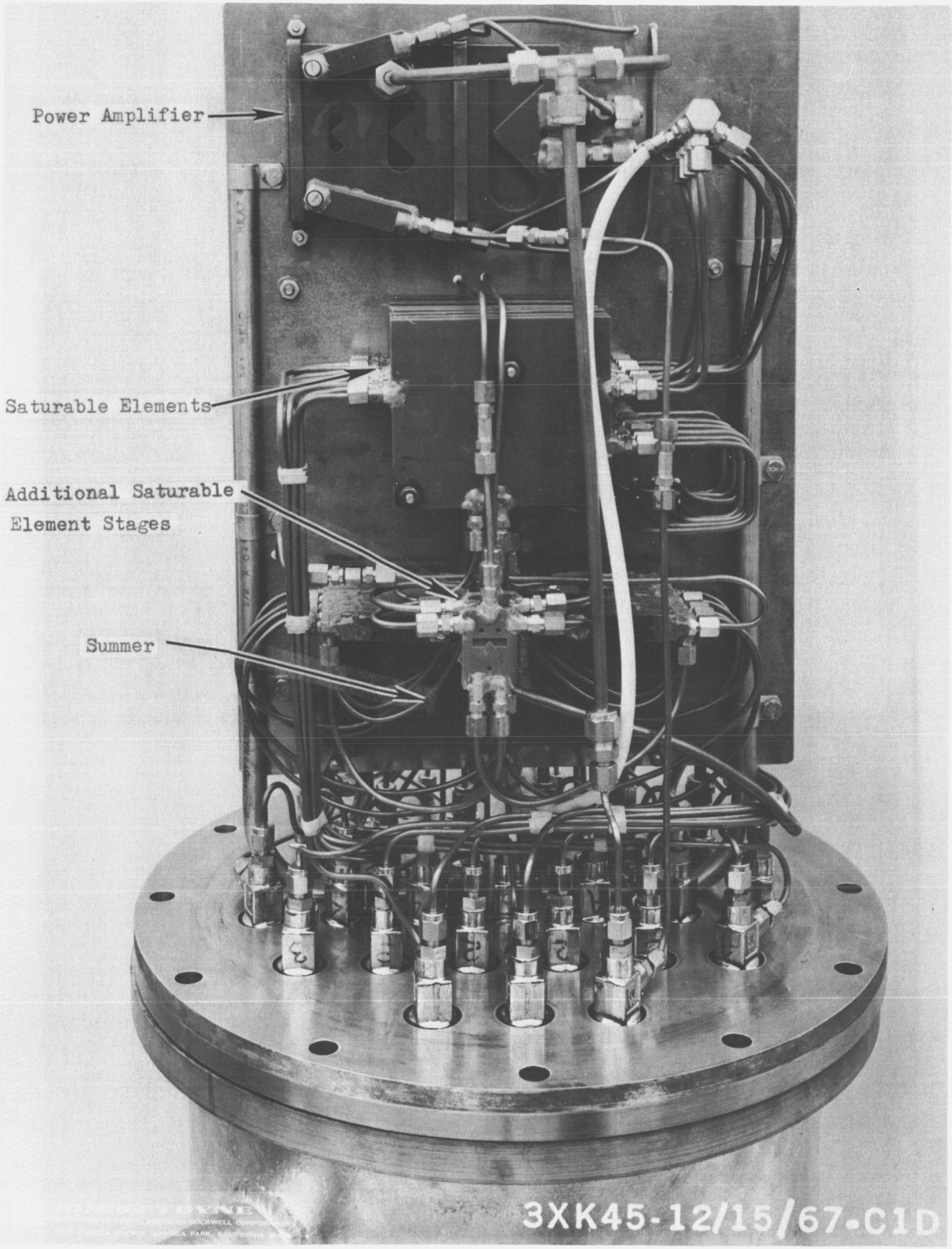

Figure 36. Breadboard Log Function Generator - Internal View

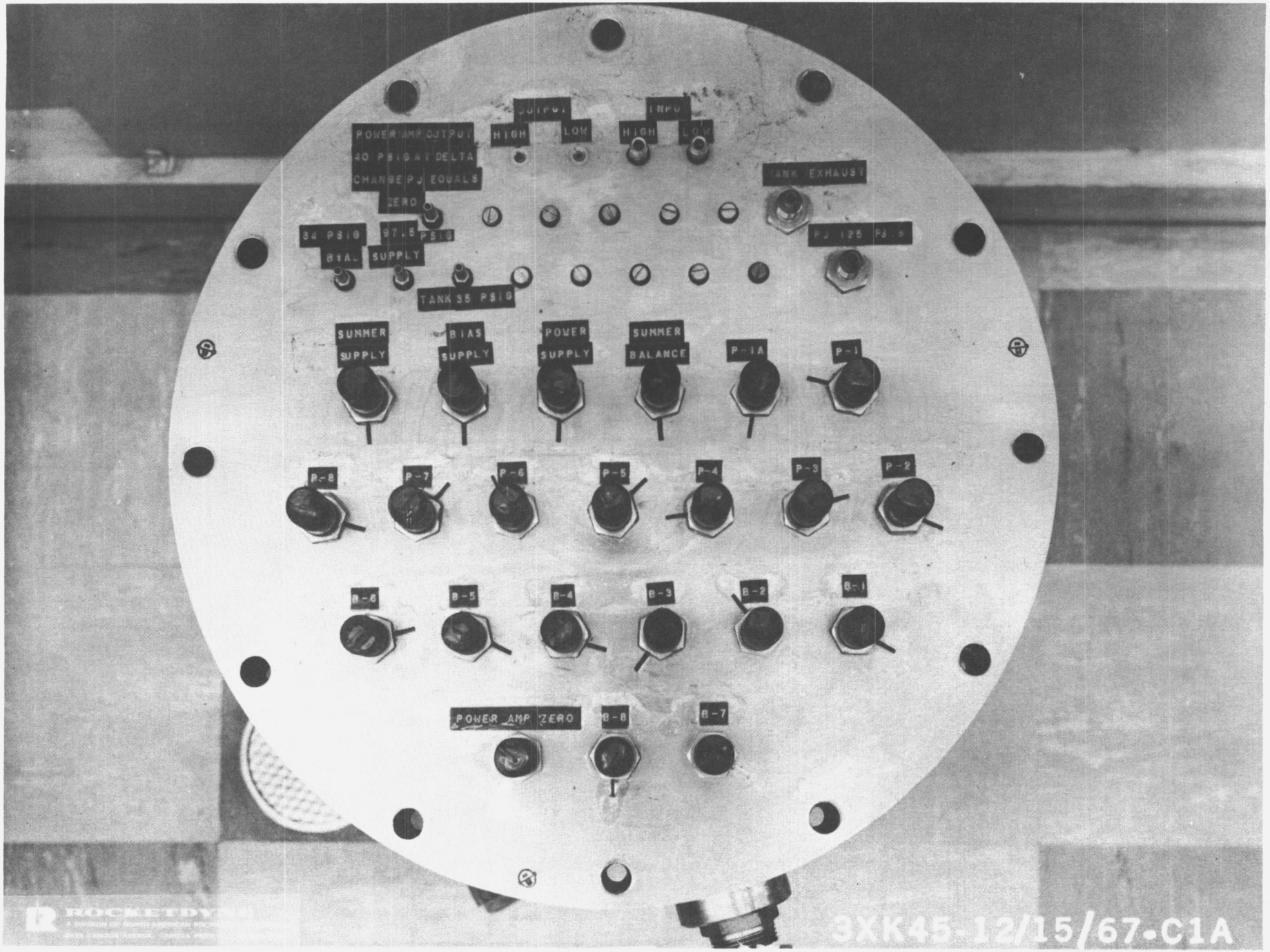

Figure 37. Breadboard Log Function Generator - Top View

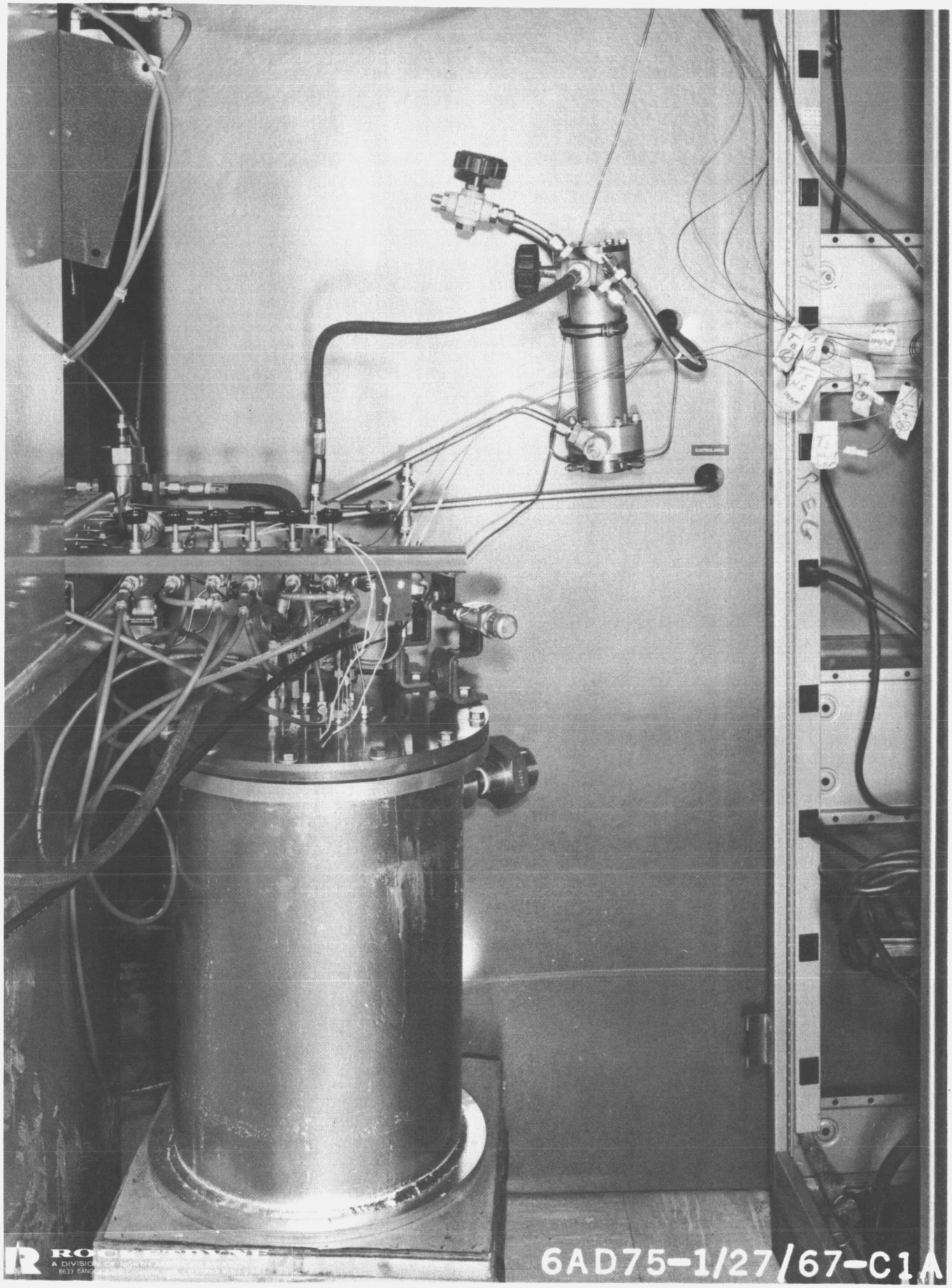

Figure 38. Breadboard Log Function Generator and Temperature Equalizer Installed for Laboratory Evaluation Tests

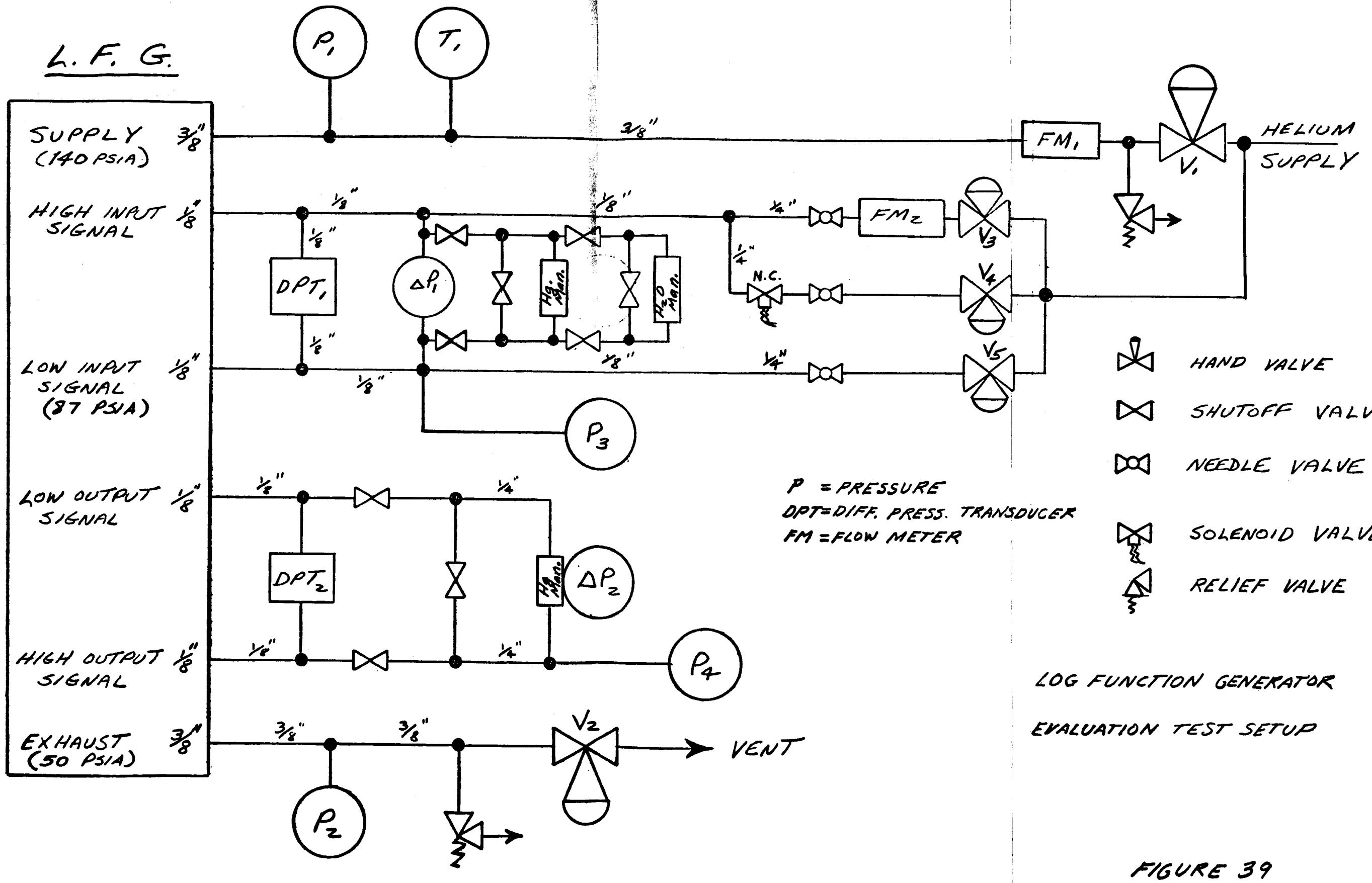

LOG FUNCTION GENERATOR

EVALUATION TEST SETUP

FIGURE 39

C. MANGION (11-4-66)

CHANGED - MILLEMAN ~~(5-16-67)~~ (5-25-67)

FOLDOUT FRAME 1

FOLDOUT FRAME 2

FIGURE 40

LOG GENERATOR CALIBRATION
31 MAY 1967

SUPPLY PRESSURE - 125 psig
VENT PRESSURE - 35 psig
ROOM TEMPERATURE GHe

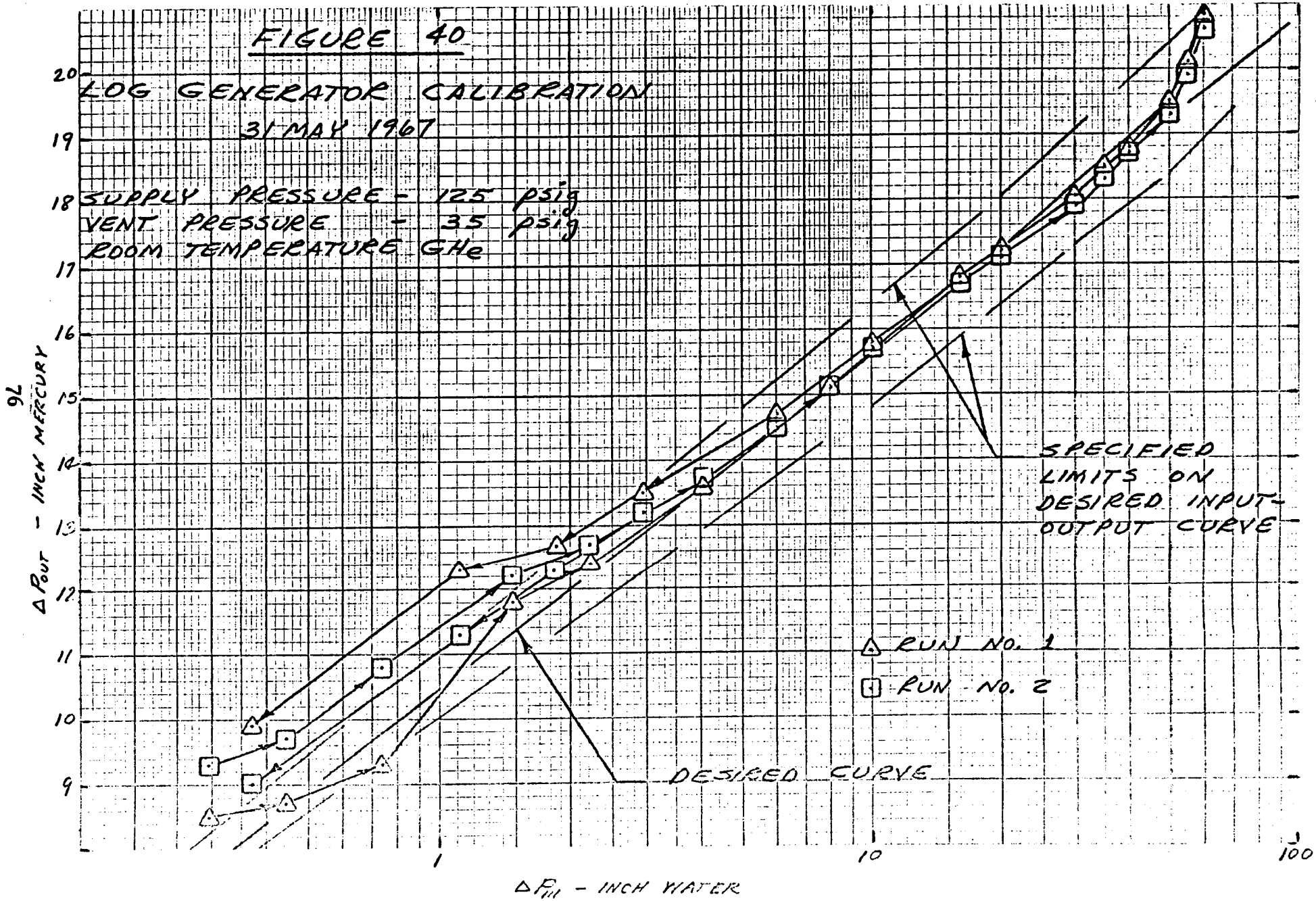

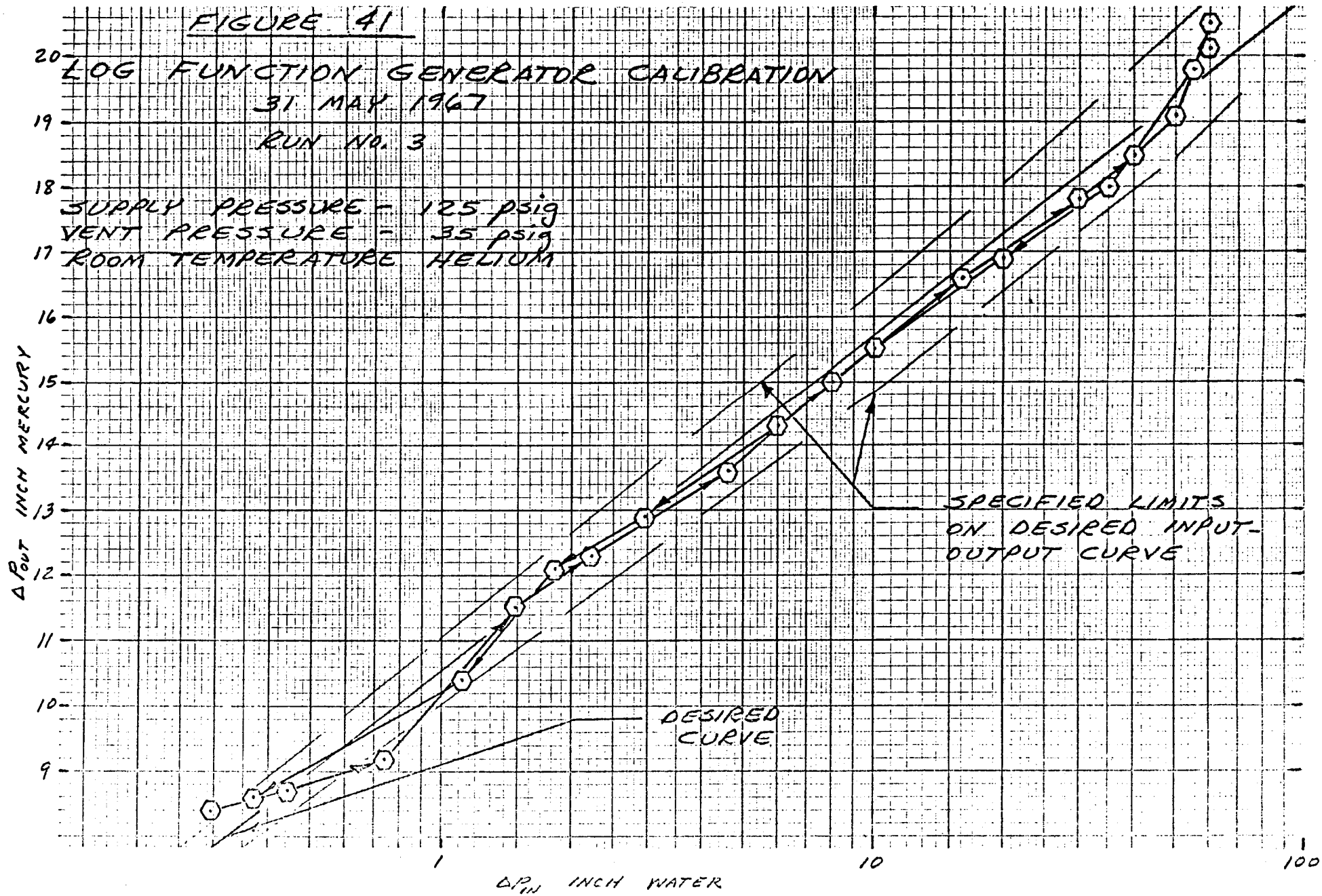
FIGURE 41
LOG FUNCTION GENERATOR CALIBRATION
31 MAY 1967
RUN No. 3
SUPPLY PRESSURE - 125 psig
VENT PRESSURE - 35 psig
ROOM TEMPERATURE HELIUM
20
19
18
17
16
15
14
13
12
11
10
9
ΔPOUT INCH MERCURY
SPECIFIED LIMITS ON DESIRED INPUT-OUTPUT CURVE
DESIRED CURVE
1
10
100
ΔPIN INCH WATER

FIGURE 42

LOG FUNCTION GENERATOR TRANSIENTS

1 June 1967

0.5 SEC/CM
INPUT - 49.5 to 55.1 in HG.
OUTPUT - 19.35 to 20.0 in HG. (noisy)

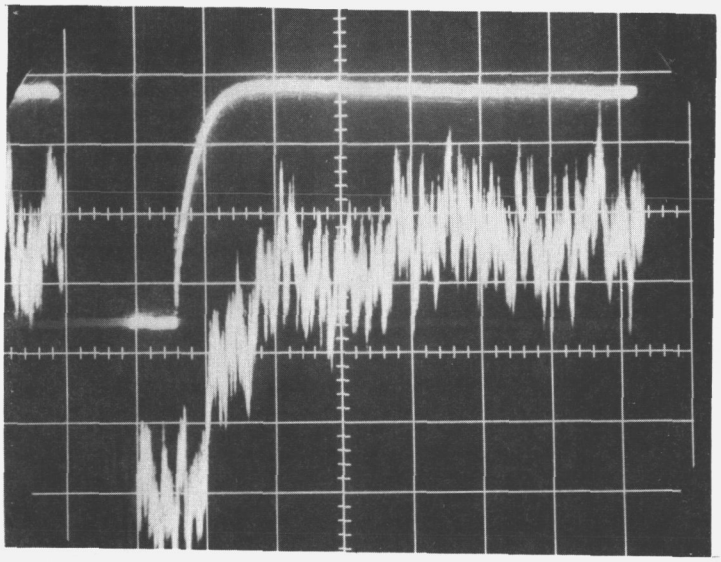

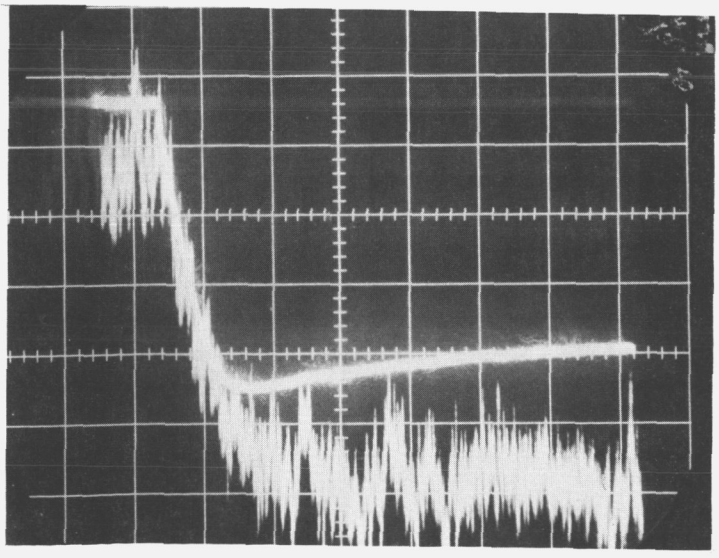

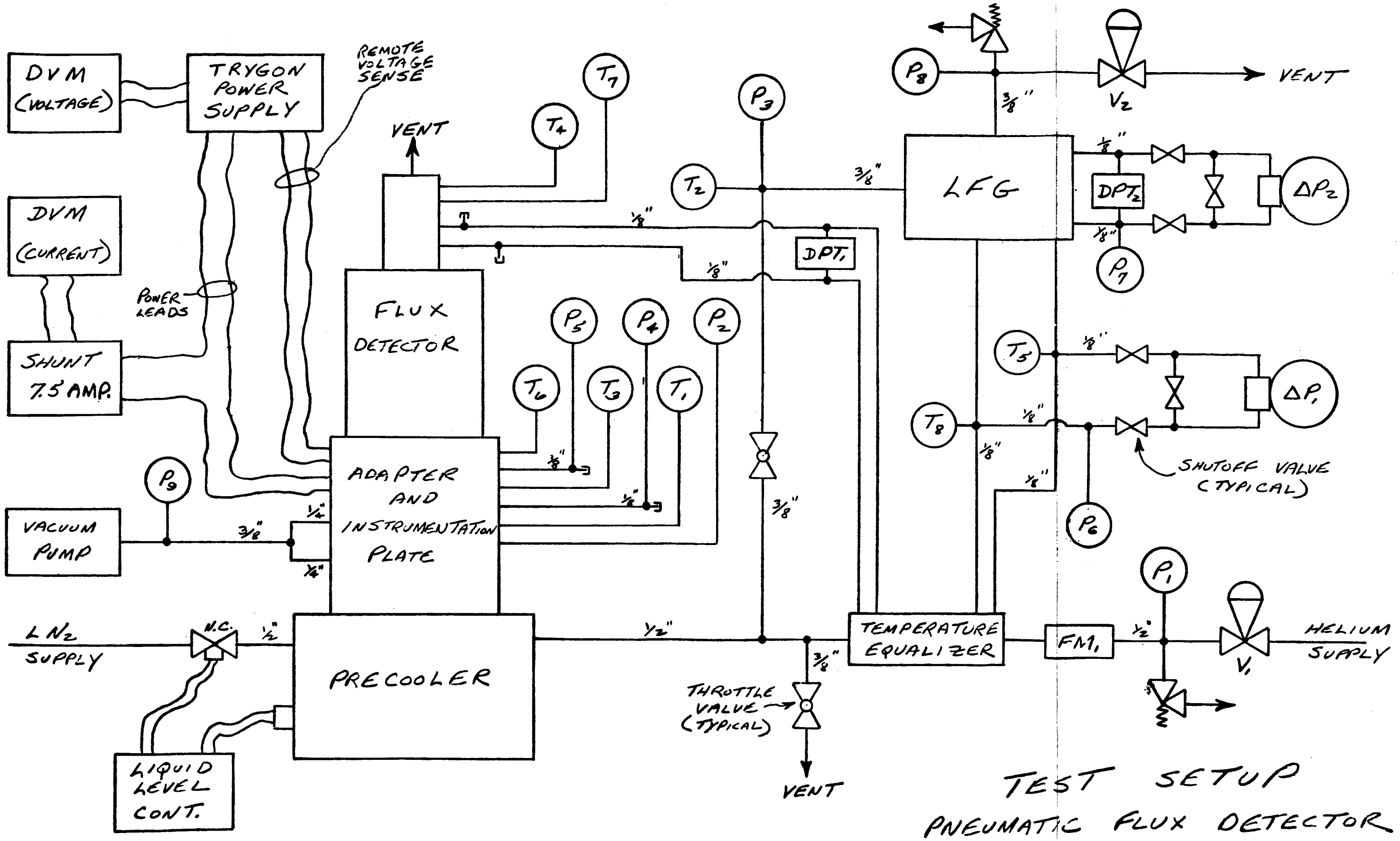

TEST SETUP
PNEUMATIC FLUX DETECTOR SYSTEM

FIGURE 43

C. MANGION
(11-8-66)

FOLDOUT FRAME 1

FOLDOUT FRAME 2

LEGEND FOR INSTRUMENTATION SHOWN

P_1	Regulated Helium Supply Pressure
P_2	Sensing Element Supply Pressure
P_3	LFG Supply Pressure
P_4	Pressure Downstream Active Element Orifice
P_5	Pressure Downstream of Compensating Element Orifice
P_6	Compensating Element Output Pressure
P_7	LFG (Log Function Generator) High Output Pressure
P_8	LFG Exhaust Pressure
P_9	Sensing Element Vacuum Pressure
ΔP_1	Differential Pressure Flux Detector Output
ΔP_2	Differential Pressure LFG Output
DPT_1	Differential Pressure Transducer Flux Detector Output
DPT_2	Differential Pressure Transducer LFG Output
T_1	Sensing Element Supply Temperature
T_2	LFG Supply Temperature
T_3	Temperature Downstream of Active Element Inlet Orifice
T_4	Temperature Downstream of Active Element Heaters
T_5	Temperature of High Input Signal to LFG
T_6	Temperature Downstream of Compensating Element Inlet Orifice
T_7	Temperature Downstream of Compensating Element Heaters
T_8	Temperature of Low Input Signal to LFG
FM_1	Flowrate of Total Helium Supply

Figure 43. (Concluded)

APPENDIX A
SAMPLE CALCULATIONS

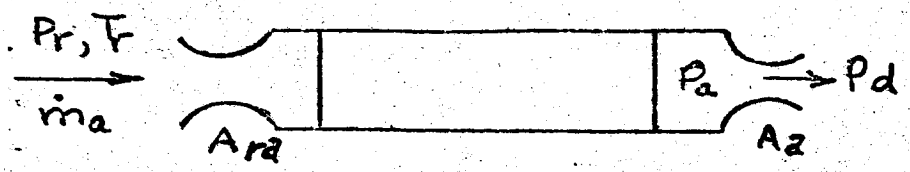

EQ'NS OF FLOW

1) $\dot{m}_a = \dfrac{P_r A_{ra} f\left(\frac{P_a}{P_r}\right)}{\sqrt{T_r}}$

2) $\dot{m}_a = \dfrac{P_a A_a f\left(\frac{P_d}{P_a}\right)}{\sqrt{T_a}}$

HEAT TRANSFER

3) $q_a = \dot{m}_a c_{pa} (T_a - T_r)$

COMBINE 2) & 3)

4) $P_a = \dfrac{\dot{m}_a \sqrt{T_r + q_a/\dot{m}_a c_{pa}}}{A_a f\left(\frac{P_d}{P_a}\right)}$

WITH P_r & T_r CONSTANT & CHOKED ORIFICES

4a) $P_a = K_1 \sqrt{T_r + K_2 q_a}$ WHERE K_1 & K_2 ARE CONSTANTS

i.e. SIGNAL PRESSURE, P_a, IS A FUNCTION OF THE HEAT GENERATED.

ESTABLISH OPERATING RANGES & LEVELS OF PRESSURE & TEMP. FROM:

FROM EQ. 2 PG. 1

5) $$P_{a\,max} - P_{a\,min} = \frac{\dot{m}_a\sqrt{T_{a\,max}}}{A_a f\left(\frac{P_d}{P_a}\right)} - \frac{\dot{m}_a\sqrt{T_{a\,min}}}{A_a f\left(\frac{P_a}{P_r}\right)}$$

6) $$P_{a\,max} - P_{a\,min} = P_{a\,max}\left(1 - \sqrt{\frac{T_{a\,min}}{T_{a\,max}}}\right)$$

ASSUMING SUPPLY GAS TEMP CAN BE REDUCED TO LN_2 BOILING @ 14.7 psi

$T_{a\,min} = 140°R$. ASSUMING SUPPLY GAS PRESSURE @ 250 psia. From Fig. 3 . CHOOSE $T_{a\,MAX} = 340°R$

CRITICAL PRESSURE

7) $$\left(\frac{P_a}{P_r}\right)_{CRIT} = \left(1 + \frac{\gamma-1}{2}\right)^{\frac{-\gamma}{\gamma-1}}$$ where $\gamma = 1.66$

NOTE: He & N_2 PROPERTIES FROM REF. 4, 5, & 6

$$\left(\frac{P_a}{P_r}\right)_{CRIT} = .488$$

$$P_{a\,CRIT} = .488(250) = 122 \text{ psia}$$

8) $$f\left(P_a/P_r\right) \sqrt{\frac{2\gamma}{\gamma-1}\frac{g}{R}}\sqrt{\left(\frac{P_a}{P_r}\right)^{2/\gamma} - \left(\frac{P_a}{P_r}\right)^{\frac{1+\gamma}{\gamma}}}$$

for choked flow,

$$f\left(\frac{P_a}{P_r}\right) = \sqrt{\frac{2(1.66)(386)}{.66(4640)}}\sqrt{(.488)^{\frac{2}{1.66}} - (.488)^{\frac{2.66}{1.66}}}$$

$$= .2075 \frac{lbm\sqrt{°R}}{lbf\ sec}$$

@ $P_a = 129$ psia.

$$f\left(\frac{P_a}{P_r}\right) = \sqrt{\frac{2(1.66)(386)}{.66(4640)}}\sqrt{(.515)^{\frac{2}{1.66}} - (.515)^{\frac{2.66}{1.66}}}$$

$$= .207 \frac{lbm\sqrt{°R}}{lbf\ sec}$$

For $P_{a\,max} = 129$ flow change NEGLIGIBLE

CHECK Re & ΔP FOR $T_{WAX} - T_{aMIN}$

9) $\dot{m}_a = \dfrac{q_a}{C_{pa}(T_a - T_f)}$ where $q_a = .78 \frac{BTU}{sec}$ FROM REF 1

10) $Re_a = \dfrac{GD_h}{\mu} = \dfrac{\dot{m}_a D_h}{A\mu} = \dfrac{4\dot{m}_a}{\mu P_w}$

$P_w = 1.592$ in

11) $P_{ra} - P_2 = f\dfrac{L}{D_h}\dfrac{\rho V^2}{2g} = f\dfrac{L}{D_h}\dfrac{\dot{m}_a^2}{2g\rho A_f^2}$

$D_h = .0209$ in.

$A_f = .00582\ in^2$

@ T_a T_w CHOSEN

$$\dot{m}_a = \frac{.78}{1.25(200)} = 3.13 \times 10^{-3} \ \frac{lb}{sec}$$

$$Re = \frac{4(3.13)(10^{-3})}{1.592(6.75)(10^{-7})} = 11,630$$

$$P_{ro} - P_2 = .0292 \frac{2}{.0209} \frac{(3.13 \times 10^{-3})^2}{2(386)(1.125)(10^{-4})(8.32 \times 10^{-3})^2} = 4.55 \text{ psi}$$

REWRITE EQ'N 5 ON Pg 2 OF APPENDIX SO THAT $P_{a\,min}$ MAY BE USED AS BASE.

12) $$P_{a\,max} - P_{a\,min} = P_{a\,min}\left[\sqrt{\frac{T_{a\,max}}{T_{a\,min}}} - 1\right]$$

USING $P_{a\,min} = 80$ psia

$$P_{a\,max} - P_{a\,min} = 80\left[\sqrt{\frac{340}{140}} - 1\right] = 44.8 \text{ psi} \quad @100\% \text{ flow}$$

ASSUMED CHOKED HOWEVER FOR SUPPLY PRESSURE OF 250 psia.

$P_{a\,max} - P_{a\,min} = 44.6$ psi.

LOG FUNCTION GENERATOR SPECS ARE BASED UPON 80 psi and 140°R REF. PRESSURE & TEMPERATURE RESPECTIVELY.

CHECK HEAT TRANSFER IN HEATER

USE: $.7 \le P_R \le 120$ for $10,000 \le Re \le 120,000$ $\quad L/D \ge 60$

13) $$h = .023 \frac{k}{D_h} (Re)^{0.8} (P_R)^{0.4}$$ FROM REF. 7

Properties evaluated at bulk stream conditions

$$P_R = \frac{c_p \mu}{k}$$

ASSUME 240 R AS BULK TEMP.

$$h = .023 \frac{1.2(10^{-4})}{.0209} (11{,}630)^{0.8} \left[\frac{1.25\ (0.75)(10^{1})}{1.2\ (10^{-4})}\right]^{0.4}$$

$$= .00213 \frac{Btu}{sec\text{-}in^2\ ^\circ R}$$

(4) $$T_{wa} - \bar{T}_a = \frac{q_a}{h A_w} = \frac{.78}{.00213\ (3.18)} = 115^\circ R$$

$$T_{wa} = 355^\circ R$$

CALCULATE TEMP DISTRIBUTION IN HEATER. ELECTRICALLY HEATED, ASSUME UNIFORM HEAT FLUX.

USING EQ'N 13 FOR FILM COEFFICIENT

$$h = \frac{.023}{D_h} \left[\frac{4\dot{m}_2}{P_w}\right]^{0.8} \left[c_p\right]^{0.4} \frac{k_b}{\mu^{0.8}} \frac{\mu^{0.4}}{k^{0.4}}$$

& SINCE ALL TERMS EXCEPT k & μ ARE CONSTANT

$$h = .025 \frac{k^{0.6}}{\mu^{0.4}}$$

HEAT FLUX IS

$$\frac{q_a}{A_w} = \frac{.78}{3.18} = .245$$

CHOOSE 10 INCREMENTS

$$T_x = T_{x\ init.} + \int \frac{q}{c_p \dot{m}}\, dx$$

SINCE $\frac{q}{c_p \dot{m}}$ IS CONSTANT

$$\Delta T = Kx$$

$$T_{w_x} = \frac{q}{hA} + T_{init}$$

CHECK CONDUCTANCE IN SILICAN SLABS.

$$k_{silicon} = 200 \frac{BTu}{hr\,ft\,^\circ R} = .00463 \frac{BTu}{sec\,in\,^\circ R} \quad \text{(REF. 8)}$$

SLAB THICKNESS = .020

NEGLECT CONDUCTANCE

THERMAL CONTRACTION

SILICON WILL CONTRACT .02 % MAX IN RANGE OF INTEREST REF. 9

FOR 6061-T6 Al @ 140 R

$$\frac{\Delta L}{L} = .00375 \frac{IN}{IN}$$

SILICON CONTRACTION IS NEELIGIBLE

FOR AL ON .2 IN $\Delta L = .00075$

.112 IN $\Delta L = .00042$

THEREFORE ALLOWANCE MUST BE MADE IN HEATER SHELL DESIGN FOR THIS

APPENDIX A
SAMPLE CALCULATIONS

A LARGER PROBLEM IS THAT OF THERMAL STRESSES DUE TO CONTRACTION IF HEATER SHELL IS MOUNTED IMPROPERLY. CHECK DEFLECTIONS & STRESSES IN HEATER SHELL.

FROM REF. 11 THE MOMENT DISTRIBUTION ON A RECTANGULAR FRAME SUBJECTED TO UNIFORM INTERNAL PRESSURE IS:

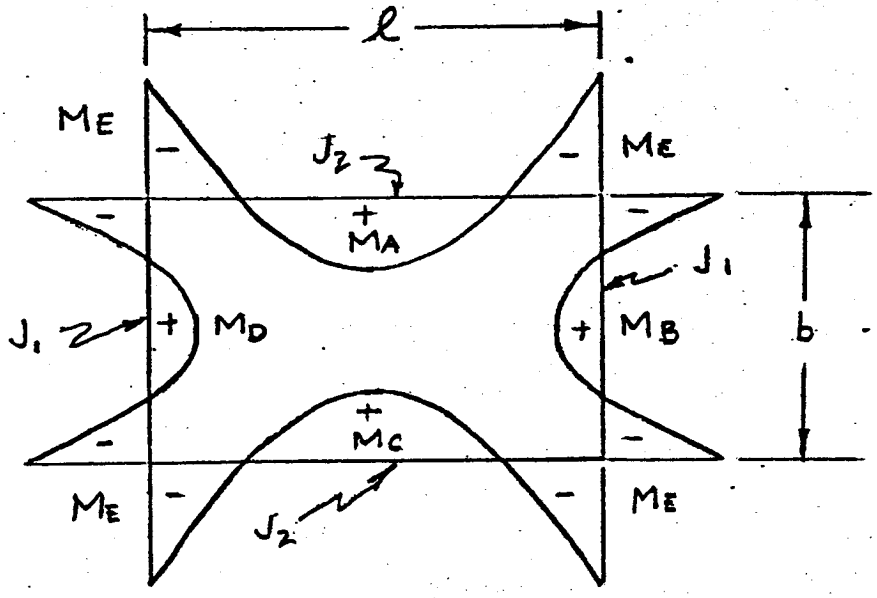

(−) INDICATES TENSION ON INSIDE

J ~ MOMENT OF INERTIA (in⁴)

N ~ AXIAL FORCE (lb)

M ~ MOMENT (in lb)

q ~ LOADING (lb/in)

$\beta \sim b/\ell$

$K \sim (J_2/J_1)\beta$

15) $N_1 = \frac{ql}{2}$

16) $N_2 = \frac{qb}{2}$

17) $M_E = -\frac{ql^2}{12}\frac{(1+\beta^2 K)}{1+K}$

18) $M_A = M_C = \frac{ql^2}{8} + M_E$

19) $M_B = M_D = \frac{qb^2}{8} + M_E$

$q = 125 \times 2 = 250$ lb/in

$N_1 = 25$ lb

$N_2 = 14$ lb

$J_1 = J_2$

$K = \beta = .56$

$M_E = -.629$ in-lb

$M_A = M_C = .621$ in-lb

$M_B = M_D = -.237$ in-lb

ON SIDE B & D SHELL DEFLECT INWARD

USE MOMENTS @ CORNERS & AXIAL FORCES AND CALCULATE DEFLECTION INWARD TREATING SIDE AS A BEAM. USE EQUATION DERIVED FROM ENERGY RELATIONSHIPS. (REF. 12)

20) $\delta \int \frac{M m \, dx}{EI}$

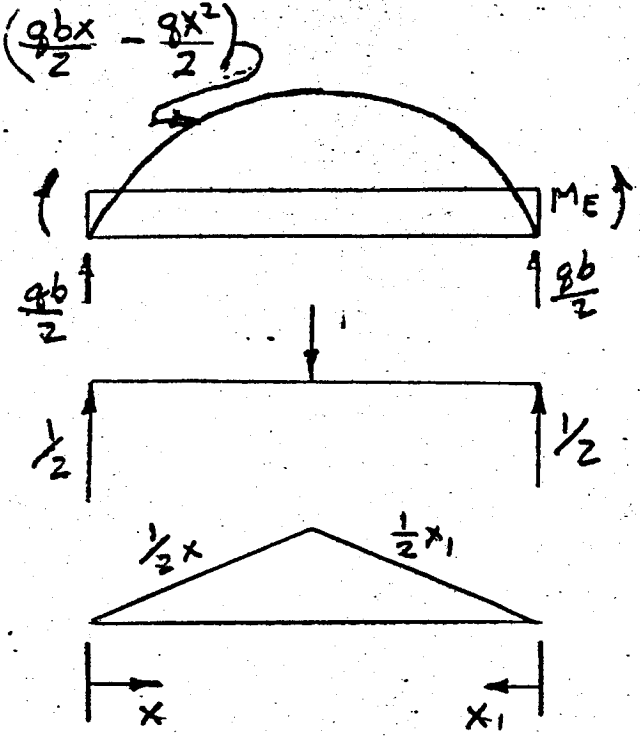

M = MOMENT DUE TO ACTUAL LOADING @ POSITION X

m = MOMENT DUE TO UNIT LOAD

$$\delta = \frac{2}{EI}\int_0^{b/2}\left(\frac{qb}{2}x - \frac{qx^2}{2} + M_e\right)\left(\frac{x}{2}\right)dx$$

$$= \frac{b^2}{8EI}\left[26b^2 + M_e\right] = \frac{.001495}{EI}$$

$E = 10.9 \times 10^6$ (REF 10)

21) $I = \frac{bh^3}{12} = \frac{2(.02)^3}{12} = 1.333(10^{-6})$

$$\delta = \frac{.001495}{(10.9)(1.333)} = 1.03 \times 10^{-4}$$

Inward deflection not excessive

LOOKING AT TOP & BOTTOM PLATE USING FLAT PLATE - SIMPLY SUPPORTED IS WORST CASE.

22) $$S = \frac{.75\, w b^2}{t^2(1+1.61\alpha^3)}$$

w = PRESSURE
b = WIDTH
a = LENGTH
t = THICKNESS
$\alpha = \frac{b}{a}$
S = stress

$b = .200$ IN
$a = 2$ IN
$t = .020$
$w = 125$ PSI

$S = 9350$ PSI

YIELD STRESS FOR 6061-T6 7.35,000PSI (REF. 10)

TENSILE STRESS FROM MOMENT IN CROSS-SECTION

23) $$S = \frac{MC}{I} \quad \frac{M\, t/2}{\frac{a t^3}{12}} = \frac{6M}{2(.02)^3} = 7500M$$

$$S = 7500(.629) = 4710$$

AXIAL STRESSES

$$S = \frac{P}{A} = \frac{125(.112)}{2 \times .02} = 322 \text{ PSI}$$

$$S = \frac{P}{A} = \frac{125(.200)}{.04} = 625 \text{ PSI}$$

APPENDIX A

SAMPLE CALCULATIONS

TOTAL CORNER STRESS

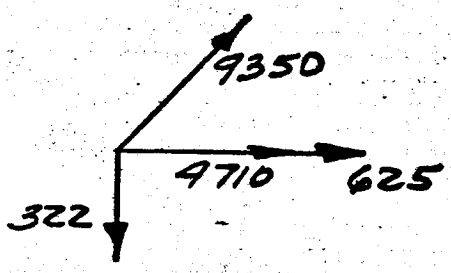

$$S = \sqrt{(322)^2 + (5335)^2 + (9350)^2}$$

$S = 10,800$ psi

M.S. = 3.24

Appendix B

LOG FUNCTION GENERATOR SPECIFICATION

Power Jet Supply

1. Fluid Media - Gaseous Helium
2. Pressure, P_f = 250 psia maximum
3. Temperature, T_f = 520°R approximately
4. Mass Flowrate - $\dot{m}_f = 6 \times 10^{-3}$ lb/sec maximum

Control Inputs

1. Fluid Media - Gaseous Helium
2. Temperature, T_{ca} and T_{cb} = 520°R approximately
3. Mass Flowrates, $\dot{m}_{ca}$ and $\dot{m}_{cb} = 1.5 \times 10^{-4}$ lb/sec maximum
4. Pressures, P_a, P_b, and $\Delta P = P_a - P_b$ as indicated in the following table.

Table I

Log Function Generator Input Pressure Signals

ABSOLUTE FLUX LEVEL, ϕ (PERCENT)	P_a (PSIA)	P_b (PSIA)	$P_a - P_b$ (PSID)
0	87.0475	87.0475	0
1	87.4873	87.0475	.4398
1.58	87.7303	87.0475	.6828
2.512	88.1196	87.0475	1.0721
3.981	88.808	87.0475	1.7606
6.3103	89.7812	87.0475	2.73376
10.6015	91.3407	87.0475	4.2319
15.8517	93.7216	87.0475	6.67414
25.12	97.3573	87.0475	10.3098
39.82	102.764	87.0475	15.7169
63.11	110.752	87.0475	23.704
100.03	121.756	87.0475	34.708
158.5	136.088	87.0475	49.041
251.27	153.425	87.0475	66.377

LOG FUNCTION GENERATOR SPECIFICATION

Output Signal

1. The output shall be a differential pressure proportional to a constant plus K ln ϕ; i.e., $\Delta P_o = C + K \ln \phi$

   $\Delta P_o \neq C + K \ln (\Delta Pi)$

2. At 0.01% flux level, P_{o1} and P_{o2} shall both be equal to 60 psia; i.e., $P_{o1} = P_{o2} = 60$ psia (with $P_{df} = 50$ psia).

3. The output, $\Delta P_o = P_{o1} - P_{o2}$, shall vary as follows:

TABLE II

Power Level (percent)	ΔP_o (psia)	P_{o1} (psia)	P_{o2} (psia)
0.01	0	60	60
0.05	1.74	60.87	59.13
0.1	2.5	61.25	58.75
1.0	5.0	62.5	57.50
10.0	7.5	63.75	56.25
100.0	10.0	65	55
150.0	10.44	65.22	54.78
200	10.76	65.38	54.62

4. The output accuracy, i.e., ΔP_o as a function of the input $P_a - P_b$, shall be within ± 5 percent absolute.
5. Frequency response shall be greater than 100 radians per second.
6. Output gain and zero adjustments are required.
7. Output noise may be filtered at frequencies greater than 80 cps.

BASIC EQUATIONS - ANALOG

MODEL OF SENSING UNIT

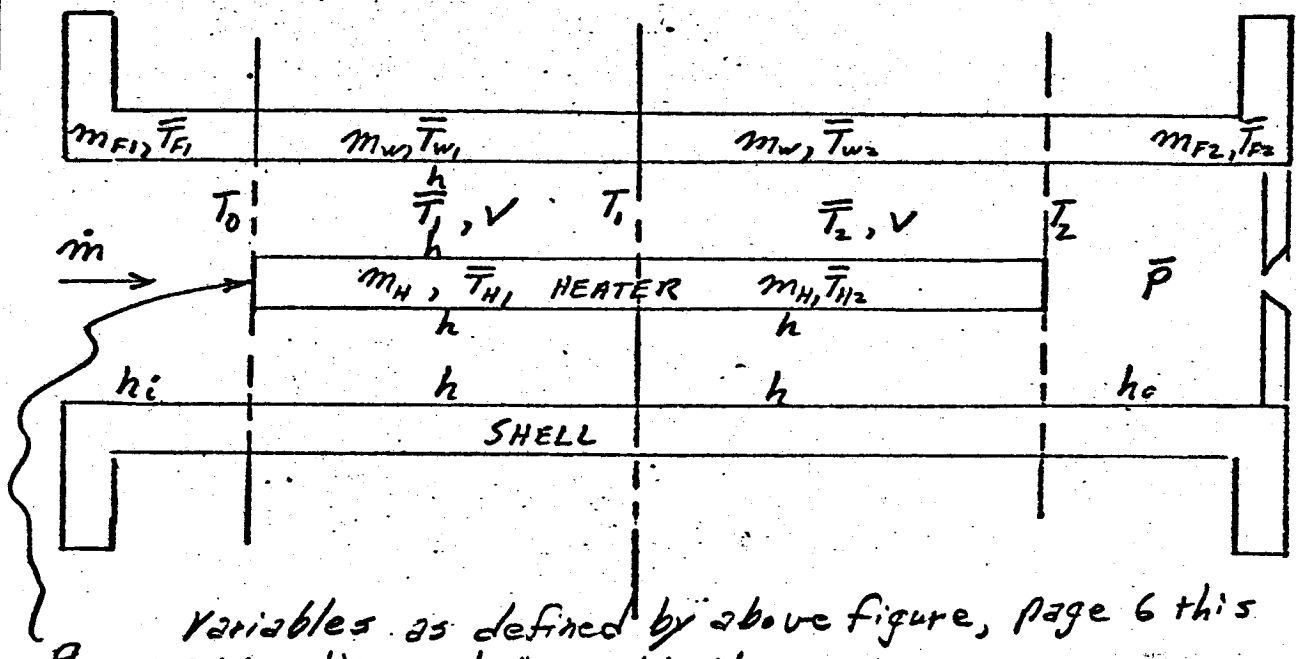

q_{IN}

Variables as defined by above figure, page 6 this appendix and Appendix H

1. $$m_H C_H \frac{d\bar{T}_{H1}}{dt} = q_{IN} - hA_H(\bar{T}_{H1} - \bar{T}_1) - K_c(\bar{T}_{H1} - \bar{T}_{w1}) + K_1(\bar{T}_{H2} - \bar{T}_{H1})$$

2. $$m_H C_H \frac{d\bar{T}_{H2}}{dt} = q_{IN} - hA_H(\bar{T}_{H2} - \bar{T}_2) - K_c(\bar{T}_{H2} - \bar{T}_{w2}) - K_1(\bar{T}_{H2} - \bar{T}_{H1})$$

3. $$\frac{\bar{P}V}{R\bar{T}_1} C_p \frac{d\bar{T}_1}{dt} = \dot{m} C_p (T_0 - \bar{T}_1) + hA_H(\bar{T}_{H1} - \bar{T}_1) - hA_w(\bar{T}_1 - \bar{T}_{w1}) + h_i A_{F1}(\bar{T}_{F1} - T_0)$$

4. $$\frac{\bar{P}V}{R\bar{T}_2} C_p \frac{d\bar{T}_2}{dt} = \dot{m} C_p (T_1 - \bar{T}_2) + hA_H(\bar{T}_{H2} - \bar{T}_2) - hA_w(\bar{T}_2 - \bar{T}_{w2}) + h_o A_{F0}(\bar{T}_{F2} - T_2)$$

5. $$m_w C_w \frac{d\bar{T}_{w_1}}{dt} = hA_w(\bar{T}_1 - \bar{T}_{w_1}) + K_2(\bar{T}_{w_2} - \bar{T}_{w_1}) - K_3(\bar{T}_{w_1} - \bar{T}_{F_1}) + K_c(\bar{T}_{H_1} - \bar{T}_{w_1})$$

6. $$m_w C_w \frac{d\bar{T}_{w_2}}{dt} = hA_w(\bar{T}_2 - \bar{T}_{w_2}) - K_2(\bar{T}_{w_2} - \bar{T}_{w_1}) - K_3(\bar{T}_{w_2} - \bar{T}_{F_2}) + K_c(\bar{T}_{H_2} - \bar{T}_{w_2})$$

7. $$m_{F_1} C_w \frac{d\bar{T}_{F_1}}{dt} = h_i A_{F_1}(T_0 - \bar{T}_{F_1}) + K_3(\bar{T}_{w_1} - \bar{T}_{F_2})$$

8. $$m_{F_2} C_w \frac{d\bar{T}_{F_2}}{dt} = h_o A_{F_2}(T_2 - \bar{T}_{F_2}) + K_3(\bar{T}_{w_2} - \bar{T}_{F_2})$$

9. $$\bar{P} = K_m \sqrt{T_2}$$

10 $$T_2 = 2\bar{T}_2 - \bar{T}_1$$

11 $$T_0 = \text{fixed}$$

12 $$T_1 = 2\bar{T}_1 - T_0.$$

PREPARED BY: RS	ROCKETDYNE A DIVISION OF NORTH AMERICAN AVIATION, INC.	PAGE NO. 3 OF 7
CHECKED BY:	NUMERICAL EQUATIONS -	REPORT NO.
DATE: 8/22/66	SENSING ELEMENT ANALOG MODEL	MODEL NO.

$$\frac{dT_{H_1}}{dt} = 7890\, q_{IN} - 18.08 \frac{h}{h_o}\left(\bar{T}_{H_1} - \bar{T}_1\right) - 0\left(\bar{T}_{H_1} - \bar{T}_{w_1}\right) + .212\left(\bar{T}_{H_2} - \bar{T}_{H_1}\right)$$

$$= 7890\, q_{IN} - \left(18.08 \frac{h}{h_o} + 0 + .212\right)\bar{T}_{H_1} + 18.08 \frac{h}{h_o}\bar{T}_1 + 0\,\bar{T}_{w_1} + .212\,\bar{T}_{H_2}$$

$$\frac{dT_{H_2}}{dt} = 7890\, q_{IN} - \left(18.08 \frac{h}{h_o} + 0 + .212\right)\bar{T}_{H_2} + 18.08 \frac{h}{h_o}\bar{T}_2 + 0\,\bar{T}_{w_2} + .212\,\bar{T}_{H_1}$$

$$\bar{P} = 6.79\sqrt{T_2}$$

$$\frac{d\bar{T}_1}{dt} = \frac{\bar{T}_1}{\bar{P}}\left[1210\left(T_o - T_1\right) + 710 \frac{h}{h_o}\left(\bar{T}_{H_1} - \bar{T}_1\right) - 13.35 \frac{h_w}{h_{wo}}\left(\bar{T}_1 - \bar{T}_{w_1}\right) + 1.69 \frac{h_F}{h_{FO}}\left(\bar{T}_{F_1} - T_o\right)\right]$$

$$= \frac{\bar{T}_1}{\bar{P}}\left[\left(1210 - 1.7 \frac{h_F}{h_{FO}}\right)T_o - 1210\,T_1 + 710 \frac{h}{h_o}\bar{T}_{H_1} - \left(710 \frac{h}{h_o} + 13.35 \frac{h_w}{h_{wo}}\right)\bar{T}_1 + 13.35 \frac{h_w}{h_{wo}}\bar{T}_{w_1} + 1.7 \frac{h_F}{h_{FO}}\bar{T}_{F_1}\right]$$

$$= \frac{\bar{T}_1}{\bar{P}}\left[1208\,T_o - 1210\,T_1 + 710\,\bar{T}_{H_1} - 723\,\bar{T}_1 + 13.35\,\bar{T}_{w_1} + 1.7\,\bar{T}_{F_1}\right]$$

$(2\bar{T}_1 - T_o)$

$$\frac{d\bar{T}_2}{dt} = \frac{\bar{T}_2}{\bar{P}}\left[1210\,(T_1 - T_2) + 710\,\frac{h}{h_o}\,(\bar{T}_{H2} - \bar{T}_2) - 13.35\,\frac{h_w}{h_{wo}}\,(\bar{T}_2 - \bar{T}_{w2}) + 1.69\,\frac{h_F}{h_{FO}}\,(\bar{T}_{F2} - \bar{T}_2)\right]$$

$$= \frac{\bar{T}_2}{\bar{P}}\left[1210\,T_1 - \left(1210 + 1.7\,\frac{h_F}{h_o}\right)T_2 + 710\,\frac{h}{h_o}\,\bar{T}_{H2} - \left(710\,\frac{h}{h_o} + 13.35\,\frac{h_w}{h_{wo}}\right)\bar{T}_2 + 13.35\,\frac{h_w}{h_{wo}}\,\bar{T}_{w1} + 1.7\,\frac{h_F}{h_{FO}}\,\bar{T}_{F1}\right]$$

$$= \frac{\bar{T}_2}{\bar{P}}\left[1210\,T_1 - 1212\,T_2 + 710\,\bar{T}_{h2} - 723\,\bar{T}_2 + 13.35\,\bar{T}_{w2} + 1.7\,\bar{T}_{F2}\right]$$

$$\frac{d\bar{T}_{w1}}{dt} = .0623\,\frac{h}{h_o}\,(\bar{T}_1 - \bar{T}_{w1}) + .1222\,(\bar{T}_{w2} - \bar{T}_{w1}) - .1438\,(\bar{T}_{w1} - \bar{T}_{F1}) + 0\,(\bar{T}_{H1} - \bar{T}_{w1})$$

$$= .0623\,\frac{h}{h_o}\,\bar{T}_1 - \left(.0623\,\frac{h}{h_o} + .2660\right)\bar{T}_{w1} + .1222\,\bar{T}_{w2} + .1438\,\bar{T}_{F1} + 0\,\bar{T}_{H1}$$

$$= .0623\,\frac{h}{h_o}\,\bar{T}_1 - .3283\,\bar{T}_{w1} + .1222\,\bar{T}_{w2} + .1438\,\bar{T}_{F1} + 0\,\bar{T}_{H1}$$

$$\frac{d\bar{T}_{w_2}}{dt} = .0623\,\bar{T}_2 - .3283\,\bar{T}_{w_2} + .1222\,\bar{T}_{w_1} + .1438\,\bar{T}_{F_2} + O(\bar{T}_{H_2})$$

$$\frac{d\bar{T}_{F_1}}{dt} = .0177\,(T_0 - \bar{T}_{F_1}) + .323\,(\bar{T}_{w_1} - \bar{T}_{F_1})$$

$$R_1 = .0177\,T_0 - .3407\,\bar{T}_{F_1} + .323\,\bar{T}_{w_1}$$

$$\frac{d\bar{T}_{F_2}}{dt} = .0177\,\bar{T}_2 - .3407\,\bar{T}_{F_2} + .323\,\bar{T}_{w_2}$$

PREPARED BY: RS	TABLE I ROCKETDYNE A DIVISION OF NORTH AMERICAN AVIATION, INC.	PAGE NO. 6-7
CHECKED BY:	TABLE OF NOMINAL SYSTEM	REPORT NO.
DATE:	PARAMETERS	MODEL NO.

PARAMETER	SYMBOL	VALUE *
1. Heater element equivalent lumped mass	m_H	.001014 lb_m
2. Wall equivalent lumped mass	m_W	.00346 lb_m
3. End flange equivalent lumped mass	m_F	.001538 lb_m
4. Heater element specific heat	C_H	.125 $\frac{BTU}{lb_m\,^\circ R}$
5. Wall & flange material specific heat	C_W	.20 $\frac{BTU}{lb_m\,^\circ R}$
6. Overall heat transfer coeff- heater to gas	hA_H	2.29×10^{-3} $\frac{BTU}{sec\,^\circ R}$
7. Overall heat transfer coeff- gas to wall	hA_W	4.31×10^{-5} $\frac{BTU}{sec\,^\circ R}$
8. Overall heat transfer coeff- gas to flange	$h_i A_{F_i}$	$.545\times10^{-5}$ $\frac{BTU}{sec\,^\circ R}$
9. Conductance between heater element lumps	K_1	2.69×10^{-5} $\frac{BTU}{sec\,^\circ R}$
10. Conductance between heater and wall	K_C	0 $\frac{BTU}{sec\,^\circ R}$
11. Conductance between wall lumps	K_2	8.46×10^{-5} $\frac{BTU}{sec\,^\circ R}$
12. Conductance between wall and flange	K_3	9.95×10^{-5} $\frac{BTU}{sec\,^\circ R}$

* all values are on a per lump basis (see schematic)

ANALOG MODEL PNEUMATIC FLUX DETECTOR SENSING ELEMENT

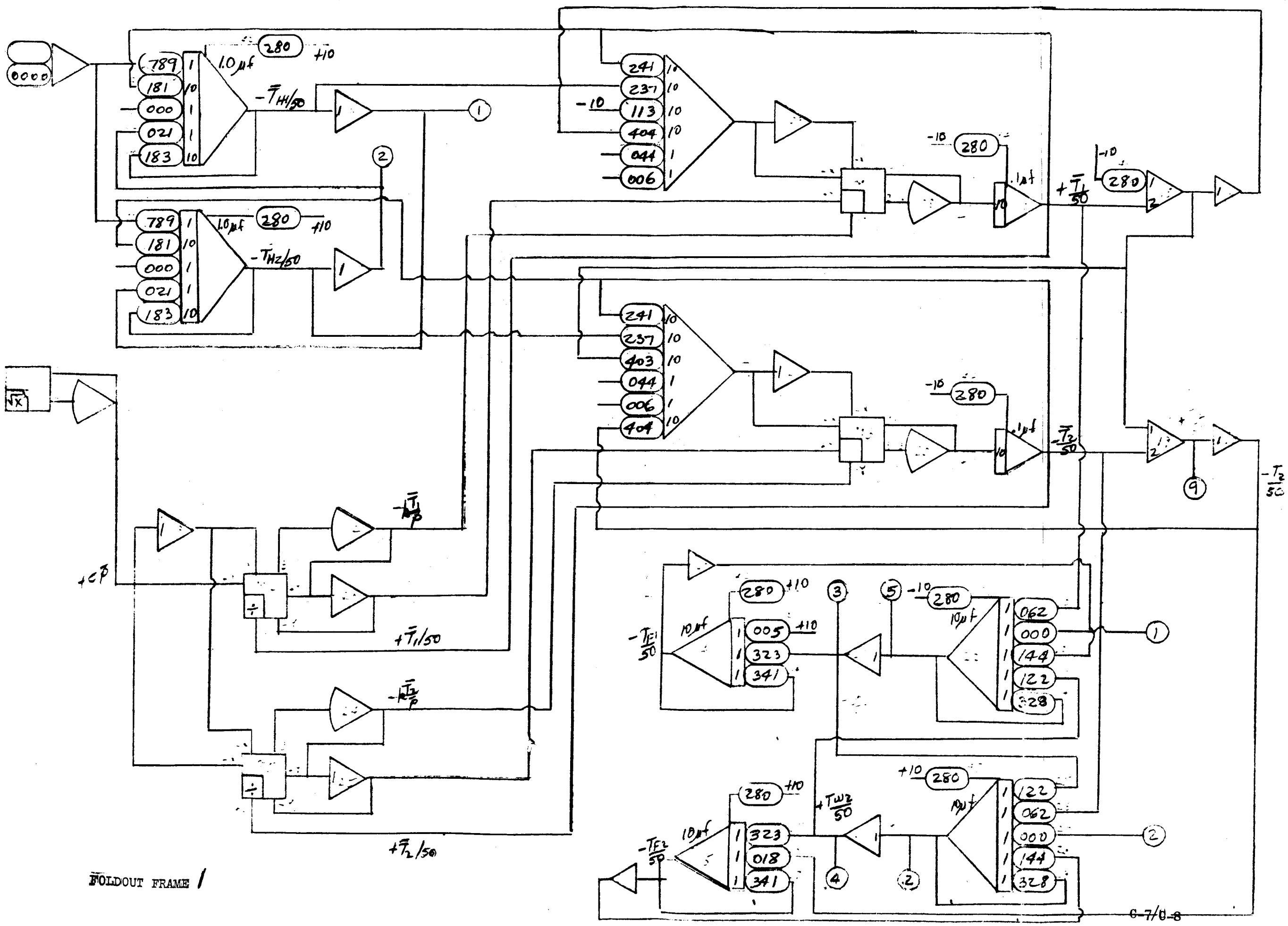

FOLDOUT FRAME 1

FOLDOUT FRAME 2

APPENDIX D

PRECOOLER CALCULATIONS

DEWPOINT OF MIL-SPEC HELIUM = -70° F
EXTROPOLATING FROM DATA OF KEENAN & KEYES, COOLING TO -116° SHOULD ICE OUT 90% OF THE WATER VAPOR.

$$\left(W_S = .0001227 \frac{16 H_2O}{16 H_C} \text{ @ AMBIENT}\right)$$

USE 4 - $\frac{1}{4}$" OD TUBE, .020 WALL (.210 ID) TO ACCOMPLISH THIS.

$$\dot{m} = \frac{.00624}{4} \text{ 16m/SEC} = .001565 \text{ LB}_m\text{/SEC}$$

ASSUME $0\Delta t$ ACROSS TUBE WALL.

$$N_R = \frac{4\dot{m}}{\pi d \mu} = \frac{4(.001565)(12)}{\pi (.210)(.000672)\mu} = \frac{169.4}{\mu}$$

WHERE μ IS IN CENTIPOISES

$$P_r = \frac{C_p \mu}{K}$$ FOR HELIUM, P_r IS RELATIVELY CONSTANT

WITH $(P_r)^{0.4} \sim .855$

TO START WITH, INTEGRATE OVER 10" LONG SECTOR

$$hA = \frac{hD}{K}\frac{K}{D} A = .023 (N_R)^{.8} (P_R)^{.4} \frac{H}{D} A$$

$$= .023 (N_R)^{.8} (.855) \frac{K}{.210} (12) \frac{\pi (.210)(10)}{144}$$

$$= \underline{\underline{.0515 (N_R)^{.8} K}}$$

ON BOILING SIDE, USE CORRELATION FOR STABLE POOL FILM BOILING AROUND A HORIZONTAL TUBE WITH

$$\left(\frac{q}{A}\right)\frac{(LEG)^{\frac{1}{4}}}{C_5} = f(\Delta T)$$

(WALL SUPERHEAT)

$LEG = D = .250/12 = .02083$

$C_5 = 0.62$

$$q = f(\Delta T)\, A \frac{C_5}{(LEG)^{\frac{1}{4}}} = \frac{.250\,\pi\,(10)}{144}\frac{(.62)}{.380} f(\Delta t)$$

$$= \underline{\underline{.0890\, f(\Delta t)}}$$

① $T_o = 560\,F \quad N_R = \dfrac{169.4}{2040 \times 10^{-5}} = 8300$

$hA = .0515\,(1370)(.090) = 6.35$

$q = 6.35\,(560 - T_w) = .089\, f(T_w - 140)$

$T_w = 500 \qquad .089\,(4700) = 419$

$T_w \;\; 381$

$495 \qquad .089\,(4600) = 409$

413

$q = 410$

$$\tilde{T}_1 = T_o - \frac{q}{C_{pm}} = T_o - \frac{q}{1.248\,(.001565)(3600)}$$

$$= T_o - \frac{q}{7.03}$$

$= 560 - 58.3 = 560.0$

501.7

$2 \overline{)1061.7}$

530.8

$$\tilde{T}_1 = 560 - \frac{390.8}{420.0}(58.3) = 560 - 55.2 = 504.8$$

$$560.0$$

$$1064.8$$

$$T_{AV} = 532.4$$

$$N_R = \frac{169.4}{1950 \times 10^{-5}} = 8690$$

$$hA = .0515(1420)(.0865) = 6.32$$

$$632(532.4 - T_w) = .0890 f (T_w - 140)$$

$T_w = 480$ $\quad .0890(4450) = 396$

331

$T_w = 475$ $\quad .0890(4400) = 391$

363

$T_w = 470$ $\quad .0890(4300) = 383$

394.5

$g = 386 \quad T_w\ 472$

$$\tilde{T}_1 = 560 - \frac{386}{7.03} = 560 - 54.9$$

$$= 505.1 \quad VS \quad 504.8$$

② $T_{AV} = 338 + 140 = 478$

$$N_R = \frac{169.4}{1840 \times 10^{-5}} = 9210$$

$$hA = .0515(1490)(.0810) = 6.21$$

$$6.21(478 - T_w) = .0890 f (T_w - 140)$$

$T_w = 430$ $\quad .0890(380) = 338$

236

$T_w = 425$ $\quad .0890(375) = 334$

329

$g = 334 \quad T_w\ 425$

$$\tilde{T}_2 = 505 - \frac{3.34}{7.03} = 505 - 47.5 = 457.5$$

457.5
505.0
$2\overline{)962.5}$
481.2

$T_{av} = 480$

$6.21(480 - T_w) = .0890 f (T_w - 140)$

$T_w = 425$ $\quad .0890(375) = 334$
342

$T_w = 426$
335 $\quad q = 335 \quad T_2 = 457$

③

$T_{av} = 296. + 140 = 436$

$N_R = \frac{169.4}{1720 \times 10^{-5}} = 9850$

$hA = .0515\ (1580)(.076) = 6.19$

$6.19(436 - T_w) = .0890 f (T_w - 140)$

$T_w = 385$ $\quad .0890(326) = 290$
316

$T_w = 388$ $\quad .0890(330) - 294$
297

$q = 295$

$T_3 = 457 - \frac{295}{7.03} = 457 - 42$

415
557
$2\overline{)872}$
436 OK.

④

$T_{av} = 257 + 140 = 397$

$N_R = \frac{169.4}{1620 \times 10^{-5}} = 10460$

$hA = .0515\ (1640)(.0717) = 6.16$

$6.16\,(397 - T_w) = .0890 f\,(T_w - 140)$

$T_w = 352 \qquad .0890\,(287) = 256$

277

$T_w = 354 \qquad .0890(290) = 258$

265

$f = 258 \qquad T_w = 355$

$T_4 = 415\,\frac{258}{7.03} = 415 - 367 =$

$= 378.3$

$2\overline{)793.3}\quad 415.0$

396.6 vs 397 ✓

CONCLUSION: 50 IN. ARE REQUIRED TO REACH
$T - 140 = 204°R.$

PRESSURE DROP FOR THIS TUBING

$e = .001 \quad \frac{e}{d} = \frac{.001}{.210} = .00476$

USE INLET $N_R = 8300$, $\rho = \frac{80}{386(12)(560)} = 3.09 \times 10^{-5}$ lb/in^3

$f = .04$

$\Delta P/50'' = f\frac{l}{d}\rho\frac{V^2}{2g} = f\frac{l}{d}\frac{\dot{m}^2}{2\rho A^2 g} \qquad A = .0346$

$= \frac{.04}{.04}\left(\frac{50}{.21}\right)\left(\frac{.001565^2}{2 \times 3.09\times10^{-5}(.0346)^2(386)}\right)$

$= .817$ PSI

FOR A FACTOR OF SAFETY OF 6, USE 300"
↳ 5 PSI ΔP (10 COILS, 10" DIA.)
(9 COILS, 17" DIA.)

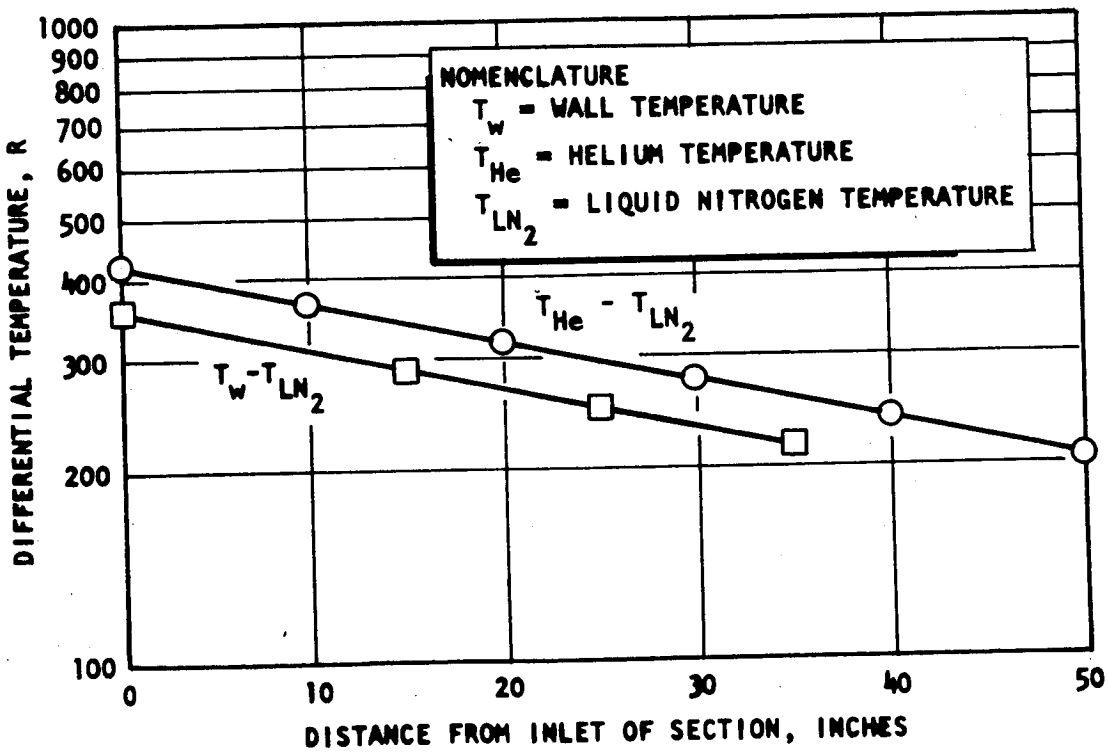

Figure D-1. Temperature Distribution De-Icing Section of Precooler

THE REMAINDER OF THE HEAT EXCHANGER WILL SERVE TO DROP THE TEMP. FROM $-116 = 344\,^{\circ}R$ TO $142\,^{\circ}R$.
I ASSUME 15 PARALLEL PATHS OF $\frac{1}{8}$" OD, .020 WALL TUBING

$$\dot{m} = .000417 \text{ lbm/SEC}$$

$$N_R = \frac{4(.000417)(12)}{\pi(.85)(.000672)\mu} = \frac{116.0}{\mu}$$

WE INTEGRATE OVER 20" LONG SECTIONS

$$hA = .023(N_R)^{.8}(.855)\frac{k}{.085}(12)\frac{\pi(.085)(20)}{144/12}$$

$$= .1030(N_R)^{.8}k$$

$$LEG = \frac{.125}{12} = .01042$$

$$q = f(\Delta T)\frac{.125\pi}{144}(20)\frac{(.62)}{.317}$$

$$= .1068 f(\Delta T)$$

$$T_i = T_{i-1} - \frac{q}{1.248(.000417)(3600)}$$

$$= T_{i-1} - \frac{q}{1.874}$$

① $T_o = 344\,^{\circ}R \quad N_R = \frac{116.0}{1470\times10^{-5}} = 7890$

$$hA = .1030(1320)(.0655) = 8.90$$

$$8.90(344 - T_w) = .1068 f(T_w - 140)$$

$T_w = 320$		$.1068(2500) = 154$
214		
$T_w = 315$		$.1068(2420) = 258$
258		

$$\bar{T}_1 = 344 - \frac{258}{1.874} = 344 - 133.7$$

$$\begin{array}{r} 133.7 \\ \hline 210.3 \\ 344.0 \\ \hline 2\overline{)554.3} \\ 277.1 \end{array}$$

$$\bar{T}_1 = 344 - \frac{137.1}{204}(133.7) = 344 - 88.9$$

$$\begin{array}{r} 89 \\ \hline = 255 \\ 344 \\ \hline 599 \end{array}$$

$$T_{aw} = 300$$

$$N_R = \frac{116.0}{1350 \times 10^{-5}} = 8600$$

$$h_A = .1030\,(1400)(.060) = 8.65$$

$$8.65\,(300 - T_w) = .1068 f\,(T_w - A_0)$$

$T_w = 280$ $\qquad .1068\,(2000)$

173 $\qquad = 214$

$T_w = 276$ $\qquad .1068\,(1950)$

208 $\qquad = 208$

$$\bar{T}_1 = 344 - \frac{208}{1.874} = 344 - 111 = \begin{array}{r} 233 \\ 344 \\ \hline 2\overline{)577} \\ 288.5 \end{array}$$

$T_{aw} = 292$

$$8.65\,(292 - T_w) = .1068 f\,(T_w - 140)$$

$T_w = 270$ $\qquad 199$

190 $\qquad$ SAME

$T_w = 269$

199

$$\bar{T}_1 = 344 - 106.2 \qquad \begin{array}{r} 344 \\ 237.8 \\ \hline 581.8 \\ 290.9 \end{array}$$

(2)

$T_{av} = 63 + 140 = 203$

$N_R = \frac{116.0}{1020 \times 10^{-5}} = 11380$

$h_A = .1030(1770)(.0464) = 8.45$

$8.45\,(203 - T_w = .1068f\,(T_w - 140)$

$T_w = 190 \qquad .1068(840) = 89.7$

110

$T_w = 192 \qquad .1068(860) = 91.9$

93.0

$q = 92$

$\tilde{T}_2 = 237.8 - \frac{92}{1.874} = 237.8 - 49 - 1 = 188.7$

426.5

$213.2 = T_{ai}$

$T_{ai} = 210$

$8.45(210 - T_w) = 1068f\,(T_w - 140)$

$T_w = 198 \qquad 1068(950) = 100.6$

101.5

$q = 101$

$\tilde{T}_2 = 237.8 - \frac{101}{1.874} = 237.8 - 54.0 - 183.8$

$T_{av} = 210.8$

(3) $T_{av} = 172$

$N_R = \frac{116.0}{900 \times 10^{-5}} = 12900$

$LA = .1030(1820)(.0415) = 7.78$

$7.78\,(172 - T_w) = .1068f\,(T_w - 140)$

$T_w = 165 \qquad .1068f(490) - 52.3$

54.4

$T_w = 165.2$

52.9 $\qquad\qquad$ 52.5

$\bar{T}_3 = 183.8 - 28.00 =$

155.8

$2\overline{)339.6}$

169.8

$T_{av} = 171$

$7.78(171 - T_w) = .1068f(T_w - 140)$

$T_w = 164.5$ $\qquad$ $.1068(480) = 51.3$

50.6

$g = 51$

$\bar{T}_3 = 183.8 - 27.2$

27.2

156.6

340.4 $\qquad$ $T_3 = 157$

170.2

④ $T_{av} = 151.8$

$N_R = \dfrac{116.0}{850 \times 10^{-5}} = 13660$

$LA = .1030(2000)(.038) = 7.83$

$7.83(151.8 - T_w) = .1068f(T_w - 140)$

$T_w = 148$ $\qquad$ $.1068(210) = 22.4$

29.8

$T_w = 148.8$ $\qquad$ $.1068(245) = 26.2$

23.5

$T_w = 148.6$ $\qquad$ $.1068(240) = 25.6$

25.0

$g = 25.3$

$\bar{T}_1 = 157 - 13.5 = 143.5$ $\qquad$ 143.5 / 157.0 / 300.5 $\qquad$ $150.2\ T_{av}$

$T_{av} = 151$

$7.83(151 - T_w) = .1068f(T_w - 140)$

$T_w = 148$ $\qquad$ 22.4

23.5

$T_w = 147.9$

22.7 $\qquad$ SAY $g = 22.5$

$T_4 = 157 - 12 = 145$ ✓ $\qquad$ 157

$2\overline{)302}$

151 ✓

SO IN 80" WE GET DOWN TO 145°R

USING A FACTOR OF SAFETY OF 5,

THIS SAYS 400".

ASSUME MINIMUM COIL DIA = 3"

42 COILS 396"

FOR 18" COIL HEIGHT .429 COIL SPACING OK.

ASSUME FOLLOWING COIL CONFIGURATION

INNER $\qquad\qquad\qquad\qquad\qquad\qquad\qquad\qquad$ OUTER

1 - 1 - 1 - 1 - 2 - 2 - 2 - 2 3

3" 3.75" 4.50" 5.25" 6.00" 6.75" 7.50" 8.25 9.00

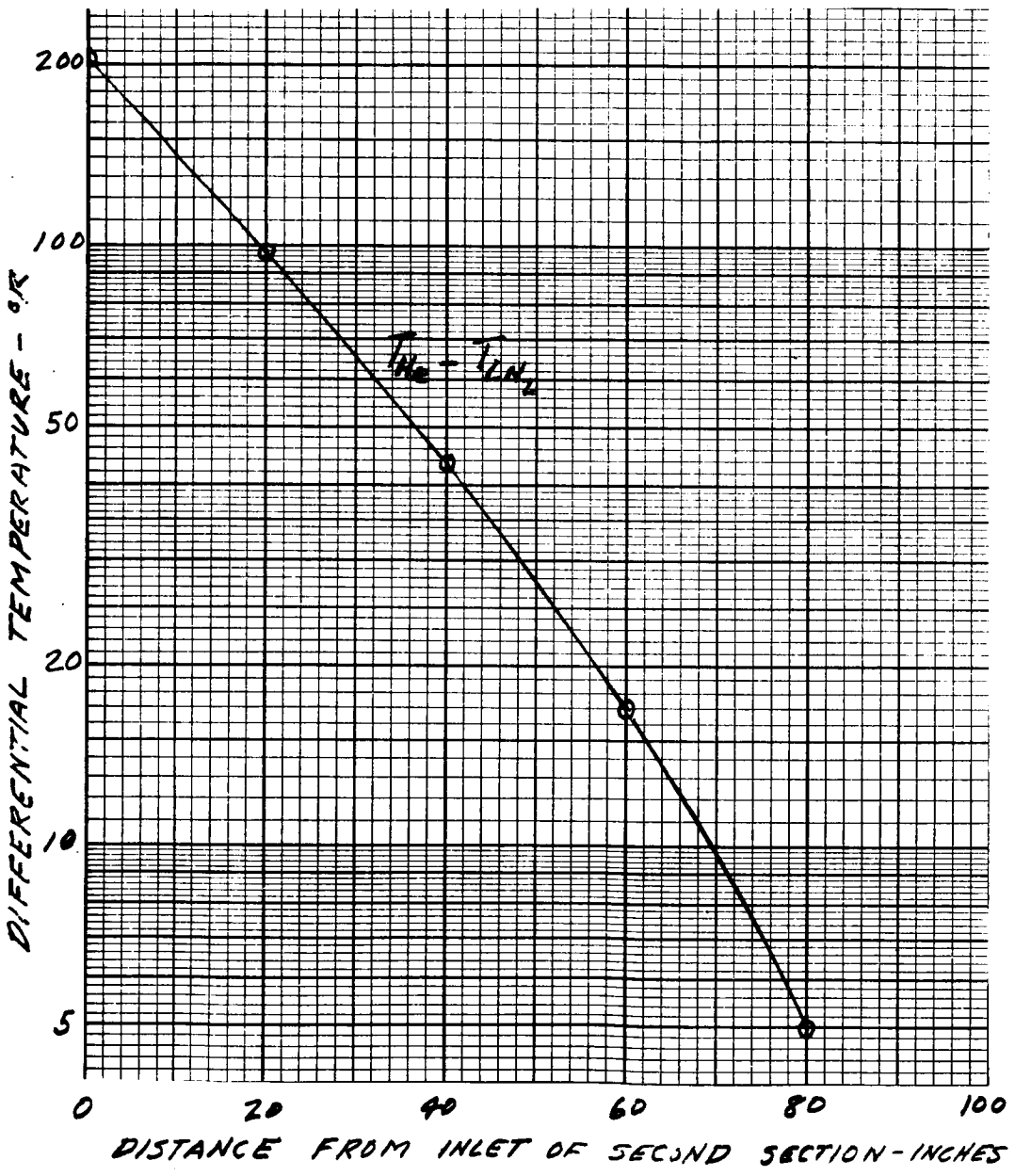

Figure D-2. Temperature Distribution Second Section of Precooler

CHECK PRESSURE DROP IN SECOND SECTION

$T_{av} \sim 300\ ^\circ R$
$N_R = 8600$

$$\rho = \frac{80}{386\,(12)(300)} = .0000576 = 5.76 \times 10^{-5}$$

$$\frac{e}{D} = \frac{.001}{.085} = .0118 \qquad A = .00567 \text{ IN}$$

$$f = .041$$

$$\Delta P = .041 \left(\frac{400}{.085}\right) \frac{(.000417)^2}{2\,(5.76 \times 10^{-5})(.00567)^2(386)}$$

$$= 2.34 \qquad \text{OK}$$

ESTIMATE TOTAL DROP FOR PRECOOLER (INCLUDING ENTRANCE AND EXIT LOSSES, DROPS DUE TO CURVATURE OF TUBING, ETC) $\sim$ 30 PSI.

NITROGEN REQUIREMENTS

.00626 LB/SEC He

$\Delta T = 560 - 140 = 420^\circ R$

$C_p = 1.248 \frac{BTU}{LB\ ^\circ R}$

$q = .00626\ (1.248)(420) = 3.28\ BTU/SEC$

HEAT OF VAPORIZATION OF LN_2 $= 98.25 - 12.51$
$85.74\ BTU/LB$

LN_2 EVAPORATE

$= \frac{3.28}{85.74} = .0382\ LB/SEC$

$= 138\ LB/HR$

AT 14.7 PSIA, $\rho_G = .285\ LB/FT^3 = .000165\ LB/IN.^3$

i.e., $\frac{0382}{.285} = .134 \frac{FT^3}{SEC} = 232\ IN^3/SEC$

FOR 0.1 PSI ΔP THROUGH SENIOR

$$A = \frac{\dot{m}}{\sqrt{2g\rho\Delta P}} = \frac{.0382}{\sqrt{2(386)(.000165)(.1)}}$$

$$= \frac{.0382}{\sqrt{.01272}} = \frac{.0382}{.1127} = 34\ IN.^2$$

APPENDIX E

TEMPERATURE EQUALIZER CALCULATIONS

CONFIGURATION

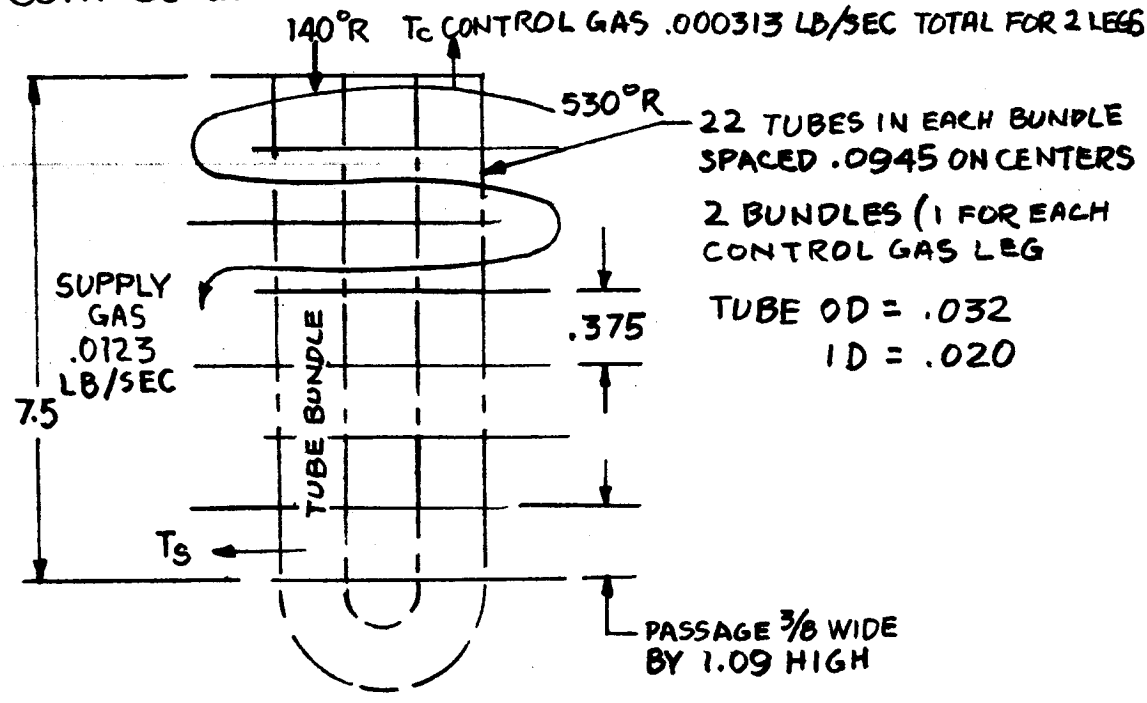

ESTIMATE FOR $T_S \approx T_C$

$$.0123\,(530 - T_C) = .000313\,(T_C - 140)$$

$$T_C = 521^\circ R$$

(ESSENTIALLY CONSTANT TEMPERATURE ON SUPPLY SIDE)

$$Q = .000313\,(1.248)(3600)(521 - 140)$$

$$= 536 \text{ BTU/HR}$$

$$q_T = 14.9 \ \frac{\text{BTU}}{\text{HR - TUBE}}$$

INSIDE TUBE : $N_R = \frac{4\dot{m}}{\pi d \mu} = \frac{9.89}{\mu}$ (μ IN C.P.)

REYNOLDS NUMBERS WILL BE LAMINAS

FOR TUBE INTERIOR, USE CORRELATION OF Mc ADAMS FIG. 9.17, USING k EVALUATION AT

$$T_{av} = \frac{521+140}{2} = 330\,^{\circ}R$$

FOR TUBE EXTERIOR, USE CORRELATION OF McADAMS EQ 10-11A P. 272

$$\frac{h_m D_o}{k_f} = 0.33 \left[\frac{c_p \mu}{k}\right]^{\frac{1}{3}} \left[\frac{D_o G_{max}}{\mu}\right]^{0.6}$$

ESSENTIALLY CONSTANT PROPERTIES AT 520°R

$$\frac{c_p \mu}{k} \approx .65$$

$$G_{MAX} = \frac{\dot{m}}{A} = \frac{.0123(144)}{(1.09-12\ (.032))(.375)}$$

$$= 6.68$$

$$\frac{D_o G_{max}}{\mu} = \frac{.032}{12}\left(\frac{6.68}{.000672\ (1950\times10^{-5})}\right)$$

$$= 1360$$

$$\frac{h D_o}{k} = 0.33\,(.87)\,(76) = 21.8$$

$$h = \frac{.086}{.032}\,(12)\,(21.8) = 703$$

$$hA = 703\,(\pi)\,\frac{(.032)}{12}\,\frac{(15)}{12} = 7.36 \text{ FOR 15" TUBING}$$

BACK TO THE COLD SIDE:

FOR 44 .020 I.D. TUBES

$$\dot{w} = \frac{.000313}{44}(3600) = .0256 \ {}^{lb}/_{m} - \text{TUBE}$$

$$k_{330} = .0635$$

$$\frac{\dot{w} c_p}{kL} = \frac{.0256(1.248)(12)}{.0635(15)} = .403$$

$$\frac{h_{av} D}{k} = .25$$

$$h_{av} A = \frac{h_{av} D}{k} \frac{k}{D} \pi DL = .25(.0635)\pi\left(\frac{15}{12}\right)$$

$$= .0623$$

NOTE THAT THIS IS TWO ORDERS OF MAGNITUDE LESS THAN THE hA ON THE HOT SIDE. SO WE CAN SAY $T_{w_{av}} = 520°R$

$$Q = .0623(520 - 330) = 12 \text{ BTU/hm}$$

OK - ADD SOME LENGTH TO TUBE INLET AND EXIT SECTION AND AROUND BENDS AND WE'RE IN. (ALSO NOTE FLOW RATE AT 140° R INLET WILL BE LESS THAN MAX LFG FLOW RATE)

ΔP ON COLD SIDE

UPPER BOUND FOR ΔP OCCURS IF ALL FLOW OCCURS AT 80 PSI, 520°R.

$$\text{THEN } N_R = \frac{4\dot{m}}{\pi d \mu} = \frac{4(.000313)}{44\pi(.020)(108.6\times10^{-8})}$$

$$= 417$$

$$f = \frac{64}{N_R} = \frac{64}{417} = .1536$$

$$\Delta P = f\frac{L}{D}\,\frac{m\cdot 2}{2\rho A^2 G} \qquad \rho = 3.32\times10^{-5}\ LB/IN^2$$

$$\dot{m}^2 = \left(\frac{.000313}{44}\right)^2$$

$$= .506\times10^{-10}$$

$$= .1536\left(\frac{18}{.020}\right)\frac{.506\times10^{-6}}{2(3.32\times10^{-5})(9.87\times10^{-8})(386)}$$

$$= \underline{2.77}\ \text{PSI}$$

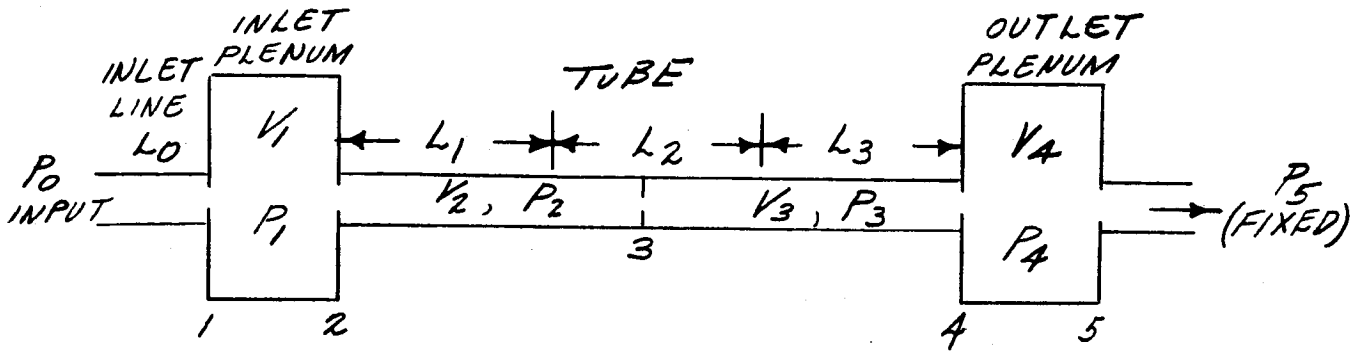

$$\dot{m}_1 = \int \frac{G A_0}{L_0} \left(P_0 - P_1 - R \dot{m}_1 / \dot{m}_1 / \right)$$

$$P_1 = \int \frac{c_1^2}{G V_1} \left(\dot{m}_1 - \dot{m}_2 \right)$$

$$\dot{m}_2 = \int \frac{G A_1}{L_1} \left(P_1 - P_2 - R \dot{m}_2 \right)$$

$$P_2 = \int \frac{c_2^2}{G V_2} \left(\dot{m}_2 - \dot{m}_3 \right)$$

$$\dot{m}_3 = \int \frac{G A_2}{L_2} \left(P_2 - P_3 - R \dot{m}_3 \right)$$

$$P_3 = \int \frac{c_3^2}{G V_3} \left(\dot{m}_3 - \dot{m}_4 \right)$$

$$\dot{m}_4 = \int \frac{G A_3}{L_3} \left(P_3 - P_4 - R \dot{m}_4 \right)$$

$$P_4 = \int \frac{c_4^2}{G V_4} \left(\dot{m}_4 - \dot{m}_5 \right)$$

$\dot{m}_5$ (FIXED) OR $K P_4$

1. $\dot{m}_1 = \int .0841 (P_0 - P_1) - 1.4 \times 10^6 \dot{m}_1 / \dot{m}_1 /$

2. $P_1 = \int 21.5 \times 10^6 (\dot{m}$

3. $\dot{m}_2 = \int .571 (P_1 - P_2) - .262 \times 10^4 \dot{m}_2$

4. $P_2 = \int 22.4 \times 10^6 (\dot{m}_2 - \dot{m}_3)$

5. $\dot{m}_3 = \int .571 (P_2 - P_3) - .262 \times 10^4 \dot{m}_3$

6. $P_3 = \int 84.8 \times 10^6 (\dot{m}_3 - \dot{m}_4)$

7. $\dot{m}_4 = \int .571 (P_3 - P_4) - .262 \times 10^4 \dot{m}_4$

8. $P_4 = \int 81.4 \times 10^6 (\dot{m}_4 - \dot{m}_5)$

9. $\dot{m}_5 = .0001565$

LOG FUNCTION GENERATOR CALCULATIONS

GIVEN: GENERAL FORM OF EQUATION $\Delta P_o = C + K \, L_N \, \phi$

ALSO GIVEN TABLE 2 IN LOG FUNCTION GENERATOR SPECIFICATION, AND TABLE 1

FROM TABLE 1 THE ASSUMPTION: $\Delta P_i = B\phi$ WAS MADE.

THIS ASSUMPTION IS GOOD UP TO $\phi = 100\%$

NOW: $\Delta P_o = C + K \, L_N \left(\frac{\Delta P_i}{B}\right)$

$\Delta P_o = C + K \, (L_N \, \Delta P_i - L_N B)$

$\Delta P_o = C - K \, L_N B + K \, L_N \, \Delta P_i$

NOW: $\Delta P_o = C^1 + K L_N \, \Delta P_i$

WHERE $C^1 = C - K \, L_N B$

@ $\phi = .01$, $\Delta P_o = 0$ FROM TABLE 2 (Appendix B)

$0 = C + K \, L_N \, (.01)$

$C = 2 \, K$

@ $\phi = 100$ $\Delta P_o = 10$ FROM TABLE 2 (Appendix B)

$10 = 2K + K \, L_N \, (100)$

$10 = 4 \, K \quad K = 2.500$

@ $\phi = 1$ $\Delta P_i = .602$ FROM TABLE 1 (Appendix B)

$1 \cdot B = .602 \quad B = .002$

SO: $\Delta P_o = 5 - 2.5 \, L_N \, .602 + 2.5 \, L_N \, \Delta P_i$

$L_N \, .602 = .2202$

$\Delta P_o = 5 + .5505 + 2.5 \, L_N \, \Delta P_i$

$$\boxed{\Delta P_o = 5.550 + 2.5 \, L_N \, \Delta P_i}$$

NOW FOR ERROR CALCULATION

$$\Delta P_o = 5.550 + 2.5\ L_N\ \Delta P_i$$

HOWEVER: ΔP_o AS A FUNCTION OF THE INPUT ΔP_i SHALL BE WITHIN ± 5% ABSOLUTE.

OR
$$\Delta P_{o\ max.} = 5.550 + 2.5\ L_N\ (\Delta P_i + .05\ \Delta P_i)$$
$$\Delta P_{o\ min.} = 5.550 + 2.5\ L_N\ (\Delta P_o - .05\ \Delta P_i)$$

NOW:
$$\Delta P_{o\ max.} = 5.550 + 2.5\ L_N\ (\Delta P_i\ (1+.05))$$
$$= 5.550 + 2.5\ (L_N\ \Delta P_i + L_N\ (1.05))$$
$$= 5.550 + 2.5\ (L_N\ \Delta P_i + .0212)$$

$$\Delta P_{o\ max.} = 5.603 + 2.5\ L_N\ (\Delta P_i)$$
$$\Delta P_{o\ min.} = 5.494 + 2.5\ L_N\ (\Delta P_i)$$

GAIN EQUATIONS

START WITH $\Delta P_o = C^1 + K\ L_N\ \Delta P_i$

WHERE $C^1 = 5.55$

$K = 2.5$

NOW IF WE DIFFERENTIATE THE EQUATION WITH RESPECT TO ΔP_o WE GET:

$$\frac{D \cdot \Delta P_o}{D\ \Delta P_i} = \frac{DC^1}{D\Delta P_i} + K\ \frac{D\ L_N \Delta P_i}{D\Delta P_i}$$

NOW $\frac{D\ \Delta P_o}{D\ \Delta P_i} = G_p$ = PRESSURE GAIN

SO: $G_p = K\ \frac{1}{\Delta P_i}$

OR
$$G_p = \frac{2.5}{\Delta P_i}$$

TABLE 1

GAIN REQUIREMENTS

ϕ	ΔP_i	G_p
.01	.006	416.7
.02	.012	208.3
.05	.029	86.2
.10	.061	41.0
.20	.122	20.5
.50	.306	8.17
1.0	.602	4.15
2.0	1.23	2.03
5.0	3.04	.822
10.0	6.04	.414
20.0	11.9	.210
50.0	28.6	.087
100.0	53.8	.046
150.0	76.9	.032
200.0	98.1	.025

- CONTINUED -

OVERALL SYSTEM

NOTE THAT $P_o \text{ max.} = 5.603 + 2.5 \text{ LN } (\Delta P_i)$

$P_o \text{ min.} = 5.494 + 2.5 \text{ LN } (\Delta P_i)$

$P_o \text{ error} = .109$

SO: THE ERROR ALLOWED IS INDEPENDENT OF THE INPUT SIGNAL LEVEL.

ALSO: $\Delta P_o \text{ MAX.} = 10.76$ @ $\phi = 200$

SO: $\frac{\text{SIGNAL}}{\text{NOISE}} = \frac{10.76}{.109} = 98.7$

NOW 98.7 IS A HIGH RATIO FOR AN AMPLIFIER WITH AN OVERALL GAIN OF BETTER THAN 400. WE NEED FILTERS. WHAT OUTPUT NOISE FREQUENCY IS PERMISSIBLE?

NOW SINCE THE DESIRED EQUATION HAS BEEN OBTAINED, WE NEED TO FIND A WAY OF DESCRIBING THE FLUIDIC APPROXIMATION. AFTER SEVERAL TRIES IT WAS FOUND THAT THE OUTPUT OF A PROPORTIONAL AMPLIFIER COULD BE APPROXIMATED BY:

$$\Delta P_o = A P_i \text{ SIN } \frac{\pi}{2} \frac{\Delta P_i}{BP_i} + K$$

AN EXAMPLE OF THE FIT OF THIS EQUATION AND EXPERIMENTAL DATA IS SHOWN IN FIGURE 1.

THEREFORE, IT WAS ASSUMED THAT THE SATURABLE AMPLIFIERS COULD BE APPROXIMATED BY:

$$\Delta P_o = A P_i \text{ SIN } \frac{\pi}{2} \frac{\Delta P_i}{BP_i}$$

FOR $0 \leq \Delta P_i \geq BP_i$

AND $\Delta P_o = A P_i$

FOR $\Delta P_i > B P_i$

- CONTINUED -

TABLE F-2

LOG FUNCTION GENERATOR REQUIREMENTS

Power Level (Percent) ϕ	Output Differential (psi) ΔP_o
0.01	0
0.05	1.74
0.10	2.5
1.0	5.0
10.0	7.5
100.0	10.0
150.0	10.44
200.0	10.76

EXAMPLE OF CURVE FIT TO EXPERIMENTAL DATA FOR FLUID AMPLIFIER

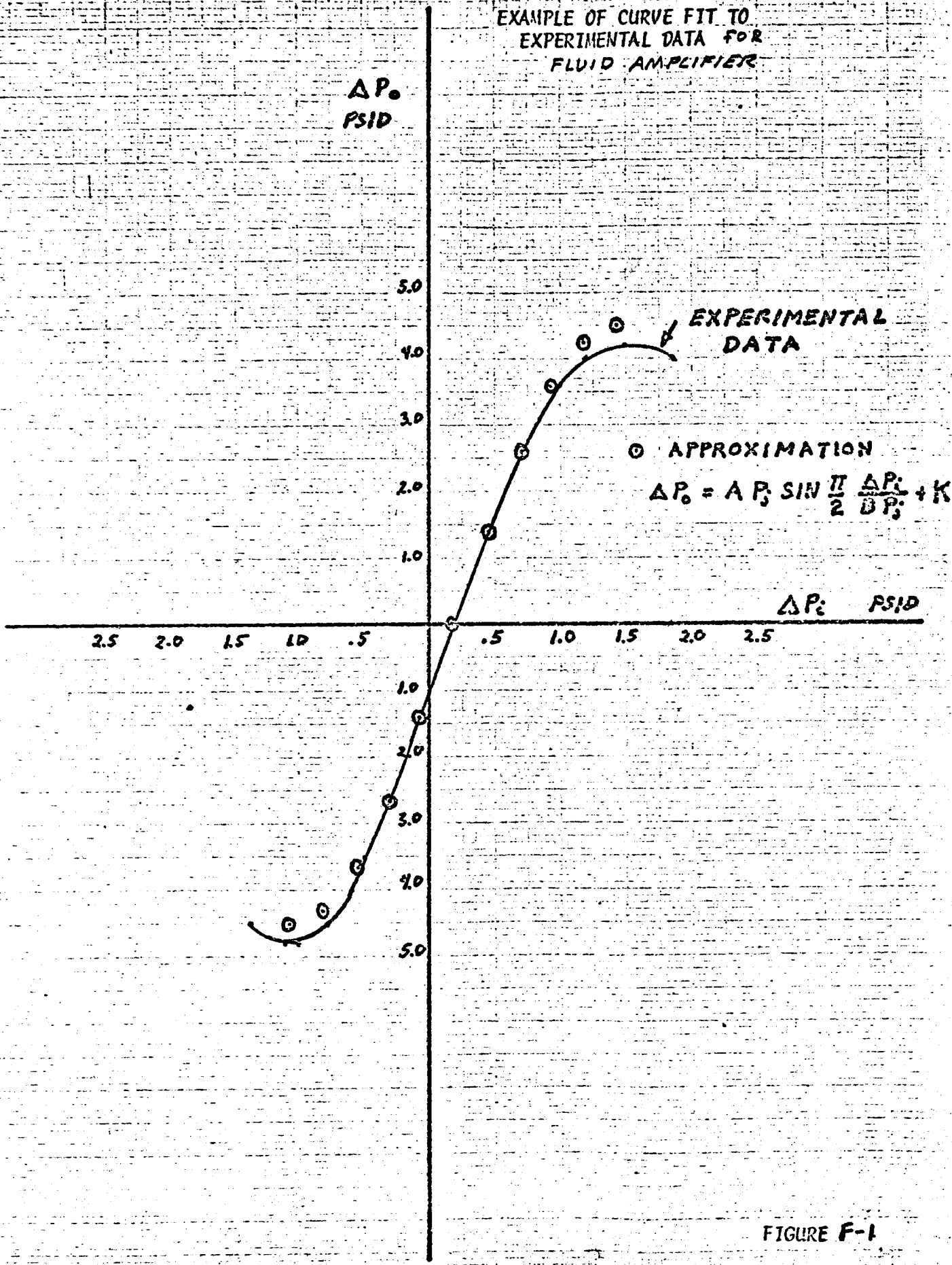

FIGURE F-1

APPENDIX G

HEATER DEVELOPMENT PROGRAM

INTRODUCTION

The objective of this program was to develop and evaluate by laboratory tests an electrical heater system which would meet the requirements of the all-pneumatic neutron flux detector. Two basic heater versions were investigated, both of the resistance type. The first version was an improvement of the original silicon semiconductor heater. The second, and successful, version was the lamination of a metal resistance foil on a metal substrate.

CONCLUSIONS AND RECOMMENDATIONS

The results of this program indicate the following conclusions:

1) The original semiconductor heater, 99-108390, proved to be unsatisfactory for use as a heat source in this application due to thermally induced materials failure at the contact pads.

2) An alternate heater, Figure 7, which utilizes a thin metallic resistance foil epoxyed on a stainless steel substrate, has demonstrated that it can satisfactorily meet the specified heating and environmental requirements for Contract NAS 3-7989 with more than adequate margin.

It is recommended that a heater configuration similar to that of Figure 7 be utilized to provide the simulated nuclear heating for the All-Pneumatic Neutron Flux Detector Sensor Assembly.

PROBLEM SUMMARY

The heaters which failed during the Flux Detector tests were fabricated to the specifications given in Table I. The heater consists of a homogenous .020 inch thick silicon pad into which boron is

diffused .005 inch on each side. The basic silicon substrate is a high-resistance "N"-type semiconductor while the boron diffusion causes its two surface layers to become low-resistance "P"-type semiconductors. These layers are tailored to produce either 3.05 or 1.83 ohms per side. To facilitate interconnecting the three heater slabs used in the heater system, gold film contact pads are diffused into the ends of each heater on both sides.

Each side of each of the heaters is connected in series by the use of two .010 inch diameter gold wires in parallel soldered between the gold contact pads. A photograph of a heater slab with leads attached at one end and both sides connected in series at the other end is shown in Figure 1. One low resistance heater is located between two high resistance heaters and the three are mounted in the spacers shown in Enclosure (6). The total heater resistance is then 15.86 ohms. The required maximum heat of 850 watts is obtained by applying 7.33 amps at 116 volts.

The heaters and spacers are mounted in a heater support tube. Gaseous helium at 250 psia and 140°R is applied upstream of the inlet orifice and is heated as it flows over the heaters and exhausts through the exit orifice. The pressure downstream of the heaters is a function of the heat consumed by the gas and is used as an analog output signal. The inlet and exit orifices are sized to give the heater pressure range and flow shown in Table I. Inasmuch as the heater surface and internal temperatures are affected by these gas flow conditions, as well as the electrical power applied, care must be exercised in design to ensure against overheating.

The initial attempts to use these heaters in the sensor tests for the All-Pneumatic Neutron Flux Detector proved fruitless. It was not possible to apply power to the heaters as they indicated an electrical open. The Flux Detector Sensor Assembly was disassembled and most of the heaters were found to be broken or otherwise damaged.

The six slabs removed from the two heater assemblies contained in the sensor were found in the following condition:

1) 2 intact slabs.
2) 2 slabs broken in two or more pieces.
3) 3 slabs with solder pads lifted (includes one of the broken slabs).

Photographs of some of the lifted solder pads are shown in Figures 2-5. In every case the silicon just under the pad is still attached to the pad. The failure occurred in the silicon itself.

The broken slabs could be explained by shock loads applied during disassembly since the sensor parts had been eppxyed in place and many had to be hammered apart. Later attempts to re-fabricate a new heater assembly using the visually intact slabs failed when those slabs were found to be electrically open. Closer inspection under a microscope revealed hairline cracks across the heater surface "P"-layers in the vicinity of the contact pads. It appeared that the failure mode was associated with these contact pads but at this time the cause of failure was unknown.

HEATER EVALUATION PROGRAM

At this point it was decided that additional heater tests should be conducted with sufficient dynamic instrumentation to provide adequate information for failure analysis. In addition, if the first failure had been caused by poor test procedure or by mishandling of the sensor assembly, these tests would provide a basis for confidence in the future performance of the heaters. Accordingly additional heaters were purchased and a single heater assembly was fabricated. A special test jig was also fabricated and a heater evaluation test program was designed. This program called for continuous oscillograph monitoring of the heater assembly electrical continuity, the heater pressure drop, the pressure downstream of the heaters, and the temperatures upstream

and downstream of the heaters. It included room temperature flow tests up to 250 psia and electrical power tests to full power at LN_2 temperatures and 250 psia.

The heaters were installed and warm temperature tests at 50 psig were begun. Heater continuity was obtained by applying 100 ma to the heaters and monitoring the voltage drop across a series resistor. Prior to test, heater continuity was good. Immediately upon commencement of flow the current through the heaters began to oscillate between 0 to 100 ms, indicating an intermittant open-circuit condition. The frequencies observed were several between 850 cps and 1100 cps. No pressure oscillations were observed, nor heater assembly vibrations felt. When the supply pressure was cut off rapidly, in approximately 50 ms, the heater assembly immediately indicated an open.

The heaters were removed from the heater support tube and all three were found to have broken or have had the solder pad lifted out at the front ends. A photograph of these three is shown in Figure 6.

Two theories as to the cause of failure were considered. The first was that the damage was due to flow-induced flutter of the heater slabs. The second was that the damage was of a thermal nature but still of causes unknown. This latter theory was supported by post observations of other thermally damaged silicon parts, Reference 1. This view was strengthened by conversations with Autonetics Materials Research personnel specializing in silicon research, Reference 2.

A second series of tests were conducted to test the validity of the flutter theory. The heaters tested in the first evaluation series were cut just in back of the broken solder pads and re-mounted in the heater support tube. This assembly was flow tested for 15 minutes at room temperature and 250 psia and for 15 minutes at 250 psia and temperature between 190°F and 240°R. No electrical continuity measurements were made. In both cases, vibrations of the heater support

tube were noted. The frequencies noted in the oscillograph pressure measurements were between 300 cps and 900 cps. No further damage to the heaters was observed indicating the silicon substrates were structurally sound at these conditions.

A closer examination of the original design criteria for choosing the materials at the contact pad was made in the light of these results. It was decided, at the recommendation of materials research personnel, Reference 2, to fabricate new contact pads from Kovar or Invar rather than from gold and to weld the fold leads on these pads rather than solder them on. Either of these two materials have low temperature coefficients of expansion which are near that of silicon. Although the expansion coefficient of gold is different than that of silicon, it was originally believed that this would cause no problem since gold is quite malleable. The solder was eliminated because it was another large mass with a different temperature expansion coefficient.

Since neither Kovar nor Invar can be directly bonded to silicon at temperatures low enough to keep from disturbing the silicon dopent level, it is necessary to use a very thin film of gold as a bonding agent. To obtain a bond with a good ohmic electrical resistance rather than one with a diodetype electrical resistance, it is necessary to pay close attention to the relative electron levels of the gold, silicon and Invar. If a diode bond develops, a high resistance results at the contact pads with ensuing local hot spots and consequent high probability of thermally induced failure. It is preferable to use doped gold and Invar to effect this desired result by creating an electrically homogenous bond between the silicon and gold and between the Invar and gold. The gold is about one mil or less in thickness. The three materials are placed in close contact by the application of a light force, heated to about 400°C and mechanically rubbed together until the gold diffuses into both the silicon and the Invar, forming a bond between the two.

The contact pads of four still useable heater slabs from previous tests were cut off and Invar pads were mounted as described above. One of these pads, while cooling to room temperature after being bonded, experienced the same type of failure previously noted. The silicon below the contact pulled out of the silicon substrate. Another of the slabs was tested by passing about three amperes of electrical current through it at room temperature. It failed in the same manner.

The most likely cause of failure of the heaters appears to be in the contact pad bonding process, both at Rocketdyne and at Kulite Semiconductor, the original fabricator. While several ideas of how to circumvent the above outlined problems by closer control of various fabrication parameters could be postulated, it was felt that other types of heaters would be easier to fabricate within the remaining time and budget.

Accordingly, a second type of heater was designed with ruggedness as a prime criteria. A sketch of this design is shown in Figure 7. available materials dictated several of the parameters. Stainless steel substrates were cut which measured 2x.2x.018 inch. A resistance foil .0035 inch thick, .125 inch wide and 4 inches long was epoxyed to both sides of the substrate as shown. The epoxy was used both as a bonding agent and as an electrical insulator.

Two types of off-the-shelf foils which appear satisfactory because of their small resistance change with temperature, their small geometry and their resistance values were chosen. They are known by the trade names of Tophet C and Evenohm. Both are fabricated in many sizes from as small as .001 inch in thickness and resistances in the range of 1 to 6 ohms/foot. The foil obtained was .0035 inch thick Evenohm which was specified as 1.2 ohms/foot.

Three of the heater slabs of the configuration shown in Figure 7 were

fabricated and installed in a heater support tube. Due to the somewhat excessive bulkiness of these elements (over .025 inches thick) this heater assembly had to be forced together and was rather crowded in the vicinity of the contact pads. In fact, the flow path below the bottom heater was substantially blocked by the two .010 diameter gold electrical lead wires. The total heater assembly resistance, at room temperature and prior to any flow tests, was found to be between .7 and .825 ohms. The resistance measurements were made with three separate instruments, including an impedance bridge.

Although the measured resistance was at least 40% below that expected it was decided to proceed with the evaluation. Fabrication of another heater assembly was scheduled to be completed while tests were conducted on the first assembly. A successful series of tests were conducted on the assembly up to 900 watts of power. These tests were conducted at inlet temperatures at least 30% greater than the 140°R which the Flux Detector Sensor test set-up has been shown to be able to provide and at about 73% of the helium flowrate which the heaters will experience in the same test set-up. Both of these observations add up to the conclusion that the heaters tested possess a safety margin over the actual Flux Detector Sensor test conditions since the evaluation tests provide less heater cooling capability. In addition, the bottom heater appeared to have run under even more stringent conditions as a post-test inspection revealed it to be blackened throughout its entire length on one side.Figure 8 shows the three heaters after conclusion of the evaluation tests. This was the heater which appeared to have much of its flow area blocked by the inlet wires and it apparently did run in a "gas starved" condition. As the heaters were epoxyed in place in this assembly, no vibrations or pressure flucitons were encountered during the tests.

A final observation of these test results concerns the apparent heater assembly total resistance and results in the conclusion that some of

the individual slabs actually produced over twice the heat specified. If this is so, and it appears highly likely, the tests conducted were greatly in excess of those necessary to provide confidence in these heaters for the conditions of interest. This hypothesis is supported by the resistance measurements made before, during, and after the flow tests, all with the same instrument. Additional resistance values are inferred from the voltage and current applied during the tests.

Prior to the tests, and at zero power during the tests, the resistance was about .8 ohm, the resistance of only two heaters. During the tests, the resistance decreased with power applied to just below .6 ohm, almost down to the resistance of a single heater, at 900 watts. Since Evenohm has a small but positive thermal resistance coefficient, this observation is opposite the expected effect. After the last test, the resistance measured 1.3 ohms. After disassembly, the resistance of the individual heaters was .42 ohms each or a total of 1.26 ohms for the assembly. The expected resistance, based on the manufacturer's specification for this type of Evenohm, was about 1.2 ohms total. The current and voltage expected to produce 900 watts and based on 1.2 ohms, were 27.4 amperes and 32.9 volts. The current and voltage necessary to produce 900 watts output from the power supply were 40 amperes and 23 volts.

Based on these observations, it is concluded that two of the heaters were initially in contact in the heater assembly, electrically shorting two heater slab sides, the equivalent of one entire heater. In addition, the remaining heater must have been in close proximity to one of the other two. When power was applied, the heaters slightly expanded and contacted each other, partially shorting out an additional heater. This hypothesis is supported by the condition of the center and bottom heaters at their downstream ends. Matching discolored bluish bands, indicating hot spots, extend across the top of the bottom heater and across the bottom of the center heater.

If one heater were shorted when 900 watts was applied to the assembly, then the two remaining heaters were producing the total heat, or each was producing 150% of rated heat. If more than one heater was shorted, the remaining heater, or parts of heaters, had to produce even more above its or their rating. In the case considered the current was 40 amperes and the resistance of one side of a heater was .21 ohms at room temperature. This results in 336 watts or over twice the rated power of 150 watts per side.

The all-metallic heater meets the desired heater specifications for the All-Pneumatic Neutron Flux Detector. It is exceedingly rugged and is capable of operating at more than twice the specified heating rate without adverse effects. The design configuration for the flux detector application will use .001 inch thick by .200 inch wide, 5 ohms/foot Tophet C resistance foil. This type of foil exhibits less resistance change with temperature than does Evenohm. The foil will be epoxyed on a .015 inch thick by .200 inch wide stainless steel substrate. The total heater thickness will be .019 inch and will be compatible with the existing heater spacer. The heaters will be epoxyed in place in the heater assembly. Use of .200 inch wide foils will eliminate electrical shorting between heater elements since the foils will extend into the spacers and will thus be physically restrained from moving toward each other. Thirteen (13) amperes at sixty-six (66) volts will produce the maximum heating rate desired.

APPENDIX G

REFERENCES

1 J. W. Bice; Rocketdyne D/991-347; personal communication.

2 W. A. Bailey; Autonetics, D/548-083; personal communication.

TABLE I

SPECIFICATION - ALL-PNEUMATIC NEUTRON FLUX DETECTOR ELECTRICAL HEATER SYSTEM

Heater Slabs Required	3
Maximum Heat Generation, watts	
One Slab	195
Two Slabs, each	327
Total, Three Slabs	850
Size, each See Enclosure (5)	
Length, in	2.0
Width, in	0.2
Thickness, in	0.02
Spacing See Enclosures (6) and (4)	
Slab-to-Slab, in	.017
Slab-to-Container, in	.010
Environment	
Gas	Helium
Pressure Range, psig	70-130
Gas Inlet Temperature, ^{o}F	-320
Gas Flowrate, lb/sec	.0032

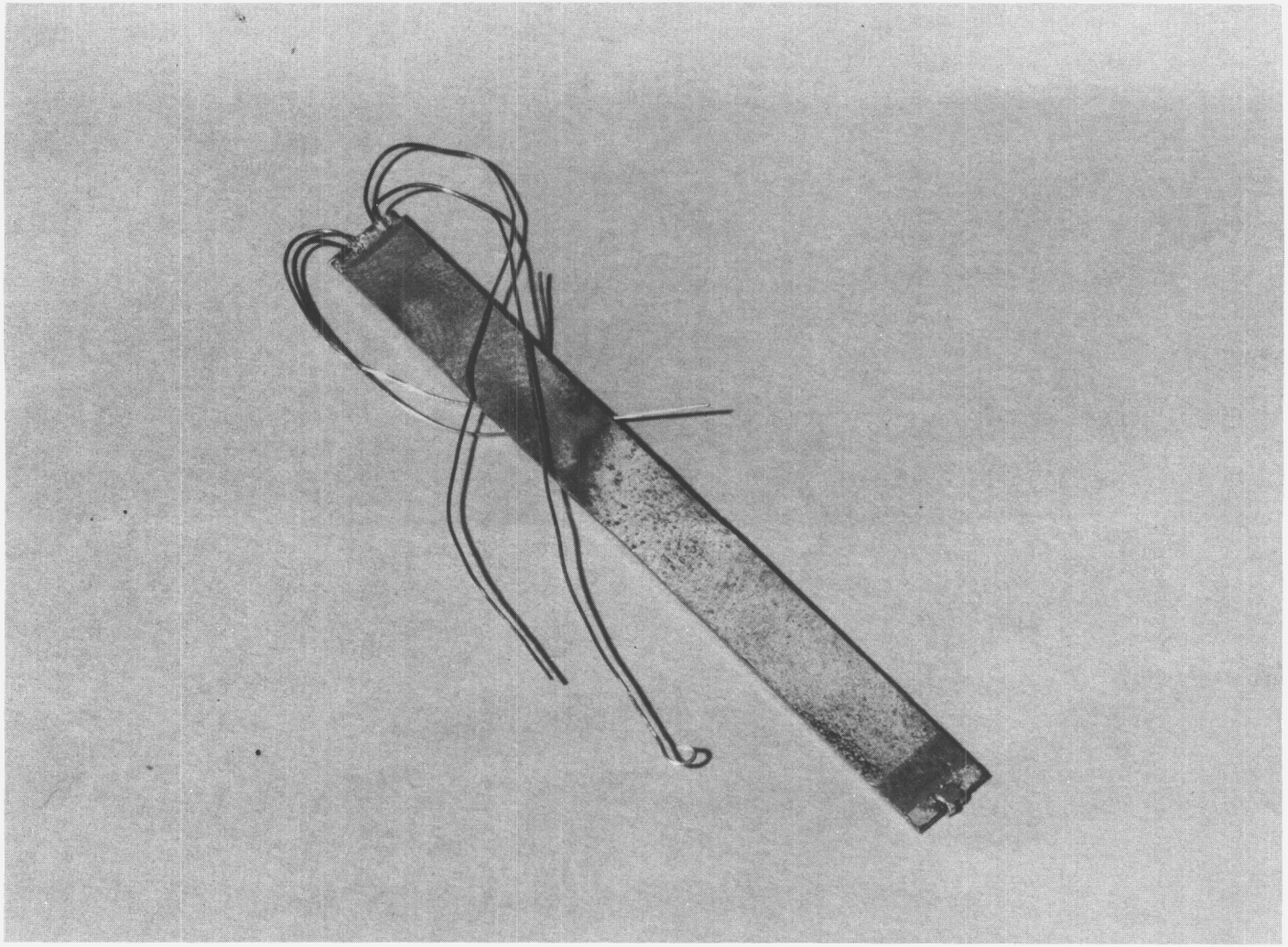

5AH61-11/10/66-S1A

Figure G-1. Silicon Flux Detector Heater Slab

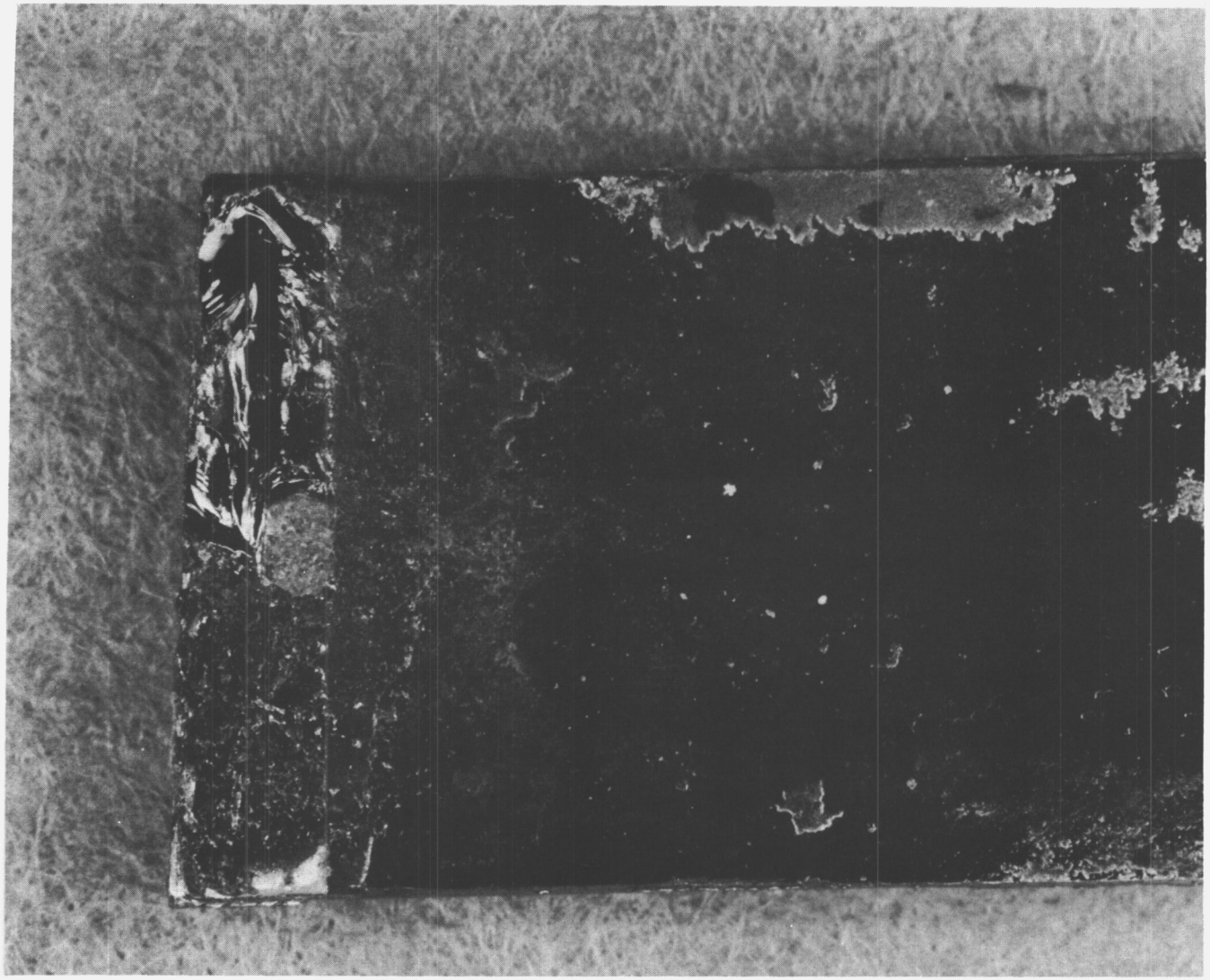

3XK45-9/28/67-C1A

Figure G-2. Failure Mode, Silicon Flux Detector Heater Slab

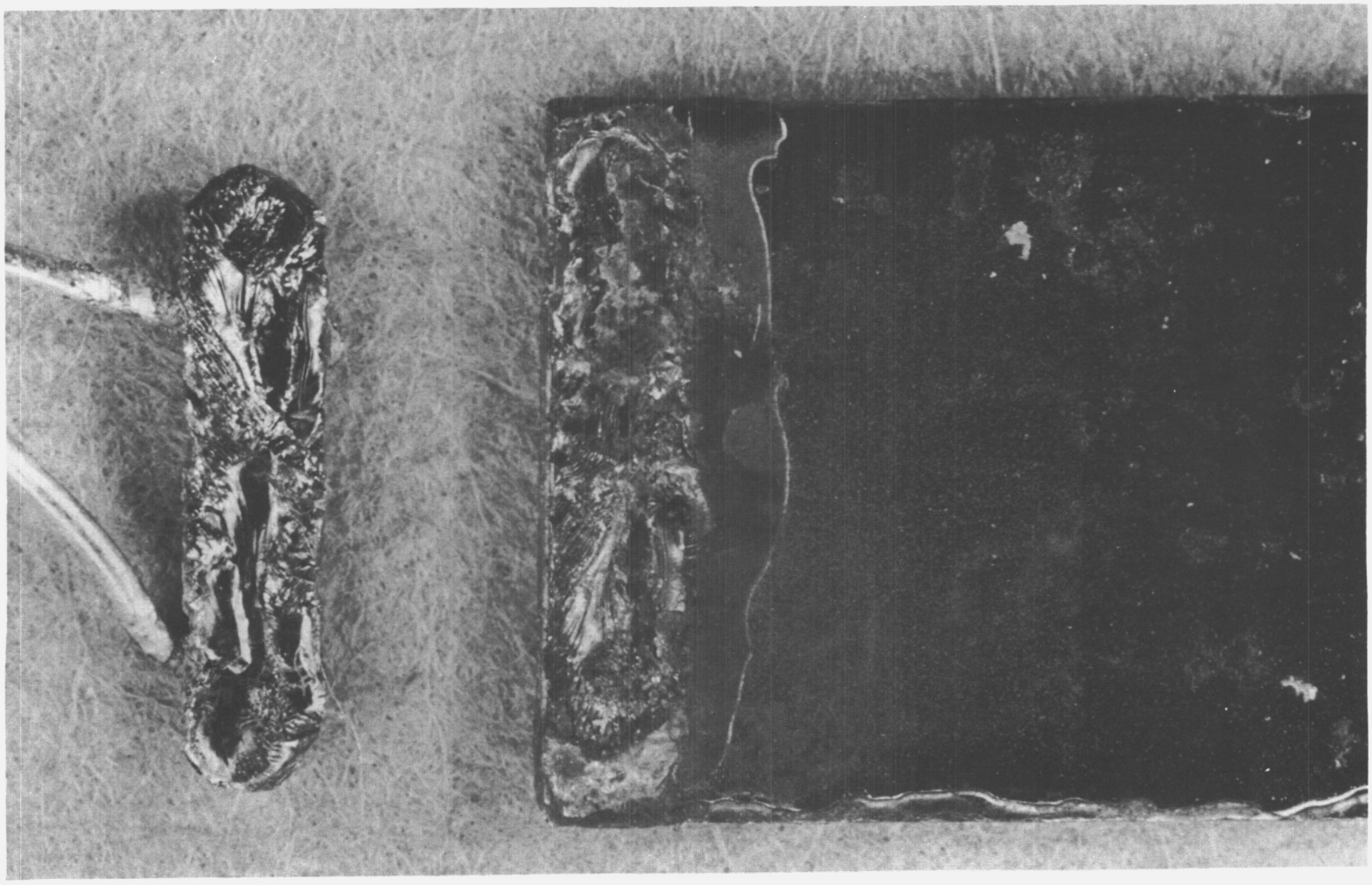

3XK45-9/28/67-C1B

Figure G-3. Failure Mode, Silicon Flux Detector Heater Slab

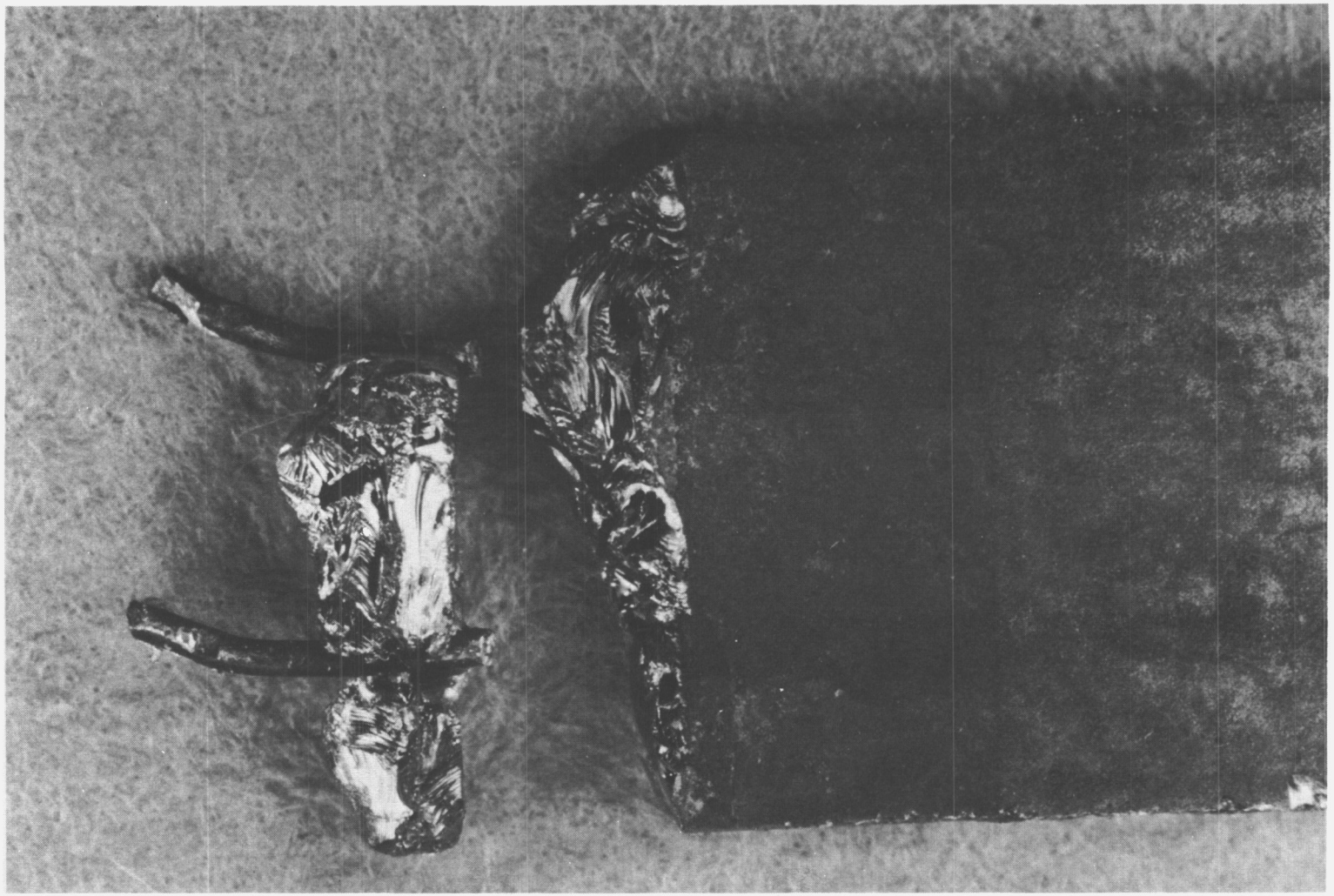

3XK45-9/28/67-C1C

Figure G-4. Failure Mode, Silicon Flux Detector Heater Slab

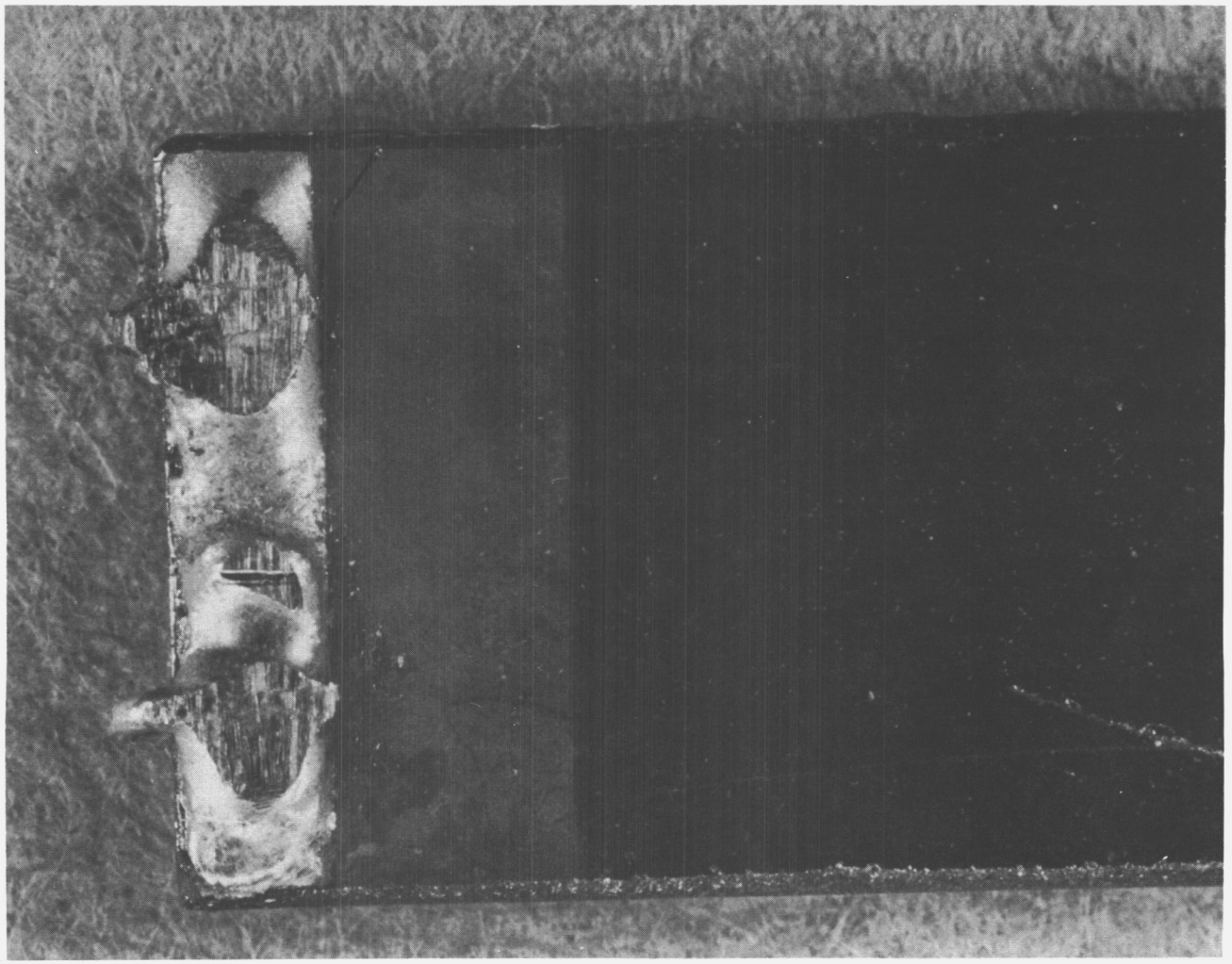

3XK45-9/28/67-C1D

Figure G-5. Failure Mode, Silicon Flux Detector Heater Slab

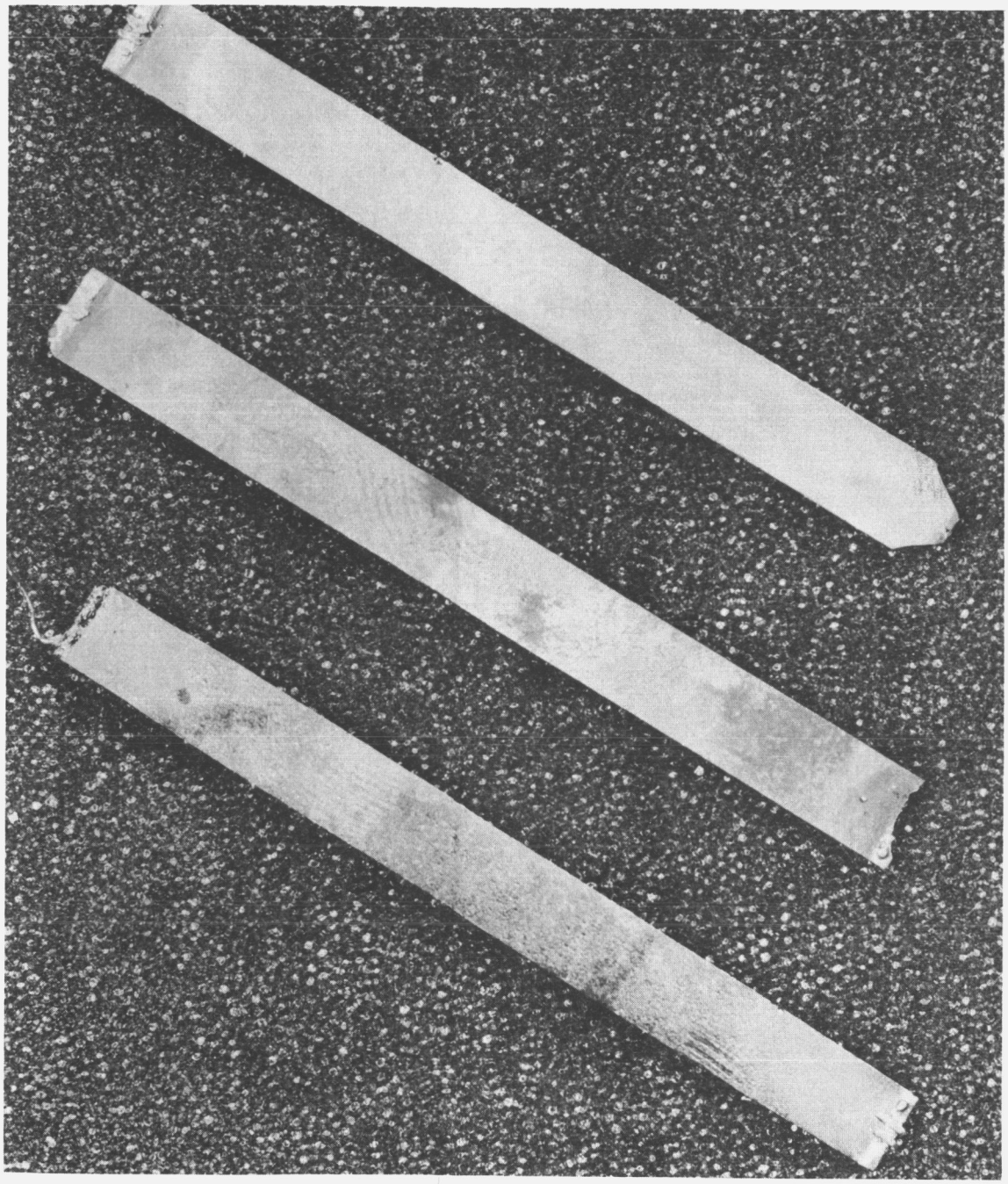

1CT91-9/25/67-S2B

Figure G-6. Heaters Failed in First Heater Evaluation Test, Silicon Flux Detector Heater Slabs

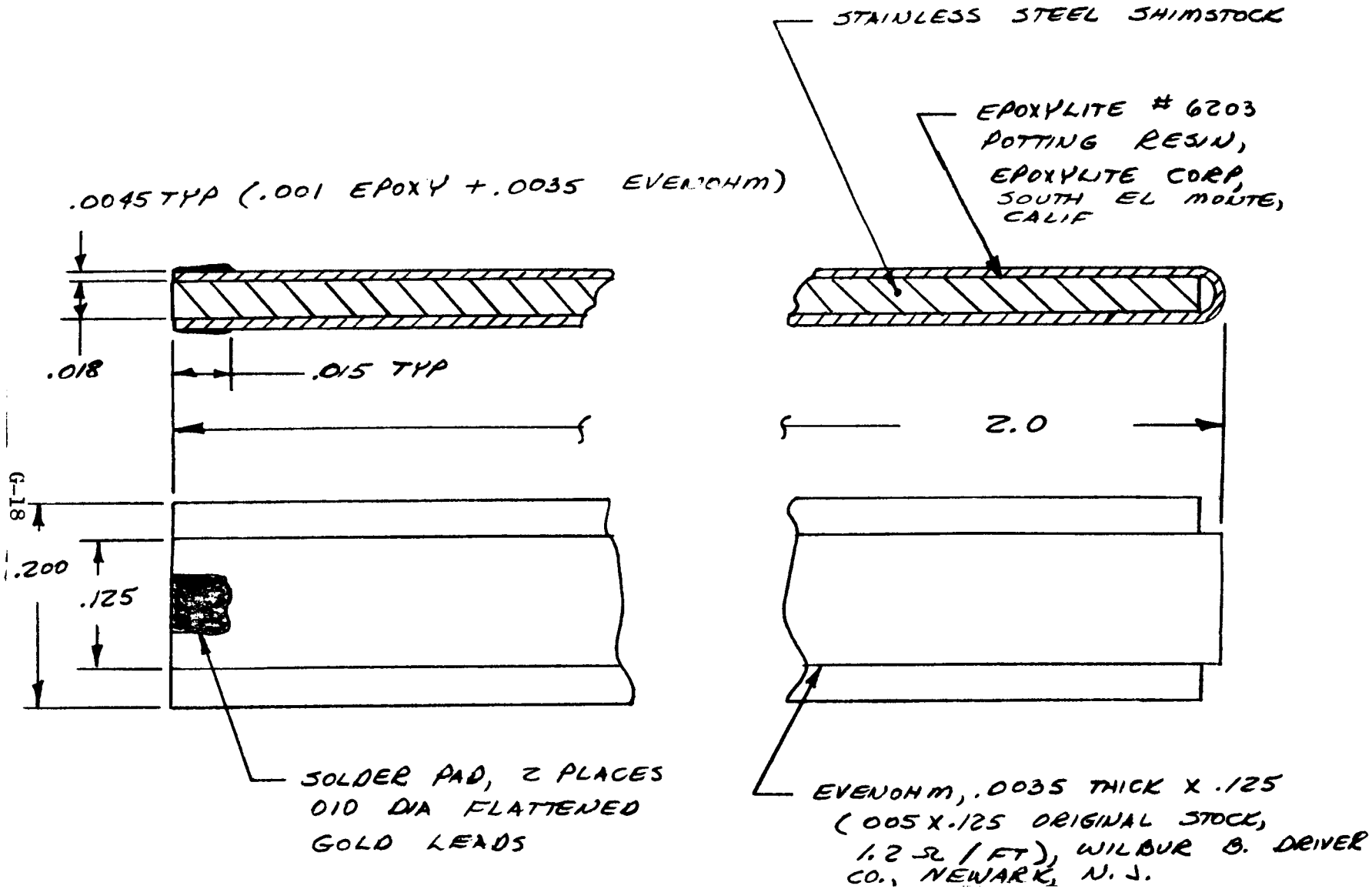

Figure G-7. Heater Assembly, Metallic Foil

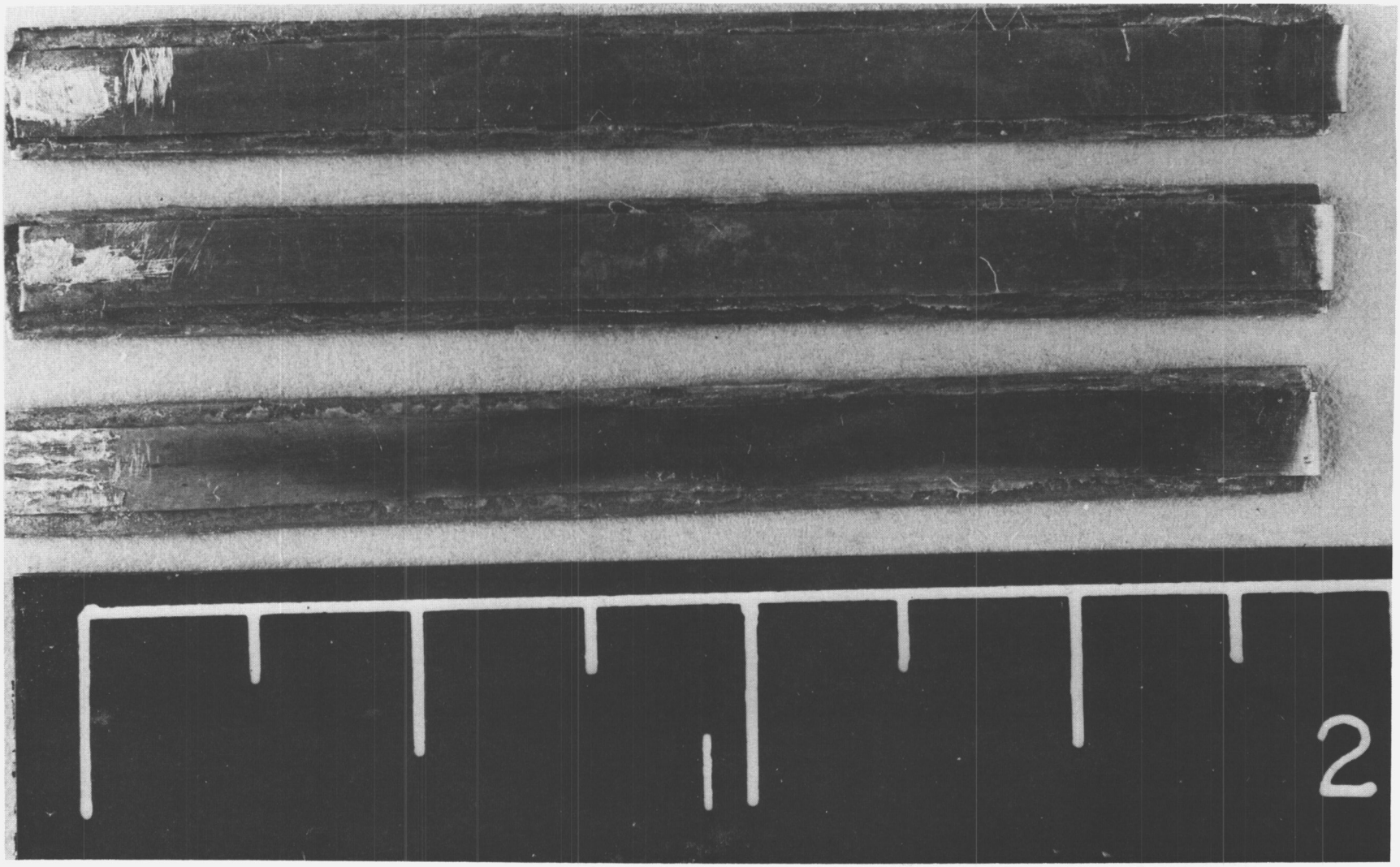

3XK42-11/2/67-C1B

Figure G-8. Posttest View of Heaters Used in Successful Metal Foil Heater Evaluation Tests

APPENDIX H

Unless otherwise noted the following nomenclature applies to equations and figures presented in the text. Many of these variables are illustrated in Fig. 1 of the main text.

NOMENCLATURE

A	Area
P	Total pressure
T	Absolute temperature
ΔP	Differential pressure
q	Heat input rate
Re	Reynolds Number
C_D	Coefficient of discharge
C_p	Heat capacity of gas at constant pressure
$\dot{m}$	Mass flowrate
$f(P_{i+1}/P_i$	Compressible flow function
K_m	A constant defined by requirements of the equation and identified by m = integer. Also conductance
C_m	Heat capacity of solid material in element
M	Effective mass of solid material in element
γ	Heat capacity ratio
R	Gas constant
g	Gravitational constant
G	Mass velocity of gas in duct
μ	Viscosity
ρ	Density of gas
D	Diameter
L	Length of duct or slab, linear dimension

f	Friction factor
P_w	Wetted perimeter
P_r	Prandtl Number
h	Film heat transfer coefficient
k	Gas thermal conductivity
D_r	Hydraulic radius
ΔT	Differential temperature
ΔL	Incremental change in length

SUBSCRIPT

$( )_a$	Active element
$( )_b$	Compensating element
$( )_r$	Element inlet (no subscript for outlet)
$( )_{(max)}$	Maximum value
$( )_{(min)}$	Minimum value
$( )_d$	Downstream from discharge
$( )_i$	i location or element
$( )_{i+1}$	i + 1 location or element, next location or element in series
$( )_{crit}$	Critical ratio
$( )_w$	Wall
$( )_f$	Function generator
$( )_o$	Output
$( )_c$	Sensing line from element

SUPERSCRIPTS

$\overline{( )}$	Average Value

PRESCRIPTS

$\Delta ( )$	Difference, delta change, differential or incremental

DISTRIBUTION LIST

Recipient	No. of Copies
NASA-Lewis Research Center 21000 Brookpark Road Cleveland, Ohio 44135 Attention: Dr. John C. Liwosz	1
NASA-Lewis Research Center 21000 Brookpark Road Cleveland, Ohio 44135 Attention: Miles O. Dustin	4
NASA-Lewis Research Center 21000 Brookpark Road Cleveland, Ohio 44135 Attention: Norman T. Musial	1
NASA-Lewis Research Center 21000 Brookpark Road Cleveland, Ohio 44135 Attention: L. V. Humble	1
NASA Headquarters Washington, D.C. 20546 Attention: John E. Morrissey	1
NASA-Ames Research Center Moffett Field, California 94035 Attention: Library	1
NASA-Goddard Space Flight Center Greenbelt, Maryland 20771 Attention: Library	1
NASA-Langley Research Center Langley Station Hampton, Virginia 23365 Attention: Library	1
NASA-Marshall Space Flight Center Huntsville, Alabama 35812	1
NASA-Lewis Research Center 21000 Brookpark Road Cleveland, Ohio 44135 Attention: Thomas J. Flanagan C&NR Procurement Section	1

Recipient	No. of Copies
U.S. Atomic Energy Commission Technical Information Service Ext. Post Office Box 62 Oak Ridge, Tennessee 37830	3
NASA-Lewis Research Center 21000 Brookpark Road Cleveland, Ohio 44135 Attention: Contract & Administrative Office	1
Battelle Memorial Institute 505 King Avenue Columbus, Ohio 43201 Attention: REIC	1
NASA-Lewis Research Center 21000 Brookpark Road Cleveland, Ohio 44135 Attention: Isidore Warshawsky	1
NASA-Lewis Research Center 21000 Brookpark Road Cleveland, Ohio 44135 Attention: Library	5
National Aeronautics and Space Administration Washington, D.C. 20546 Attention: NPO/T. C. Schwenk	3
NASA-Lewis Research Center 21000 Brookpark Road Cleveland, Ohio 44135 Attention: Office of Reliability and Quality Assurance	3
NASA-Flight Research Center Post Office Box 273 Edwards, California 93523 Attention: Library	1
NASA-Manned Spacecraft Center Houston, Texas 77001 Attention: Library	1
NASA-Western Operations 150 Pico Boulevard Santa Monica, California 90406	1
Jet Propulsion Laboratory 4800 Oak Grove Drive Pasadena, California 91103 Attention: Library	1

Recipient	No. of Copies
NASA Scientific and Technical Information Facility Box 5700 Bethesda, Maryland 20546 Attention: NASA Representative	6
U.S. Atomic Energy Commission Technical Reports Library Washington, D.C. 20545	3
NASA-Lewis Research Center 21000 Brookpark Road Cleveland, Ohio 44135 Attention: Report Control Office	1

Unclassified

Security Classification

DOCUMENT CONTROL DATA - R & D

(Security classification of title, body of abstract and indexing annotation must be entered when the overall report is classified)

1. ORIGINATING ACTIVITY (Corporate author) Rocketdyne, a Division of North American Rockwell Corporation, 6633 Canoga Avenue, Canoga Park, California 91304	2a. REPORT SECURITY CLASSIFICATION Unclassified 2b. GROUP

3. REPORT TITLE

Development of a Breadboard Model of an All-Pneumatic Neutron Flux Detector

4. DESCRIPTIVE NOTES (Type of report and inclusive dates)

5. AUTHOR(S) (First name, middle initial, last name)

S. E. Milleman

6. REPORT DATE	7a. TOTAL NO. OF PAGES	7b. NO. OF REFS
23 May 1968	160	14

8a. CONTRACT OR GRANT NO.	9a. ORIGINATOR'S REPORT NUMBER(S)
NAS3-7989 b. PROJECT NO. c. d.	R-7492 9b. OTHER REPORT NO(S) (Any other numbers that may be assigned this report)

10. DISTRIBUTION STATEMENT

11. SUPPLEMENTARY NOTES	12. SPONSORING MILITARY ACTIVITY
	Technical Management, NASA Lewis Research Center, Cleveland, Ohio, Nuclear Rocket Technology Office, Miles Dustin

13. ABSTRACT

A breadbaord Model was constructed of an All-Pneumatic Neutron Flux Detector. Subassemblies of the detector consisted of a sensing element which was electrically heated to simulate neutron heating effects, a precooler, a temperature equalizer, and a fluid interaction logarithmic function generator. The detector was designed to produce a penumatic output signal proportional to the logarithm of incident neutron flux. Performance tests were made on all system subassemblies except the sensing element. Sensing element heater development tests were completed.

DD FORM 1 NOV 65 1473

Unclassified

Security Classification

14. KEY WORDS	LINK A		LINK B		LINK C	
	ROLE	WT	ROLE	WT	ROLE	WT